Renewable and Sustainable Energy Reviews 36 (2014) 370–411

Contents lists available at ScienceDirect

Renewable and Sustainable Energy Reviews

journal homepage: www.elsevier.com/locate/rser

Artificially roughened solar air heater: Experimental investigations

Anil Singh Yadav [a,*], Manish Kumar Thapak [b]

[a] Mechanical Engineering Department, Technocrats Institute of Technology-Excellence, Bhopal, MP 462021, India
[b] Mechanical Engineering Department, Dr. K.N. Modi University, Newai, Rajasthan 304021, India

ARTICLE INFO

Article history:
Received 27 July 2013
Received in revised form
15 March 2014
Accepted 27 April 2014
Available online 28 May 2014

Keywords:
Solar energy
Solar air heater
Artificial roughness
Heat transfer
Pressure drop
Thermohydraulic performance parameter

ABSTRACT

Solar air heater is the cheapest and extensively used solar energy collection device for drying of agricultural products, space heating, seasoning of timber and curing of industrial products. The use of an artificial roughness on a surface is an effective technique to enhance the rate of heat transfer to fluid flow in the duct of a solar air heater. Use of artificial roughness in solar air heater has been topic in research for the last thirty years. In the present article an attempt has been made to present holistic view of different kinds of roughness geometry used for creating artificial roughness in solar air heater for performance enhancement by experimental approaches. In this article thirty eight experimental studies have been reported on solar air heater, roughened with different kinds of roughness geometry. However, no comprehensive comparative study has been carried out or found in the literature so far, in order to investigate the relative performance of different types of artificially roughened solar air heater. The objective of this article is to perform such a study. In this article twenty known different shapes and orientations of roughness elements are considered for comparative analysis. In order to obtain the results numerically, codes are developed in MATLAB-7. Correlations for heat transfer and friction factor, developed by various investigators for artificially roughened solar air heaters have been reported in this article. The effects of various rib parameters on heat transfer and fluid flow processes are also discussed.

Contents

* Corresponding author. Tel.: +91 9229220126.
E-mail address: anilsinghyadav@gmail.com (A. Singh Yadav).

http://dx.doi.org/10.1016/j.rser.2014.04.077
1364-0321/

1. Introduction

Energy is the primary force in the universe. Energy defines the Earth's biomes and sustains life. All life, from single-celled microbes to blue whales, exists in a continuous process of consuming, using, and storing energy [1]. In general, energy is the ability of a system to cause exterior impacts, for instance a force across a distance. Input or output of work changes the energy content of a body. Energy exists in many different forms such as:

- Mechanical energy
- Potential energy
- Kinetic energy
- Thermal energy
- Magnetic energy
- Electrical energy
- Radiation energy
- Nuclear energy
- Chemical energy [2].

According to the degree of conversion, energy carriers are classified as primary or secondary energy carriers and as final energy carriers (Fig. 1). Primary energy carriers are substances which have not yet undergone any technical conversion, whereby the term primary energy refers to the energy content of the primary energy carriers and the primary energy flows. Secondary energy carriers are energy carriers that are produced from primary or other secondary energy carriers, either directly or by one or several technical conversion processes (e.g. gasoline, heating oil, rape oil, electrical energy), whereby the term secondary energy refers to the energy content of the secondary energy carrier and the corresponding energy flow. Final energy carrier and final energy respectively are energy streams directly consumed by the final user (e.g. light fuel oil inside the oil tank of the house owner, wood chips in front of the combustion oven, district heating at the building substation). Useful energy refers to the energy available to the consumer after the last conversion step to satisfy the respective requirements or energy demands (e.g. space heating, food preparation, information, transportation) [3,4].

Worldwide energy consumption has been increasing rapidly, in fact almost exponentially, since the industrial revolution. Industrialization of developing nations and the population increase in the world. At present, most of the energy requirement worldwide is met by the combustion of fossil fuels (i.e., coal, petroleum oils, natural gas, etc.), which have become an essential and integral part of modern civilization, being increasingly relied upon since the industrial revolution. Only a very small proportion of the energy comes from nuclear and hydro power, and a much smaller portion from renewable energy sources, such as solar, wind, hydro, geothermal, tidal wave, and so on [5]. Basically all the forms of energy in the world as we know it are solar in origin. The greatest advantage of solar energy as compared with other forms of energy is that it is clean and can be supplied without environmental pollution. Over the past century, fossil fuels provided most of our energy, because these were much cheaper and more convenient than energy from alternative energy sources, and until recently, environmental pollution has been of little concern [6].

Solar air heater is one of the basic equipment through which solar energy is converted into thermal energy. The main applications of solar air heater are space heating, seasoning of timber, curing of industrial products and these can also be effectively used for curing/drying of concrete/clay building components. A solar air heater is simple in design and requires little maintenance. However, the value of the heat transfer coefficient between the absorber plate and air is low and this results in a lower thermal efficiency. The thermal efficiency of solar air heater is low because of low value of convective heat transfer coefficient between the flowing air and absorber plate (heat transferring surface) due to the formation of thin laminar viscous sub-layer on its absorber plate. The efficiency of solar air heater can be improved by modifying the boundary layer developed on the heated surface. One of the well-known methods of modifying the boundary layer is to break the laminar viscous sub-layer formed on the heat transfer surface by creating artificial roughness in the form of repeated ribs, grooves or combination of ribs and grooves. The artificially roughened surface has wide application namely in cooling of gas turbine blades, nuclear reactors, solar air heating systems etc. The artificial roughness breaks the laminar viscous sub-layer and create local wall turbulence due to the flow separation and flow reattachment between the consecutive ribs, which reduces the thermal resistance, increases heat transfer and thereby efficiency. The application of artificial roughness enhances the heat transfer at the cost of increased value of friction factor and power penalty. The efforts of the researchers are always directed towards the proper selection of the shape and arrangement of the artificial roughness, which modifies the boundary layer, enhances the heat transfer coefficient with minimum pressure drop i.e. power penalty [7]. Hence, it is necessary to review different types of artificial roughness used on the heat transferring surface to study effect of roughness on the heat transfer coefficient (Nusselt number) and friction factor.

Numbers of experimental investigations involving roughness elements of different shapes, sizes and orientations with respect to flow direction have been carried out in order to obtain an optimum arrangement of roughness element geometry. The objective of present article is to review various types of artificial roughness geometries used and tested experimentally in solar air heater for performance enhancement by various investigators and provides critical analysis of data on heat transfer and friction characteristics of roughened surface to facilitate designers and investigators to make best use of it in future.

This paper is divided into eleven sections some of which are further divided into various subsections. Current section deals with the brief introduction and structure of this article. Section 2 deals with the basic of conventional solar air heater and its classification. Section 3 deals with the various heat transfer enhancement techniques for solar air heater. Section 4 deals with the concept of artificial roughness and its application in the areas of cooling of gas turbine, electronic equipment, nuclear reactors, and compact heat exchangers etc. investigated by various investigators. Section 5 deals with the use of artificial roughness in the solar air heater for heat transfer enhancement and also presents a brief discussion of various roughness parameters. Section 6 deals with the methods of testing to determine the thermal performance of a conventional solar air heater. In Section 7, results of 38 experimental investigations of the effect of geometrical/operating parameters of various roughness geometries on heat transfer and fluid flow characteristics in a solar air heater have been reported.

Nomenclature

A_a	gross collector aperture area, mm^2
A_c	surface area of absorber plate, mm^2
A_f	frontal area, mm^2
D	equivalent or hydraulic diameter of duct, mm
d	print diameter of dimple/protrusion or geometric parameter of broken rib, mm
e	rib height, mm
g	groove position/width of gap, mm
H	depth of duct, mm
H	heat transfer coefficient, W/m^2 K
I	intensity of solar radiation, W/m^2
k	thermal conductivity of air, W/m K
L	length of test section of duct or long way length of mesh, mm
m	mass flow rate, kg/s
P	pitch, mm
Q_l	heat loss from collector, W
Q_t	heat loss from top of collector, W
q_u	useful heat flux, W/m^2
Q_u	useful heat gain, W
S	length of discrete rib or shortway length of mesh, mm
T_a	ambient temperature, K
T_{am}	mean air temperature, K
T_i	fluid inlet temperature, K
T_o	fluid outlet temperature, K
T_{pm}	mean plate temperature, K
U_L	overall heat loss coefficient, W/m^2 K
v	velocity of air in the duct, m/s
W	width of duct, mm
w	width of rib, mm
ΔP	pressure drop, Pa

Dimensionless parameters

B/S	relative roughness length
d/w	relative gap position
e/D	relative roughness height
e/H	rib to channel height ratio
$e+$	roughness Reynolds number
f	friction factor
F'	collector efficiency factor
F_R	collector heat-removal factor
f_r	friction factor for rough surface
f_s	friction coefficient of smooth surface
$G(e^+)$	heat transfer roughness function
g/e	relative gap width
g/p	relative groove position
G_d/L_v	relative gap distance
L/D	test length to hydraulic diameter ratio of duct
L/e	relative logway length of mesh
l/s	relative length of grit
Nu	Nusselt number
Nu_r	Nusselt number for rough channel
Nu_s	Nusselt number for smooth channel
P/e	relative roughness pitch
P'/P	relative roughness staggering ratio
Pr	Prandtl number
$R(e^+)$	friction roughness function
Re	Reynolds number
S/e	relative short way length of mesh
S'/S	relative roughness segment ratio
St	Stanton number
W/H	duct aspect ratio
W/w	relative roughness width

Greek symbols

$(\tau\alpha)_e$	effective transmittance-absorptance product
ϕ	wedge angle/chamfer angle, degree
α	angle of attack, deg.
δ	transition sub-layer thickness, mm
ε	dissipation rate, m^2/s^3
η_{th}	thermal efficiency
μ	dynamic viscosity, Ns/m^2
ρ	density of air, kg/m^3
ω	specific dissipation rate, 1/s

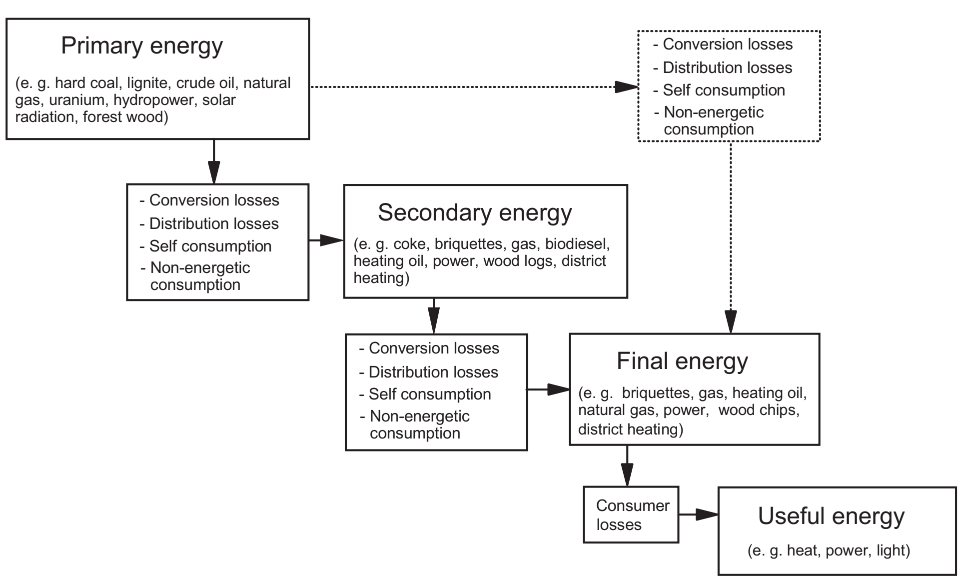


Fig. 1. Energy conversion chain [3].

Section 8 deals with the effect of important roughness parameters on heat transfer performance of a solar air heater and also presents the correlations developed by various researchers. Section 9 deals with the design considerations/strategy for an artificially roughened solar air heater. A comparative study is carried out to select best roughness geometry for heat transfer enhancement using MATLAB-7.6.0.324 in Section 10 and finally the paper is concluded with future scope in Section 11.

2. Solar air heater and its classification

A conventional solar air heater consists of an absorber plate, about 1–3 mm thickness is usually made up of aluminum, GI or steel, with a parallel plate below forming a passage of high aspect ratio through which the air is to be heated and flows (Fig. 2). A transparent glass cover of thickness 4–5 cm is provided above the absorber plate, while a sheet metal container filled with insulation is provided on the bottom and sides. Flat plate solar air heaters are almost always mounted in stationary position with an optimum tilt to horizontal and normally facing the equator (south in northern hemisphere). Fig. 3 shows the classification of solar air heater on the basis of energy storage, numbers of covers, extended surface and their tracking axis [8]. Design and construction details of a conventional smooth solar air heater systems are described by Garg and Prakash [9] Duffie and Beckman [10] and Khan [11].

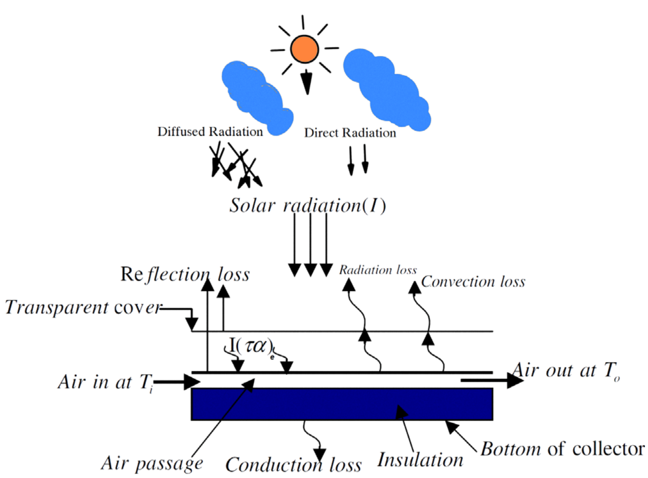


Fig. 2. Conventional solar air heater [9,10].

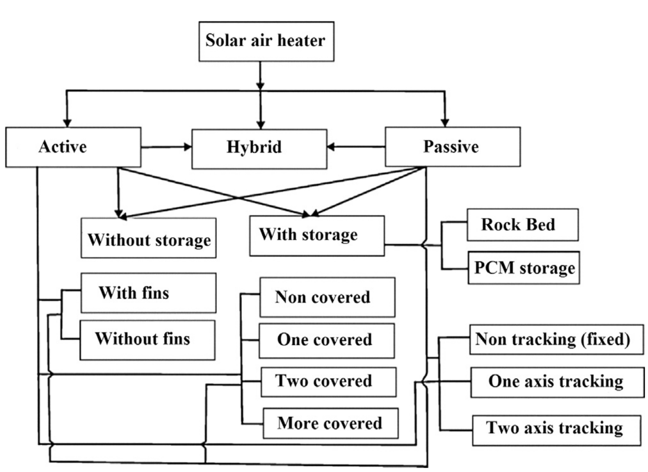


Fig. 3. Classification of solar air heater [8].

Table 1
Classification of enhancement methods [14].

Category	Technique
Surface methods	Roughened surfaces Extended surfaces Corrugated surfaces Perforated surfaces Swirl-flow devices Surface vibrations Surface rotation
Fluid methods	Fluid vibration Fluid additives Electrostatic fluids
Compound methods	Vibration/roughened Perforations/corrugations Roughened/rotation

Nusselt number and friction factor for conventional solar air heater can be obtained by Dittus–Boelter [12] and Blasius equation [13] respectively.

3. Heat transfer enhancement techniques

Various heat transfer enhancement techniques have been employed to improve the performance of a solar air heater. Constantinos [14] classified the enhancement techniques as fluid, surface and compound enhancement techniques as shown in Table 1. The thermal performance of conventional solar air heaters has been found to be poor because of the low convective heat transfer coefficient from the absorber plate to the air. The heat transfer between the absorber surface (heat transfering surface) of solar air heater and flowing air can be improved by either increasing the heat transfering surface area using extended and corrugated surfaces without enhancing heat transfer coefficient or by increasing heat transfer coefficient using the turbulence promoters in the form of artificial roughness on absorber surface. The roughness, on the absorber plate can be provided by several methods such as sand blasting, machining, casting, forming, welding ribs and or fixing thin circular wires. The use of artificial roughness in different forms and shapes is the most effective and economic way of improving the performance of a solar air heater. A lot of experimental investigations involving roughness elements of different shapes, sizes and orientations with respect to flow direction have been carried out in order to obtain an optimum arrangement of roughness element geometry.

4. Concept of artificial roughness for heat transfer enhancement

It is well known that in a turbulent flow a laminar/viscous sub-layer exists in addition to the turbulent core. The artificial roughness on heat transfer surface breaks up the laminar boundary layer of turbulent flow and makes the flow turbulent adjacent to the wall. The artificial roughness that results in the desirable increase in the heat transfer also results in an undesirable increase in the pressure drop due to the increased friction; thus the design of the flow duct and absorber surface of duct should, therefore, be executed with the objectives of high heat transfer rates and low friction losses. It is therefore desirable that the turbulence must be created only in the region very close to the heat transferring surface i.e. in the viscous sub-layer only where the heat transfer takes place and the core flow should not be unduly disturbed so as to avoid excessive friction losses. This can be done by keeping the

height of the roughness elements to be small in comparison with the duct dimensions. Artificial roughness can be produced on a surface by the following ways:

(1) Blasting sand over the heat transferring surface.
(2) Fixing grooves and ridges.
(3) Fixing wires.
(4) Fixing three dimensional roughness geometries.
(5) Fixing ribs of different geometry such as round, rectangular or V-shaped or broken ribs.

The concept of artificial roughness was first applied by Joule [15] to enhance heat transfer coefficients for in-tube condensation of steam and since then many experimental investigations were carried out on the application of artificial roughness in the areas of cooling of gas turbine, electronic equipments, nuclear reactors, and compact heat exchangers etc. Investigators have modeled the shape of internal cooling passage of gas turbine as a rectangular channel with two opposite rough walls and two smooth walls. Several types of surface roughness have been used; they may be broadly classified as regular geometric roughness and irregular roughness. Irregular surface roughness can be produced by sand blasting the surface. Regular surface roughness is of many types in the form of cavities and ribs depending on the shape, arrangement and orientation of roughness elements on the heated plate.

An early study of the effect of roughness on friction factor and velocity distribution was performed by Nikuradse [16], who conducted a series of experiments with pipes roughened by sand grains. Based on law of the wall similarity, author developed friction correlations in terms of roughness function R and roughness Reynolds number e^+. These correlations were presented as

$$R = \sqrt{(2/f)} + 2.5\ \ln(2e/D) + E \tag{1}$$

and

$$e^+ = \sqrt{(f/2)}Re(2e/D) \tag{2}$$

The constant E in Eq. (1) was a geometric parameter dependent on the duct geometry. For pipes, author reported a value of this parameter as 3.75. For the fully rough region, author reported a constant value of 8.48 for the roughness function R.

Nikuradse found the following three flow regimes:

(1) Hydraulically smooth flow regime ($0 < e^+ \le 5$)
(2) Transitionally rough flow regime ($5 < e^+ \le 70$)
(3) Fully rough flow regime ($e^+ > 70$)

In hydraulically smooth flow regime, the friction factor is the same for the rough and smooth pipes, because the projections of the roughness elements lie entirely within the laminar sub-layer i.e. roughness has no effect on the friction factor. In transitionally rough flow regime, the projections of the roughness elements are of the same order of the thickness of the laminar sub-layer. In fully rough flow regime, the roughness function is found to be independent of the roughness Reynolds number and it attains a constant value. The projections of the roughness elements extend beyond the laminar sub-layer as the thickness of boundary layer becomes small in comparison to the roughness height.

Nunner [17] was the first who developed a flow model and likened this model to the temperature profile in smooth tube flow at increased Prandtl number. The proposed flow model predicts that roughness reduces the thermal resistance of the turbulence dominated wall region without significantly affecting the viscous region. The argument was quantified by using the Prandtl analogy and replacing Pr by $(f/f_s)Pr$. This model predicts that value of St/St_s decreases with increase in Prandtl number. The proposed flow model also predicts that St/St_s, is independent of the roughness type.

Dipprey and Sabersky [18] developed a heat momentum transfer analogy for flow in a sand-grain-roughened tube assuming that the law of wall similarity applies to both the temperature and velocity profiles. For the fully rough flow ($e^+ > 70$) authors found that the heat transfer function was a function of only two variables: roughness Reynolds number (e^+) and Prandtl number (Pr). Authors developed heat and momentum transfer analogy for flow in tubes having sand grain roughness which have been presented as

$$G(e^+,\ Pr) = [f/2S_t - 1](f/2)^{-0.5} + R(e^+) \tag{3}$$

Webb et al. [19] used the law of wall similarity employed by Nikuradse and heat transfer momentum transfer analogy extended by Dipprey and Sabersky to correlate data for tubes with rectangular transverse repeated rib roughness with $0.01 < e/D < 0.04$ and $10 < P/e < 40$. In the fully rough region the Stanton number and friction factor correlations have been presented as

$$St = \frac{f/2}{1 + \sqrt{(f/2)[4.5(e^+)^{0.28}\ Pr^{0.57} - 0.95(P/e)^{0.53}]}} \tag{4}$$

and

$$\sqrt{2/f} = 2.5in\left(\frac{D}{2e}\right) - 3.75 + 0.95(P/e)^{0.53} \tag{5}$$

Sheriff and Gumley [20] experimentally investigated the optimum roughness Reynolds number (e^+_{opt}) as 35. Kays [21] suggested that by fixing small diameter protrusion wires perpendicular to flow direction on surface of absorber plate may help to break laminar sub-layer.

Lewis [22] defined a new efficiency parameter for optimizing thermo-hydraulic performance of roughened surfaces with respect to smooth surfaces. Author presented the various parameters which control the momentum and heat transfer performance of a rough surface in a uniform channel flow in a novel way.

Han et al. [23] experimentally investigated the effects of rib shape, angle of attack and pitch-to-rib height ratio on friction factor and heat transfer coefficient. Author reported that ribs with 45° inclinations produced better heat transfer performance than ribs with 90° orientations, when compared at the same friction power.

An experimental study of fully developed turbulent air flow in square ducts with two opposite rib-roughened walls was performed by Han [24], to determine the effects of the rib pitch-to-height and rib height-to-equivalent diameter ratios on friction factor and heat transfer coefficients with Reynolds number varied between 7000 and 90,000. Based on the four-sided, smooth-duct correlation and the four-sided, ribbed-duct similarity law, a general prediction method for average friction factor and average Stanton number in rectangular ducts with two smooth and two opposite ribbed walls was developed. There was good agreement between prediction and measurements.

Han et al. [25] carried out experiments to determine the effect of rib angle of attack on the average heat transfer coefficients and pressure drop in the fully developed turbulent air flow in a square channel with two opposite rib-roughened walls for Reynolds number varied from 7000 to 90,000. The rib height-to-equivalent diameter ratio was kept at a constant value of 0.063, the rib pitch-to-height ratio was varied from 10 to 20, and the rib angle of attack was varied from 90° to 60° to 45° to 30°, respectively. The thermal performance comparison indicated that the increased heat conductance for the rib with an oblique angle to the flow (α=45–30°) was about 10–20% higher than the rib with a

90° angle to the flow, and the pumping power requirement for the angled rib was about 20–50% lower than the transverse rib. Semi-empirical correlations for friction factor and heat transfer coefficients were developed to account for rib spacing and rib angle.

Han [26] investigated the effect of the channel aspect ratio on the distribution of the local heat transfer coefficient in rectangular channels with two opposite ribbed walls for a Reynolds number range of 10,000 to 60,000. The channel width-to-height ratios (W/H, ribs on side W) were 1/4, 1/2, 1, 2, and 4. The test channels were heated by passing current through thin, stainless steel foils instrumented with thermocouples. The local heat transfer coefficients on the ribbed side wall and on the smooth side wall of each test channel from the channel entrance to the fully developed regions were measured for two rib spacing ($P/e=10$ and 20). The rib angle-of-attack was kept at 90°. The local data in the fully developed region were averaged and correlated, based on the heat transfer and friction similarity laws developed for ribbed channels, to cover the ranges of channel aspect ratio, rib spacing, rib height, and Reynolds number.

Han and Park [27] carried out experiments to determine the combined effects of the rib angle of attack and the channel aspect ratio on the distributions of the local heat transfer coefficient for developing flow in short rectangular channels ($L/D=10$ and 15) with a pair of opposite rib-roughened walls for Reynolds numbers from 10,000 to 60,000. The rib angle of attack was varied from 90° to 60°, to 45°, and to 30°, whereas the corresponding channel width-to-height ratio was varied from 1 to 2 and to 4, respectively. Semi-empirical heat transfer and friction correlations were obtained to account for rib angle, rib spacing, channel aspect ratio, rib height and Reynolds number.

Han et al. [28] carried out experiments to determine the effects of the rib angle of attack on the distributions of the local heat transfer coefficient and on the friction factors in short rectangular channels of narrow aspect ratios with a pair of opposite rib-roughened walls for Reynolds numbers from 10,000 to 60,000. The channel width-to-height ratios were 2/4 and 1/4; the corresponding rib angles of attack were 90°, 60°, 45°, and 30°, respectively. The results indicated that the narrow-aspect-ratio channels gave better heat transfer performance than the wide-aspect-ratio channels for a constant pumping power. Semi-empirical friction and heat transfer correlations were developed.

Han et al. [29] investigated the effect of the rib angle orientation on the local heat transfer distributions and pressure drop in a square channel with two opposite in-line ribbed walls for Reynolds numbers from 15,000 to 90,000. The square channel composed of ten isolated copper sections had a length to hydraulic diameter ratio of 20; the rib height to hydraulic diameter ratio was 0.0625; the rib pitch-to-height ratio was 10. Nine rib configurations were studied: 90° rib, 60° and 45° parallel ribs, 60° and 45° crossed ribs, 60° and 45° V-shaped ribs, and 60° and 45°-shaped ribs. The results showed that the 60° (or 45°) V-shaped rib performed better than the 60° (or 45°) parallel rib and, subsequently, better than the 60 ° (or 45°) crossed rib and the 90° rib. The V-shaped rib produced the highest heat transfer augmentation, while the -shaped rib generated the greatest pressure drop. The crossed rib had the lowest heat transfer enhancement and the smallest pressure drop penalty.

Han and Zhang [30] investigated the effect of the broken rib orientation on the local heat transfer distributions and pressure drop in a square channel with two opposite in-line ribbed walls for Reynolds numbers from 15,000 to 90,000. The square channel was composed of ten isolated copper sections and had a length to hydraulic diameter ratio of 20. The rib height to hydraulic diameter ratio was 0.0625, and the rib pitch to height ratio was 10. The results showed that the 60° parallel broken rib or 60° V-shaped broken rib provided a higher heat transfer augmentation than the 45° parallel broken rib or 45° V-shaped broken rib and, subsequently, higher than the 90° broken rib. The parallel broken rib or V-shaped broken rib had 2.5–4 times heat transfer augmentation compared with the previous parallel continuous rib or V-shaped continuous rib with 2–3 times heat transfer augmentation for the same amount of 7–8 times pressure drop penalty.

Han et al. [31] investigated the effect of wall heat flux ratio on the local heat transfer augmentation in a square channel with two opposite in-line ribbed walls for Reynolds numbers from 15,000 to 80,000. The square channel composed of ten isolated copper sections had a length-to-hydraulic diameter ratio (L/D) of 20. The rib height-to-hydraulic diameter ratio (e/D) was 0.0625 and the rib pitch to height ratio (P/e) was 10. Six ribbed side to smooth side wall heat flux ratios were studied for four rib orientations (90° rib, 60° parallel rib, 60° crossed rib, and 60° v-shaped rib). The results showed that the ribbed side wall heat transfer augmentation increased with increasing ribbed side to smooth side wall heat flux ratios, but the reverse was true for the smooth side wall heat transfer augmentation. The average heat transfer augmentation of the ribbed side and smooth side wall decreased slightly with increasing wall heat flux ratios. Two ribbed side wall heating provided a higher ribbed side wall heat transfer augmentation than the four-wall uniform heating. The effect of wall heat flux ratio reduced with increasing Reynolds numbers. The results indicated that the 60° V-shaped rib and 60° parallel rib perform better than the 60° crossed rib and 90° rib, regardless of wall heat flux ratio and Reynolds number.

Park et al. [32] presented the results of heat transfer and friction factor data measured in five short rectangular channels with turbulence promoters. Author investigated the combined effects of the channel aspect ratio, rib angle of attack, and flow Reynolds number on heat transfer and pressure drop in rectangular channels with two opposite ribbed walls. The channel aspect ratio (width to height, W/H, ribs on side W) varied from 1/4 to 1/2, to 1, 2 and 4, while the corresponding rib angles of attack were 90°, 60°, 45°, and 30°, respectively. The Reynolds number range was 10,000–60,000. The results suggested that the narrow aspect ratio channels ($W/H<1$) gave much better heat transfer performance than the wide aspect ratio channels ($W/H>1$). For the square channel ($W/H=1$), the 60°/45°angled ribs provided the best heat transfer performance. For the narrow aspect ratio channel ($W/H=1/4$ or 1/2), the 45°/60°angled ribs were recommended while the 30°/45°angled ribs were better for wide aspect ratio channels ($W/H=4$ or 2).

Chandra et al. [33] carried out an experimental study of surface heat transfer and friction characteristics of a fully developed turbulent air flow in a square channel with transverse ribs on one, two, three, and four walls. Tests were performed for Reynolds numbers ranging from 10,000 to 80,000. The pitch to rib height ratio, P/e, was kept at 8 and rib height to channel hydraulic diameter ratio, e/D was kept at 0.0625. The channel length to hydraulic diameter ratio, L/D, was 20. The heat transfer coefficient and friction factor results were enhanced with the increase in the number of ribbed walls. The friction roughness function, $R(e+)$, was almost constant over the entire range of tests performed and was within comparable limits of the previously published data. The heat transfer roughness function, $G(e+)$, increased with roughness Reynolds number and compared well with previous work in this area. Both correlations could be used to predict the friction factor and heat transfer coefficient in a rectangular channel with varying number of ribbed walls. The results of could be used in various applications of turbulent internal channel flows involving different number of rib roughened walls.

Lau et al. [34] carried out experiments to study the turbulent heat transfer and friction for fully developed flow of air in a square channel with discrete rib turbulators. The discrete ribs were

staggered on two opposite walls of the channel in alternate rows of three and two ribs. Nine rib configurations were examined: transverse ribs with an angle of attack (α) of 90°, discrete ribs with $\alpha = 90°$, parallel arrays of discrete ribs with $\alpha = 45°$ and $-45°$ on alternate rows, and parallel and crossed arrays of discrete ribs with $\alpha = 60°$, 45°, and 30°. The rib height to hydraulic diameter ratio and the rib pitch to height ratio were 0.0625 and 10, respectively. The Reynolds number ranges from 10,000 to 80,000. Results showed that the average Stanton number in the 90° discrete rib case was about 10–15% higher than that in the 90° transverse rib case. Turning the discrete ribs on the opposite walls 60°, 45°, or 30° in the same direction with respect to the main flow increased the average Stanton number 10–20% over that in the 90° discrete rib case. Parallel oblique discrete ribs with $\alpha = 60°$, 45°, and 30° had comparable performances and had higher overall heat transfer per unit pumping power than 90° discrete ribs. Crossed oblique discrete ribs performed poorly compared with 90° discrete ribs and were not recommended.

Lau et al. [35] carried out experiments to study the turbulent heat transfer and friction for fully developed flow of air in a square channel in which two opposite walls were roughened with 90° full ribs, parallel and crossed full ribs with angles of attack of 60° and 45°, 90° discrete ribs, and parallel and crossed discrete ribs with angles of attack of 60°, 45°, and 30°. The discrete ribs were staggered in alternate rows of three and two ribs. Results were obtained for a rib height to channel hydraulic diameter ratio of 0.0625, a rib pitch to height ratio of 10, and Reynolds numbers between 10,000 and 80,000. Parallel angled discrete ribs were superior to 90° discrete ribs and parallel angled full ribs, and were recommended for internal cooling passages in gas turbine airfoils. For angles of attack of 60° and 45°, parallel discrete ribs had higher ribbed wall heat transfer, lower smooth wall heat transfer, and lower channel pressure drop than parallel full ribs. Parallel 60° discrete ribs had the highest ribbed wall heat transfer and parallel 30° discrete ribs caused the lowest pressure drop. The heat transfer and pressure drops in crossed angled full and discrete rib cases were all lower than those in the corresponding 90° and parallel angled rib cases. Crossed arrays of angled ribs had poor thermal performance and were not recommended.

Zhang et al. [36] investigated the effect of compound turbulators on friction factors and heat transfer coefficients in rectangular channels with two opposite ribbed-grooved walls for a Reynolds number range of 10,000 to 50,000. The channel width-to-height ratio was 10. The fully developed heat transfer coefficients and friction factors on the ribbed-grooved and smooth side walls of each test channel were measured for six rib-groove spacings ($P/e = 8$, 10, 15, 20, 25, and 30). The fully developed friction and heat transfer in similar aspect ratio rectangular channels with two opposite ribbed walls with two rib spacings ($P/e = 8.5$ and 11.5) was also measured for comparison. The results showed that the

Table 2
Different types of artificial roughness geometries and important dimensionless parameters.

S. no.	Investigators	Rib geometry	Important dimensionless parameters
1	Prasad and Mullick [37]	Transverse wire rib roughness	e/D, P/e
2	Gupta et al. [54]	Inclined continuous rib roughness	e/D, P/e, α, W/H,
3	Saini and Saini [55]	Expanded metal mesh roughness	e/D, α, L/e, S/e
4	Muluwork [56]	Staggered discrete V-shaped rib roughness	e/D, α, B/S, P'/P, S'/S
5	Karwa et al. [57]	Chamfered rib roughness	e/D, P/e, α, W/H, ϕ, L/D
6	Verma and Prasad [58]	Transverse wire rib roughness	e/D, P/e
7	Karwa et al. [59]	Chamfered rib roughness	e/D, P/e, α, W/H, ϕ
8	Momin et al. [60]	V-shaped rib roughness	e/D, P/e, α
9	Bhagoria et al. [61]	Transverse wedge shaped rib roughness	e/D, P/e, W/H, ϕ
10	Karwa [62]	Transverse, inclined, V-up continuous, V-down continuous, V-up discrete and V-down discrete rib roughness	e/D, P/e, α, W/H, ϕ, B/S
11	Sahu and Bhagoria [63]	90° broken transverse rib roughness	e/D, P/e, W/H
12	Jaurker et al. [64]	Rib-grooved roughness	e/D, P/e,
13	Layek et al. [65]	Chamfered rib-grooved roughness	e/D, P/e, g/p, ϕ
14	Karmare and Tikekar [66]	Metal grit rib roughness	e/D, P/e, l/s
15	Saini and Saini [67]	Arc shaped rib roughness	e/D, P/e, α,W/H
16	Aharwal et al. [68]	Inclined continuous rib roughness with gap	e/D, P/e, α,W/H, d/W, g/e
17	Saini and Verma [69]	Dimple-shaped rib roughness	e/D, P/e
18	Varun et al. [70]	Combination of transverse and inclined rib roughness	e/D, P/e, W/H
19	Layek et al. [71]	Chamfered rib-grooved roughness	e/D, P/e, g/p, ϕ
20	Karmare and Tikekar [72]	Metal grit rib roughness	e/D, P/e, l/s
21	Aharwal et al. [73]	Inclined continuous rib roughness with gap	e/D, P/e, α, W/H, d/W, g/e
22	Bopche and Tandale [74]	Inverted U-shaped turbulators	e/D, P/e, α,W/H
23	Kumar et al. [75]	Discrete W-shaped rib roughness	e/D, P/e, α,W/H
24	Varun et al. [76]	Combination of transverse and inclined rib roughness	e/D, P/e, W/H
25	Mittal and Varun [77]	Combination of transverse and inclined rib roughness	e/D, P/e, W/H
26	Hans et al. [78]	Multi V-shaped rib roughness	e/D, P/e, α,W/w
27	Lanjewar et al. [79]	W-shaped rib roughness	e/D, P/e, α,W/H
28	Singh et al. [80]	Discrete V-down rib roughness	e/D, P/e, α, d/w, g/e
29	Lanjewar et al. [81]	W-shaped rib roughness	e/D, P/e, α,W/H
30	Tanda [82]	Angled continuous ribs, transverse continuous & broken ribs, and discrete V-shaped ribs roughness	e/D, P/e, α,W/H
31	Sethi et al. [83]	Dimple shaped elements arranged in angular fashion (arc)	e/D, P/e, α,W/H, e/d
32	Kumar et al. [84]	Multi V-shaped rib roughness with gap	e/D, P/e, α, W/H, G_d/L_v, g/e, W/w
33	Singh et al. [85]	Discrete V-down rib roughness	e/D, P/e, α,W/H
34	Yadav et al. [86]	Circular protrusions arranged in angular arc shape	e/D, P/e, α,W/H, e/d
35	Bharadwaj et al. [87]	Inclined continuous rib roughness	e/D, P/e, α, W/H,
36	Kumar et al. [88]	Multi V-shaped rib roughness with gap	e/D, P/e, α, W/H, G_d/L_v, g/e, W/w
37	Prasad [89]	Transverse wire rib roughness	e/D, P/e
38	Karwa and Chitoshiya [90]	60° V-down discrete rib roughness	e/D, P/e, α, B/S

heat transfer performance of the rib-groove roughened duct was much better than the rib roughened duct. The rib-groove roughened wall enhanced the heat transfer 3.4 times and paid 6 times the pressure drop penalty, whereas the rib roughened wall, with similar rib height and rib spacing, enhanced the heat transfer 2.4 times and paid about the same pressure drop penalty. Semi-empirical friction and heat transfer correlations were developed. Flow measurements showed that the roughened ducts had flatter velocity profiles than the smooth duct and rib-groove roughened duct produced higher turbulence intensity than the rib roughened duct. The flatter velocity profile and higher turbulence intensity were responsible for producing higher heat transfer.

Afterwards several investigators have attempted to design an artificially roughened duct which can enhance convective heat transfer with minimum pumping losses with two or four roughened surfaces. Several roughness geometries have been tested experimentally and simulated numerically so far with the aim to obtain maximum heat transfer enhancement with consumption of least pumping power.

5. Use of artificial roughness in solar air heater for heat transfer enhancement

A comprehensive review of literature in the previous section shows that several investigators have attempted to design an artificially roughened duct, which can enhance convective heat transfer with minimum pumping power with two or four roughened surfaces. These investigators studied the effect of geometric parameters of roughness elements and flow parameters on heat transfer and friction factor in gas turbine cooling and heat exchanger applications. But geometric and operating parameters relevant to solar air heater are different from the above mentioned applications. However the similar geometries can be used for the lower range of Reynolds number for solar air heater applications. Keeping this in view several investigators investigated various geometries of artificial roughness in solar air heater ducts in order to obtain an optimum thermo-hydraulic performance.

It has been found that the value of the heat transfer coefficient between the absorber plate and air is low and this result in a lower efficiency. To increase the heat transfer in the case of solar air heaters, the roughness elements have to be considered only on one wall which receives the solar radiation. Therefore, the solar air heaters are modeled as a rectangular duct having one rough wall and three smooth walls. This makes the fluid flow and heat transfer characteristics distinctly different from those found in the case of duct with two and four opposite roughened walls, roughened annular and circular tubes. Further the range of Reynolds number applicable in solar air heaters are of lower range in comparison of the studies discussed above. The flow Reynolds number in solar air heaters ranges as $3800 < Re < 18000$.

Prasad and Mullick [37] were the first who introduced the application of artificial roughness in the form of small diameter wire attached on the underside of absorber plate to improve the thermal performance of solar air heater for drying purposes. After Prasad and Mullick's work a numbers of experimental investigations [37,54–90] and computational simulation [38–52] of solar air heater involving roughness elements of different shapes, sizes and orientations with respect to flow direction have been carried out in order to obtain an optimum arrangement of roughness element geometry.

The roughness elements can be two-dimensional ribs or three dimensional discrete elements, transverse or inclined ribs or V-shaped continuous or broken ribs with or without gap. The roughness elements can also be arc-shaped wire or dimple or cavity or compound rib-grooved. The common shape of ribs is square but different shapes like circular, semi-circular and chamfered have also been considered to investigate thermohydraulic performance of solar air heater.

The key dimensionless geometrical parameters that are used to characterize artificial roughness are:

(1) *Relative roughness pitch* (P/e): Relative roughness pitch (P/e) is defined as the ratio of distance between two consecutive ribs and height of the rib.
(2) *Relative roughness height* (e/D): Relative roughness height (e/D) is the ratio of rib height to equivalent diameter of the air passage.
(3) *Angle of attack* (α): Angle of attack is inclination of rib with direction of air flow in duct.

Table 2 shows the different types of artificial roughness geometries and important dimensionless parameters, investigated experimentally by various investigators that characterized the geometry and substantially influence the performance of a solar air heater.

6. Method of testing to determine the thermal performance of a conventional solar air heater

The thermal performance of a conventional solar collector can be determined by the detailed analysis of the optical and thermal characteristics of the collector materials and collector design or by experimental performance testing under control conditions. It should be noted that the accuracy of the heat transfer analysis depends on uncertainties in the determination of the heat transfer coefficients, which is difficult to achieve, due to the non-uniform temperature boundary conditions that exist in solar collector. Such analysis is usually carried out during the development of prototypes, which are then tested under defined environmental conditions. In general experimental verification of the collector characteristics is necessary and should be done on all collector models manufactured.

A number of standards describe the testing procedures for the thermal performance of solar collectors. The most well-known is ASHRAE Standard 93:2003 [53]. This can be used to evaluate the performance of both flat-plate and concentrating solar collectors. The thermal performance of a solar collector is deter-mined partly by obtaining values of instantaneous efficiency for different combinations of incident radiation, ambient temperature, and inlet fluid temperature. This requires experimental measurement of the rate of incident solar radiation falling onto the solar collector as well as the rate of energy addition to the transfer fluid as it passes through the collector, all under steady-state or quasi-steady-state conditions. In addition, tests must be performed to determine the transient thermal response characteristics of the collector. The variation of steady-state thermal efficiency with incident angles between the direct beam and the normal to collector aperture at various sun and collector positions is also required.

ASHRAE Standard 93:2003 gives information on testing solar energy collectors using single-phase fluids and no significant internal storage. The data can be used to predict the collector performance in any location and under any weather conditions where load, weather, and insolation are known. This standard contains methods for conducting tests outdoors under natural solar irradiance and for conducting tests indoors under simulated solar irradiance. Solar collectors can be tested by two basic methods: under steady-state conditions or using a dynamic test procedure. For steady-state testing, the environmental conditions and collector operation must be constant during the testing period.

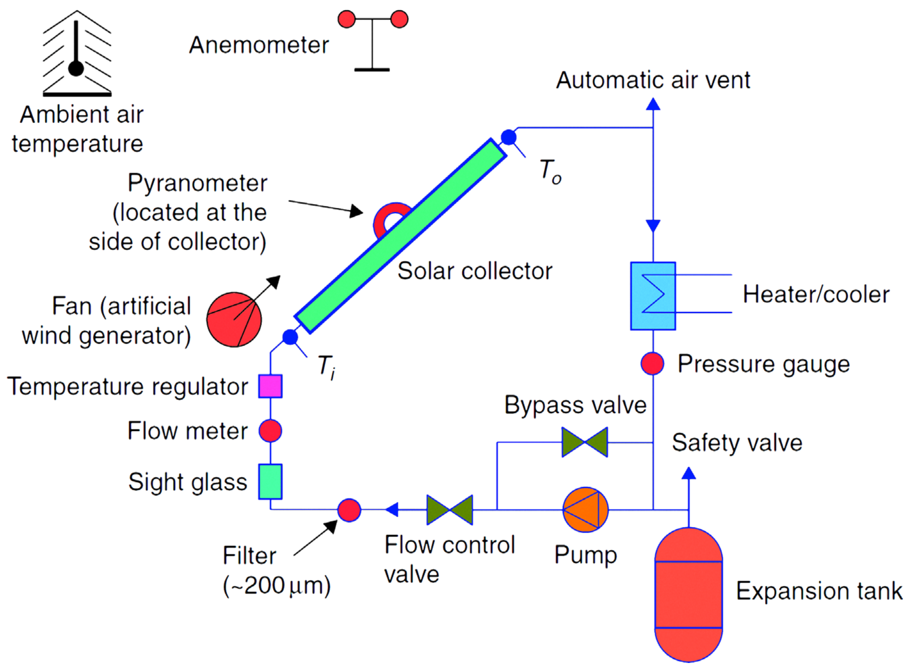


Fig. 4. Closed loop test system [53].

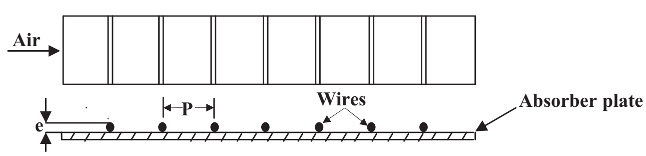


Fig. 5. Roughened absorber plate fixed with transverse continuous wires [37,58,89].

For clear, dry locations, the required steady environmental conditions are easily satisfied and the testing period requires only a few days. In many locations of the world, however, steady conditions may be difficult to achieve and testing may be possible only in certain periods of the year, mainly during summertime, and even then, extended testing periods may be needed. For this reason, transient or dynamic test methods have been developed. Transient testing involves the monitoring of collector performance for a range or radiation and incident angle conditions. Subsequently, a time-dependent mathematical model is used to identify from the transient data the collector performance parameters. An advantage of the transient method is that it can be used to determine a wider range of collector performance parameters than the steady-state method.

To perform the required tests accurately and consistently, a test rig is required as shown in Fig. 4. To evaluate the performance of a solar air heater, following parameters need to be measured:

(1) Global solar irradiance at the collector plane, G_t.
(2) Diffuse solar irradiance at the collector aperture.
(3) Air speed above the collector aperture.
(4) Ambient air temperature, T_a.
(5) Fluid temperature at the collector inlet, T_i.
(6) Fluid temperature at the collector outlet, T_o.
(7) Fluid flow rate, m.

In addition, the gross collector aperture area, A_a, is required to be measured with certain accuracy. The collector efficiency, based on the gross collector aperture area, is given by

$$\eta_{th} = \frac{m\, c_p (T_o - T_i)}{A_a G_t} \qquad (6)$$

7. Experimental investigations of artificially roughened solar air heater for performance enhancement

The thermal efficiency of solar air heaters is found to be low due to low heat transfer coefficient on the air side. Attempts have been made to enhance the heat transfer rate from the absorber plate to air by extending surfaces in the form of fins so that larger surface area could be available for convection to compensate the lower values of heat transfer coefficient. However the augmentation in heat transfer rate is accompanied by severe pressure drop penalty. In another method, heat transfer coefficient has been significantly enhanced by providing artificial roughness on absorber plate surface exposed to air which may be created, either by roughening the surface randomly with a sand grain/sand blasting or by use of regular geometric roughness. As in solar air heater the solar radiation is absorbed by absorber plate, which is the main heat transfer surface; therefore, the solar air heaters are modeled as a rectangular duct having one rough wall and three smooth walls. Different geometries of roughness elements on the underside of absorber plate studied by various investigators are discussed in this section.

Prasad and Mullick [37] introduced the application of artificial roughness in the form of small diameter wire attached on the underside of absorber plate to improve the thermal performance of solar air heater for drying purposes (Fig. 5). Authors utilized artificial roughness in the form of small diameter wires with relative roughness height, relative roughness pitch and wire diameter of 0.019, 12.7 and 0.84 mm respectively. Authors carried out investigations on rib roughened absorber plates of solar air heaters that form a system with only one roughened wall and three smooth walls. Authors used three unglazed collector channels placed side-by-side as shown in Fig. 6. Middle collector channel '*B*' was plane GI sheet, channel '*A*' was plane GI sheet having 24 gauge GI wires soldered in transverse direction on its underside and channel '*C*' was corrugated with wires soldered on the underside of absorber plate in the same way as in second channel. It was reported that protruding wires improved plate efficiency factor from 0.63 to 0.72 resulting in 14% improvement in thermal performance for a Reynolds number of 40,000. The

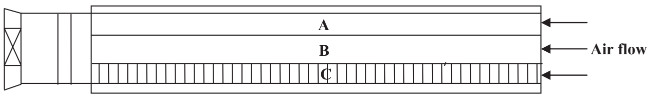


Fig. 6. Three channel portable experimental set-up. A – Galvanized iron corrugated sheet with protruding wires, B – Galvanized iron plane sheet, C – Galvanized iron plane sheet with protruding wires, D – Wooden lumber piece, E – Plywood teak, 5 mm thick, F – Diverging cone, and G – Plenum chamber [37].

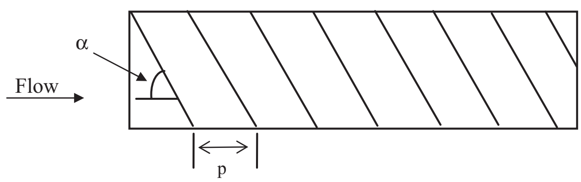


Fig. 7. Inclined continuous rib roughness [54,87].

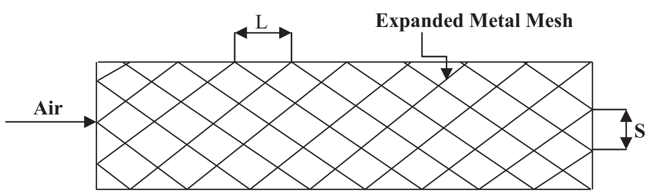


Fig. 8. Expanded metal mesh roughness [55].

agreement of the measured heat transfer coefficients with theoretical predictions was found to be satisfactory.

Gupta et al. [54] carried out an experimental investigation to determine the effect of transverse wire roughness on heat and fluid flow characteristics in transitionally rough flow region ($5 < e^+ < 70$) for rectangular solar air heater ducts with an absorber plate having transverse wire roughness on its underside as shown in Fig. 7. The investigation covered a Reynolds number range of 3000–18,000 for a duct aspect ratio (W/H) of 6.8–11.5; relative roughness height (e/D) of 0.018–0.052 at a relative roughness pitch (P/e) of 10 encompassed a range of roughness Reynolds number between 5 and 70. Simple correlations for a Nusselt number and friction factor were developed in terms of geometrical parameters of roughness, duct cross section, and the flow Reynolds number. It was observed that non-transverse ribs were advantageous when compared with transverse ribs for the enhancement of the heat transfer coefficient. For a roughened solar air heater, maximum enhancement in heat transfer and friction factor was reported to be of the order 1.8 and 2.7 times respectively corresponding to angle of inclination values of 60° and 70°, respectively. Best thermo-hydraulic performance was reported for relative roughness height (e/D) value of 0.023 and Reynolds number (Re) value of 14,000.

Saini and Saini [55] carried out an experimental investigation for fully developed turbulent flow in a rectangular duct with large aspect ratio (11:1) and having expanded metal mesh as artificial roughness to study the effect of wire mesh roughened absorber plate on heat transfer augmentation and friction characteristics of solar air heater as shown in Fig. 8. The investigation considered relative long-way length of mesh (L/e) in range of 25–71.87, relative short-way length of mesh (S/e) in range of 15.62–46.87, relative roughness height (e/D) in range of 0.12–0.039 and Reynolds number (Re) in range of 1900–13,000. It was reported that the maximum heat transfer of order 4 times over the smooth duct was obtained corresponding to angle of attack of 61.9°, relative longway length of mesh (L/e) value of 46.87 and relative shortway length of mesh (S/e) value of 25. Maximum value of friction factor was reported for angle of attack of 72°, relative longway length of mesh (L/e) value of 71.87 and relative shortway length of mesh (S/e) value of 15. Correlations for Nusselt number and friction factor were developed.

Muluwork et al. [56] compared the thermal performance of staggered discrete v-apex up and down ribs with corresponding transverse staggered discrete ribs shown in Fig. 9. They studied the effect of relative roughness length ratio (B/S), relative roughness segment ratio (S'/S), relative roughness staggering ratio (p'/p) and angle of attack (α) on the heat transfer and friction factor. It was observed that the Nusselt number increased with the increase in relative roughness length ratio (B/S). Nusselt number for v-down discrete ribs was found to be higher than the corresponding v-up and transverse discrete roughened surfaces. Nusselt number increased with increase in relative roughness staggering ratio (p'/p) and attained a maximum value for relative roughness staggering ratio (p'/p) value of 0.6. Heat transfer and friction factor attained maximum values for angle of attack (α) 60° and 70°, respectively. Correlations for Nusselt number and friction factor were developed.

Karwa et al. [57] performed an experimental investigation of heat transfer and friction for the flow of air in rectangular ducts with repeated chamfered rib-roughness on one broad wall as shown in Fig. 10. The aspect ratios of the rectangular duct investigated were 4.8, 6.1, 7.75, 9.66, and 12. The roughened wall

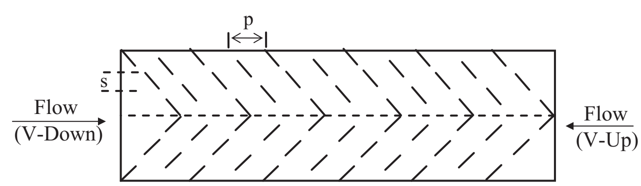


Fig. 9. Staggered discrete V-shaped rib roughness [56].

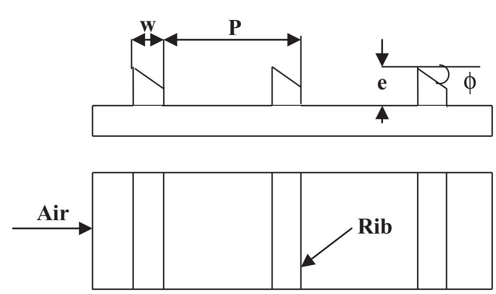


Fig. 10. Chamfered rib roughness [57].

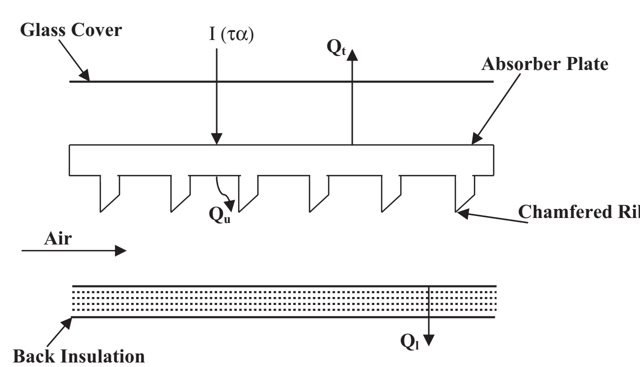


Fig. 11. Solar air heater with Chamfered rib roughened absorber plate [59].

was uniformly heated while the remaining three walls were insulated. These boundary conditions correspond closely to those found in solar air heaters. The range of parameters studied were: Reynolds numbers from 3000 to 20000; relative roughness heights from 0.014, 0.0176, 0.021, 0.027, 0.032; the relative roughness pitch of 4.5, 5.8, 7, 8.5; and rib chamfer angles of −15°, 0, 5°, 10°, 15°, 18°.The roughness Reynolds numbers corresponding to these parameters range from 5 to 60. Friction factor and heat transfer coefficient correlations were developed based on the law of wall similarity and heat-momentum transfer analogy. Authors reported: 1. As compared to the smooth duct the presence of ribs at one broad wall of the duct yielded up to about 2 and 3 times increase in the Stanton number and the friction factor respectively. 2. The highest heat transfer and also the highest friction factor occurred for 15° chamfered ribs.3. The heat transfer function increased with the increase in the aspect ratio from 4.65 to 9.66 and the roughness function decreased with the increase in the aspect ratio from 4.65 to 7.75. Thereafter both the functions attained nearly a constant value.

Verma and Prasad [58] carried out an outdoor experimental investigation for thermo-hydraulic optimization of the roughness and flow parameters for Reynolds number (Re) range of 5000–20,000, relative roughness pitch (P/e) range of 10–40 and relative roughness height (e/D) range of 0.01–0.03. Authors reported effect of transverse wire roughness on heat and fluid flow characteristics for three rectangular solar air heater ducts; two were roughened collectors and one was a plane surface. Transverse wires were fixed on underside of absorber plate as shown in Fig. 5.

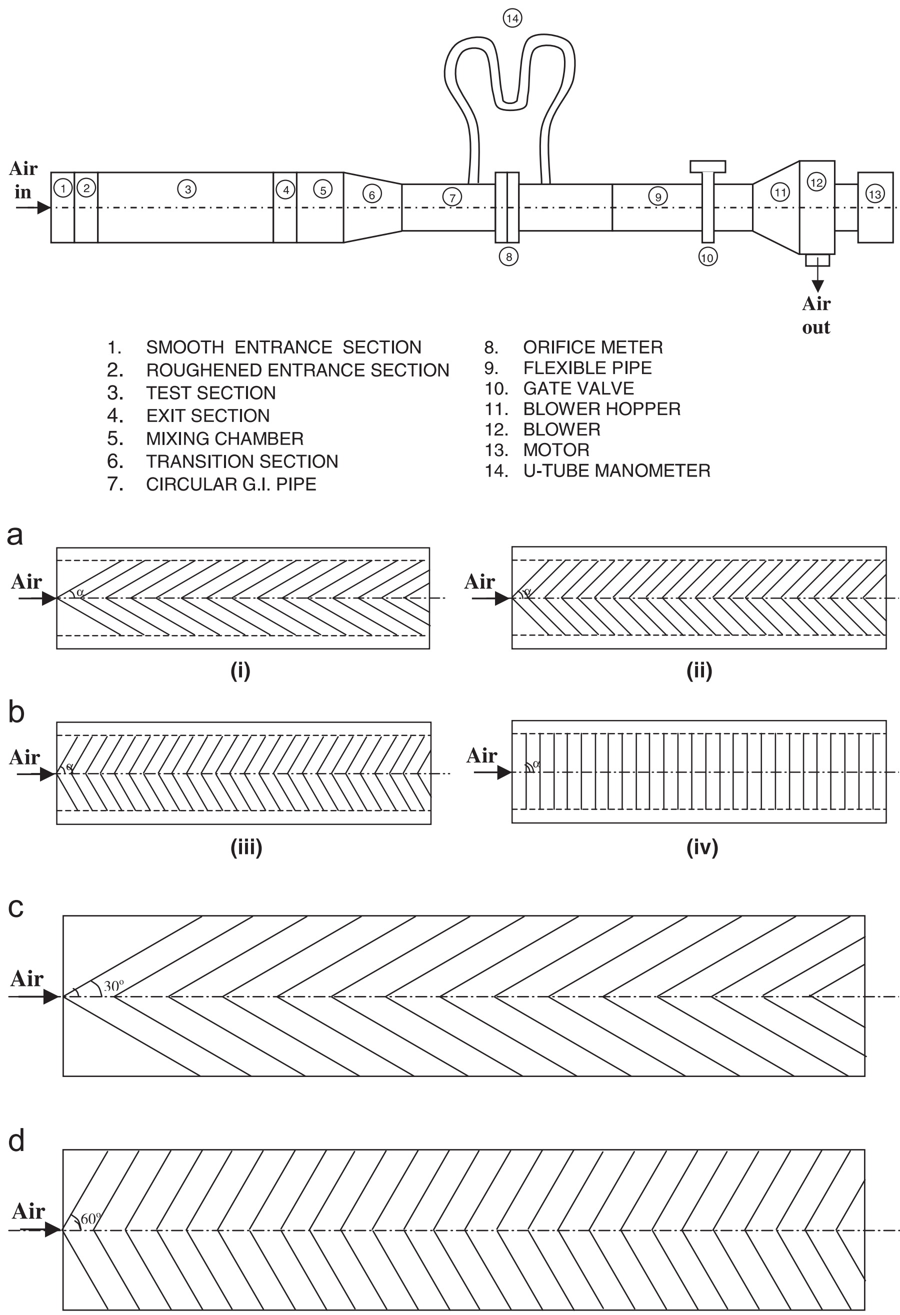


Fig. 12. (a) Schematic diagram of experimental set-up, (b) roughness elements on absorber plate, (c) schematic diagram of 30° V-shaped ribs, and (d) schematic diagram of 60° V-shaped ribs [60].

The optimal value of roughness Reynolds number (e^+) was found to be 24 and corresponding to this value, optimal thermo-hydraulic performance was reported to be 71%. Heat transfer enhancement factor (Nu_r/Nu_s) was found to vary between 1.25 and 2.08 for the range of parameters investigated. Correlations for heat transfer and friction factor were developed.

Karwa et al. [59] conducted an experimental investigation of the performance of solar air heaters with chamfered repeated rib-roughness on the airflow side of the absorber plates as shown in Fig. 11. Experiment carried out using two identical parallel ducts, one with the roughened absorber plate and the other with the smooth one. The roughened elements had a relative roughness pitch of 4.58 and 7.09 while the rib chamfer angle was fixed at 15°. For the airflow duct depths of 21.8, 21.5 and 16 mm, the relative roughness heights for the three roughened plates used were 0.0197, 0.0256 and 0.0441, respectively. The airflow rate per unit area of absorber plate was varied between 0.024 and 0.102 $kgs^{-1}\,m^{-2}$ (flow Reynolds number ranges from 3750 to 16 350). This study showed substantial enhancement in thermal efficiency (10–40%) over solar air heaters with smooth absorber plates due to the enhancement in the Nusselt number (50–120%). The thermal efficiency enhancement was also accompanied by a considerable enhancement in the pumping power requirement due to the increase in the friction factor (80–290%).

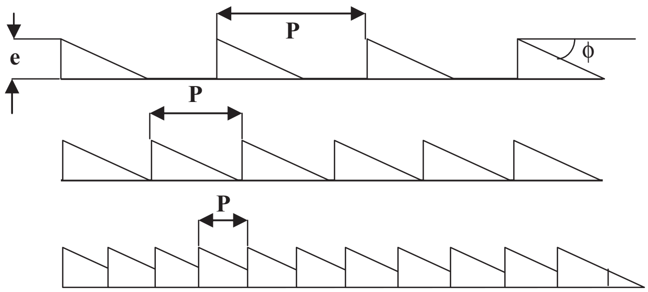


Fig. 13. Wedge shaped transverse rib roughness [61].

Momin et al. [60] experimentally investigated the effect of geometrical parameters of V-shaped ribs, shown in Fig. 12, on heat transfer and fluid flow characteristics of rectangular duct of solar air heater. The investigation covered a Reynolds number (Re) range of 2500–18000, relative roughness height (e/D) of 0.02–0.034 and angle of attack of flow (α) of 30–90° for a fixed relative roughness pitch of 10. The following important conclusions were drawn from this experiment: (1) The maximum enhancement of Nusselt number and friction factor as a result of providing artificial roughness was found to be respectively 2.30 and 2.83 times that of smooth duct for an angle of attack of 60°. It was observed that the same angle of attack corresponds to the maximum values of both Nusselt number and friction factor. (2) The thermo-hydraulic performance parameter improved with increasing the angle of attack of flow and relative roughness height and the maxima occurred with an angle of attack of 60°. (3) It was found that for relative roughness height of 0.034 and for angle of attack of 60°, the V-shaped ribs enhance the values of Nusselt number by 1.14 and 2.30 times over inclined ribs and smooth plate case at

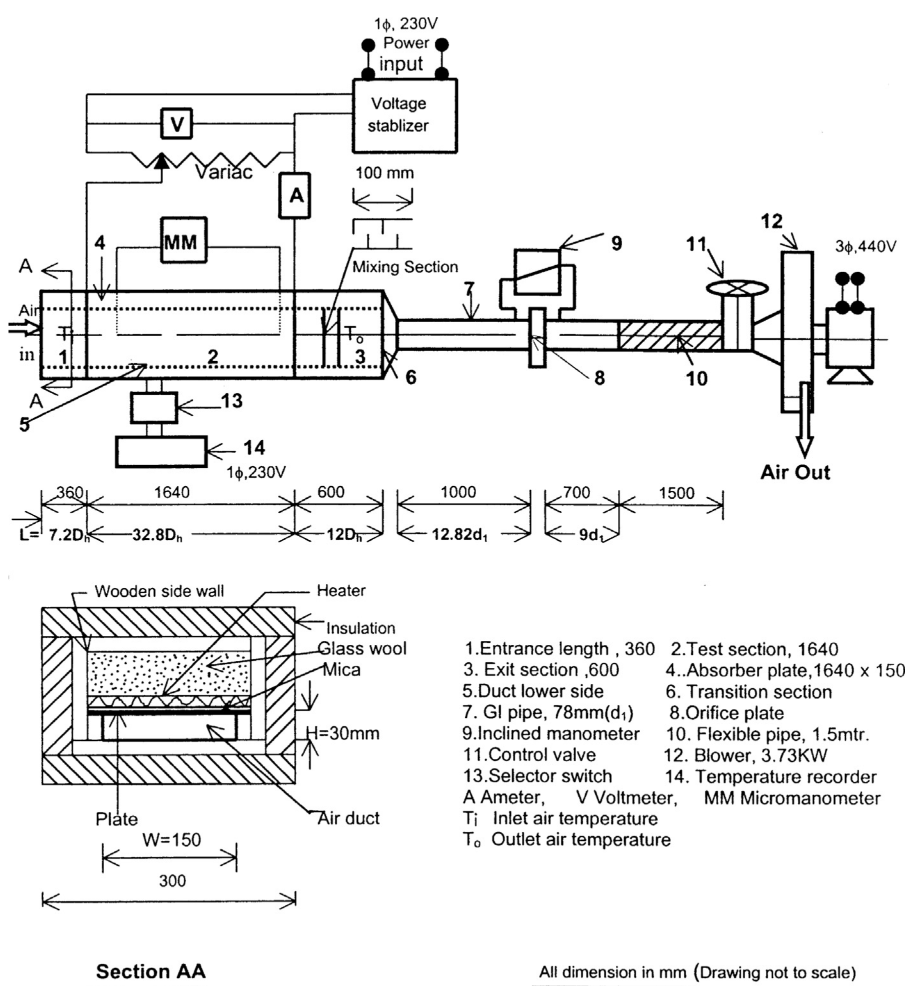


Fig. 14. Schematic diagram of experimental set-up [61].

Reynolds number of 17034. Correlations for heat transfer and friction factor were developed.

Bhagoria et al. [61] performed experiments to determine the effect of relative roughness pitch, relative roughness height and wedge angle on the heat transfer and friction factor in a solar air heater roughened duct having wedge shaped rib roughness as shown in Fig. 13. Fig. 14 shows a schematic diagram of experimental set-up for this investigation. The experiment encompassed the Reynolds number range from 3000 to 18000; relative roughness height (e/D) 0.015–0.033; the relative roughness pitch (P/e) $60.17\ \phi^{-1.0264} < P/e < 12.12$; and rib wedge angle ($\phi$) of 8, 10, 12 and 15°. Statistical correlations for the Nusselt number and friction factor were developed in terms of geometrical parameters of the roughness elements and the flow Reynolds number. The major conclusions were: (1) As compared to the smooth duct, the presence of ribs yields Nusselt number up to 2.4 times while the friction factor rises up to 5.3 times for the range of parameters investigated. (2) The maximum heat transfer occurs for a relative roughness pitch of about 7.57, while the friction factor keeps decreasing as the relative roughness pitch increases. (3) A maximum enhancement of heat transfer occurs at a wedge angle of about 10° while on either side of this wedge angle, Nusselt number decreases. The friction factor increases as the wedge angle increases.

Karwa [62] carried out a comparative experimental study of augmented heat transfer and friction in a rectangular duct with transverse, inclined, V-up continuous, and V-down continuous, V-up discrete ribs, and V-down discrete ribs for Reynolds number range of 2800–15,000, relative roughness height of 0.0467–0.050, fixed relative roughness pitch of 10, angle of attack of 60–90° and duct aspect ratio of 7.19–7.75. Roughness geometries used in this investigation are shown in Fig. 15. Stanton number and friction factor correlations were developed. The enhancement in Stanton number over smooth duct was found to be 65–90%, 87–112%, 102–137%, 110–147%, 93–134%, 102–142% for transverse, inclined, v-up continuous, v-down continuous, v-up discrete and v-down discrete rib arrangement respectively. The friction factor ratios corresponding to these arrangements were found as 2.68–2.94, 3.02–3.42, 3.40–3.92, 3.32–3.65, 2.35–2.47 and 2.46–2.58, respectively. Study revealed that the V-down discrete rib roughness secured the best thermal performance for the same power consumption.

Sahu and Bhagoria [63] investigated the effect of 90° broken ribs as shown in Fig. 16, on thermal performance of a solar air heater for fixed roughness height (e) value of 1.5 mm, Relative roughness height (e/D) value of 0.0338, duct aspect ratio (W/H) value of 8, pitch (P) in the range of 10–30 mm and Reynolds number (Re) range of 3000–12,000. It was found that the maximum Nusselt number attained for roughness pitch of 20 and

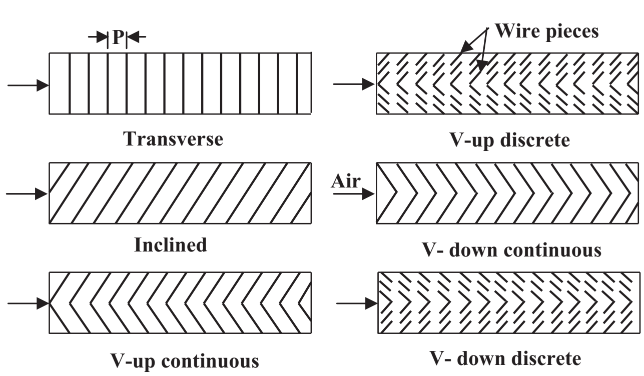


Fig. 15. Roughened absorber plate with transverse, inclined V-discrete and continuous ribs [62].

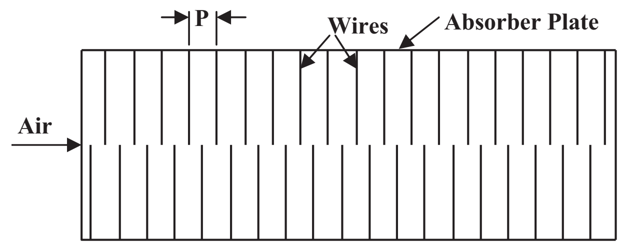


Fig. 16. 90° broken transverse rib roughness [63].

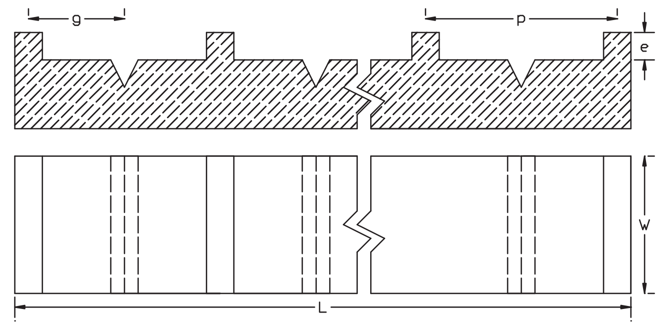


Fig. 17. Rib-grooved artificial roughness [64].

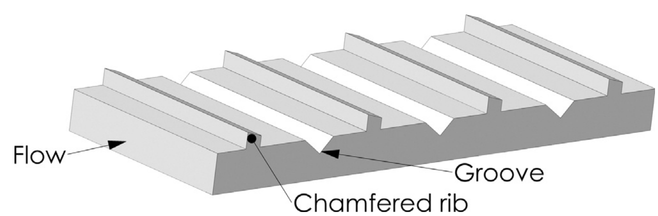


Fig. 18. Chamfered rib-grooved roughness [65,71].

decreased with an increase in roughness pitch. Roughened absorber plates increased the heat transfer coefficient by 1.25–1.4 times as compared to smooth rectangular duct under similar operating conditions at higher Reynolds number. Based on experimentation it was concluded that the maximum thermal efficiency of roughened solar air heater was to be of the order of 51–83.5% depending upon the flow conditions.

Jaurker et al. [64] experimentally investigated the heat transfer and friction characteristics of rib-grooved artificial roughness on one broad wall as shown in Fig. 17. The experimental investigation encompassed the Reynolds number range from 3000 to 21,000; relative roughness height 0.0181–0.0363; relative roughness pitch 4.5–10.0, and groove position to pitch ratio 0.3–0.7. The presence of rib-grooved artificial roughness yielded Nusselt number and friction factor up to 2.7 and 3.6 times respectively in comparison to smooth absorber plate. The maximum heat transfer occurred for a relative roughness pitch (P/e) of about 6 and relative groove (g/P) value of 0.4. It was found that the rib-grooved arrangement provided the best thermo-hydraulic performance and hence can be employed for heat transfer augmentation. Correlations for Nusselt number and friction factor were developed.

Layek et al. [65] investigated heat transfer and friction characteristics of repeated integral transverse chamfered rib-groove roughness on one broad wall as shown in Fig. 18. Experiments encompassed the Reynolds number range of 3000–21,000; relative roughness pitch of 4.5–10, chamfer angle of 5–30°, relative groove position of 0.3–0.6 and relative roughness height of 0.022–0.04.

Nusselt number and friction factor correlations were developed. Authors reported: (1) Nusselt number and friction factor increased by 3.24 times and 3.78 times respectively as compare to smooth duct. (2) The maximum heat transfer enhancement occurred for the relative roughness pitch of 6 and relative groove position of 0.4. (3) The highest Nusselt number occurred for chamfer angle of 18° but the friction factor increased monotonously with an increase in chamfer angle.

Karmare and Tikekar [66] experimentally investigated the heat transfer coefficient and friction factor characteristics of artificial roughened rectangular duct of an aspect ratio 10:1 with metal grit ribs as shown in Fig. 19. The effect of grit geometry [i.e., relative roughness height of grid (e/D), relative roughness pitch of grit (P/e), relative length of grit (l/s)] on the heat transfer coefficient and friction factor were investigated. The range of variation of system parameters and operating parameters were investigated within the limits, as e/D: 0.035–0.044, P/e: 12.5–36 and l/s: 1.72–1, against variation of Reynolds number: 4000–17,000. The main findings of the study were: (1) The presence of metal grit ribs on collector surface of the duct yielded up to two-fold enhancement in the Nusselt number and three-fold enhancement in the friction factor, for the range of Re (4000–17,000), l/s (1.00–1.72), e/D (0.035–0.044) and P/e (12.5–36). (2) Plate no. 05 [roughness parameters: $l/s=1.72$, $e/D=0.044$, $P/e=17.5$] showed the highest heat transfer performance, whereas Plate no. 06 [roughness parameters: $l/s=1.72$, $e/D=0.044$, $P/e=12.5$] yielded highest friction factor. (3) Optimum performance was observed for the Plate no. 05 having roughness parameters $l/s=1.72$, $e/D=0.044$, $P/e=17.5$ for the range of parameters studied (enhancement in Nusselt number was found to be 187% and the friction factor increased by 213%). (4) Based on the experimental data, correlations were developed for Nusselt number and friction factor.

Saini and Saini [67] experimentally studied the effect of arc shaped ribs on heat transfer and fluid flow characteristics of rectangular duct of solar air heater as shown in Fig. 20. This experimental investigation covered a Reynolds number range of 2000–17,000, relative roughness height (e/D) of 0.0213–0.0422 and relative angle of attack of flow ($\alpha/90$) of 0.3333–0.6666 for a fixed relative roughness pitch (P/e) of 10. Fig. 21 shows schematic diagram of experimental set-up for this investigation. The maximum enhancement in Nusselt number was obtained as 3.80 times corresponding to the relative arc angle ($\alpha/90$) of 0.3333 at relative roughness height of 0.0422. However, the increment in friction factor corresponding to these parameters was observed 1.75 times only. Based on the experimental values, correlations for Nusselt number and friction factor were developed.

Aharwal et al. [68] carried out an experimental investigation of heat transfer and friction factor characteristics of a rectangular duct roughened with repeated square cross-section split-rib with a gap, on one broad wall arranged at an inclination with respect to the flow direction as shown in Fig. 22. The duct had a width to height ratio (W/H) of 5.87, relative roughness pitch (P/e) of 10, relative roughness height (e/D) of 0.0377, and angle of attack (α) of 60°, relative gap width (g/e) range of 0.5–2 and relative gap

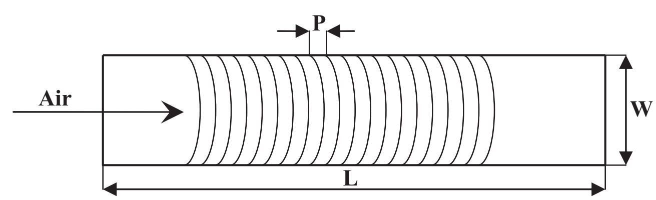


Fig. 20. Arc shaped rib roughness [67].

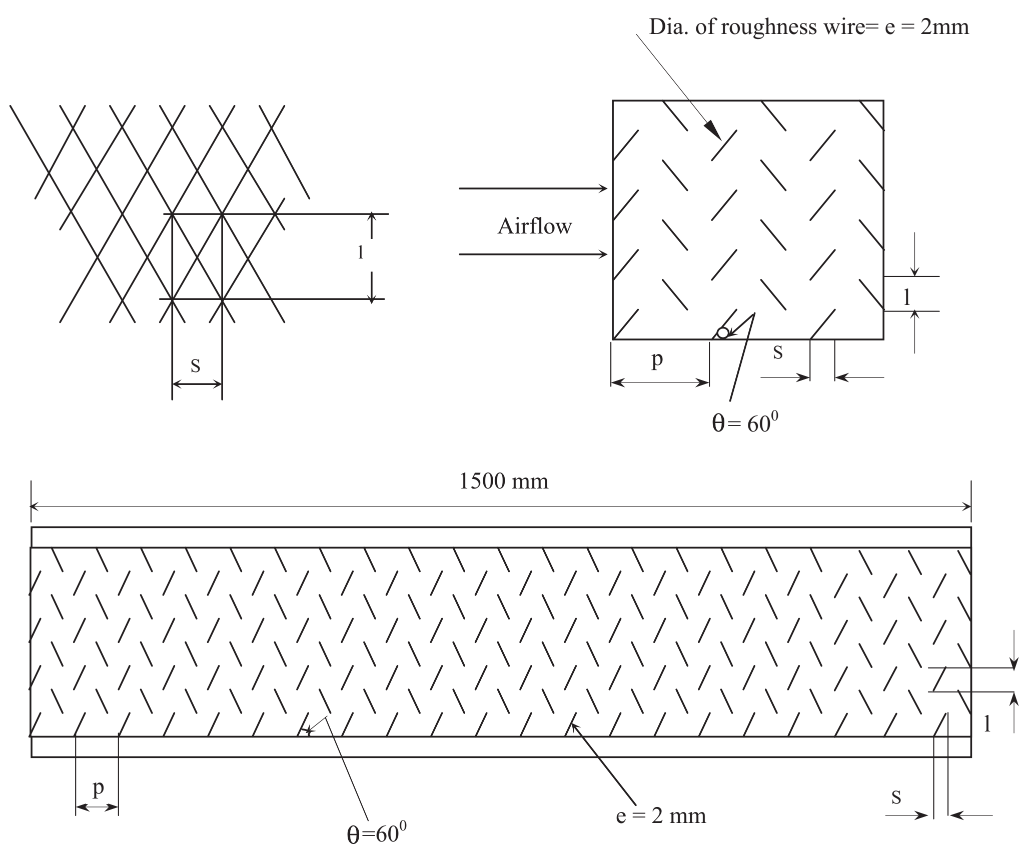


Fig. 19. Metal grit rib roughness [66,72].

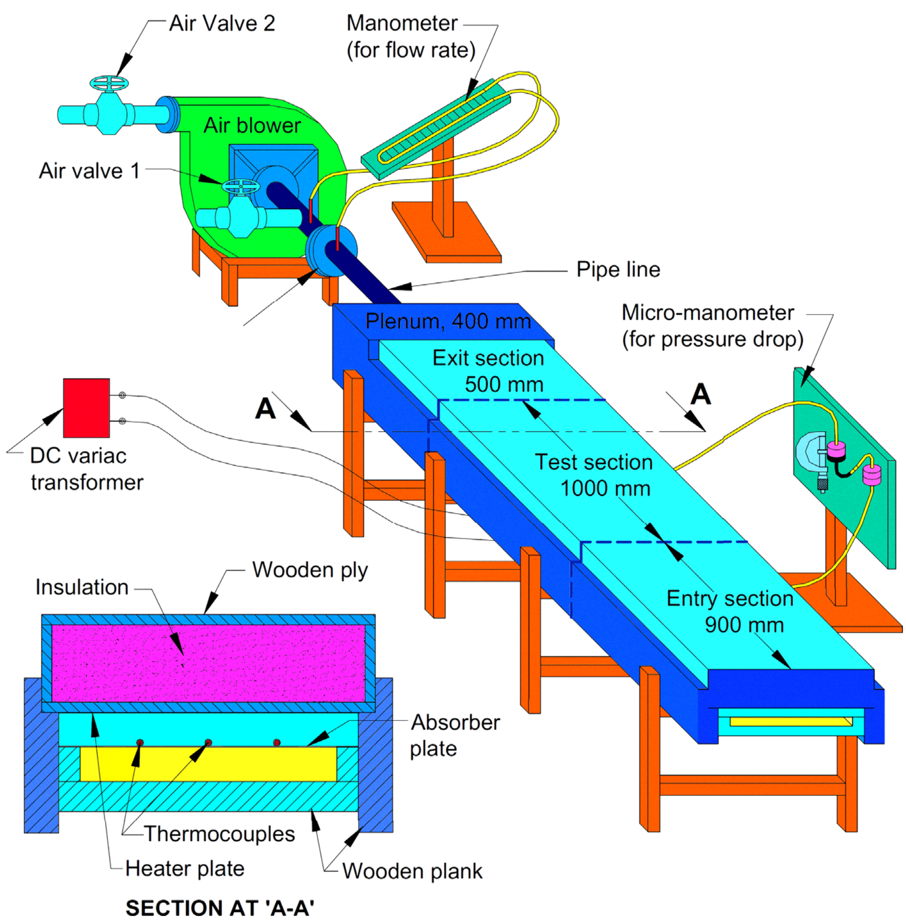


Fig. 21. Schematic diagram of experimental set-up [67].

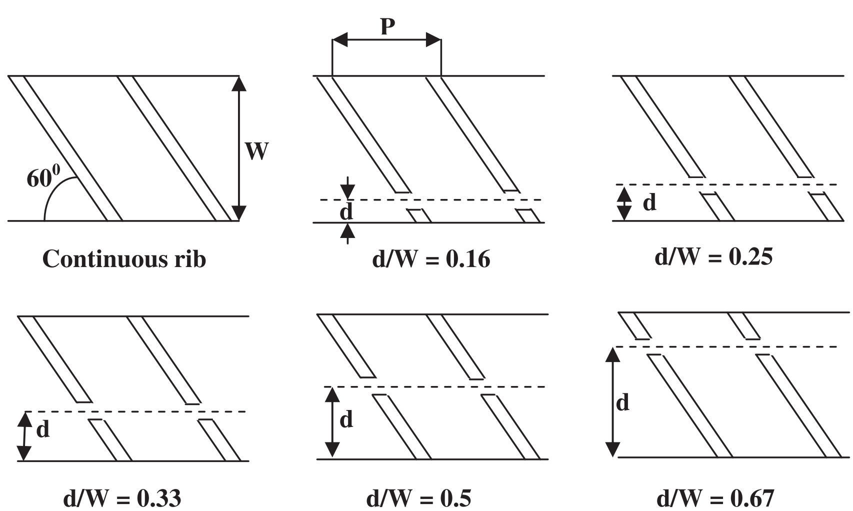


Fig. 22. Inclined rib roughness with and without a gap [68,73].

position (d/W) range of 0.1667–0.5 for Reynolds numbers range from 3000 to 18,000. Based on this experimental investigation on 60°-inclined square rib-roughened ducts with and without a gap, the following conclusions were drawn: (1) a gap in the inclined rib arrangement enhanced the heat transfer and friction factor of the roughened ducts. The increase in Nusselt number and friction factor was in the range of 1.48–2.59 times and 2.26–2.9 times of the smooth duct, respectively, for the range of Reynolds numbers from 3000 to 18,000. (2) The maximum values of Nusselt number and friction factor was observed for a gap in the inclined repeated ribs with a relative gap position of 0.25 and a relative gap width of 1.0. (3) The thermo-hydraulic performance analysis of roughened ducts showed that the relative gap width of 1.0 and a relative gap position of 0.25 results in a higher value of efficiency parameter. (4) Correlations for Nusselt number and friction factor were developed.

Saini and Verma [69] carried out an experimental investigation on fluid flow and heat transfer characteristics of solar air heater duct having dimple-shaped artificial roughness as shown in Fig. 23. The investigation covered the range of Reynolds number

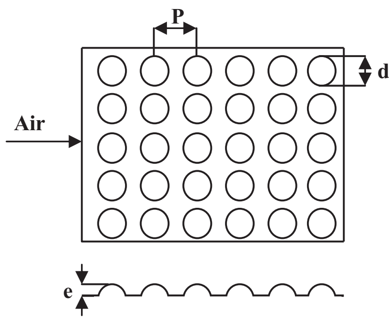


Fig. 23. Dimpled shaped rib roughness [69].

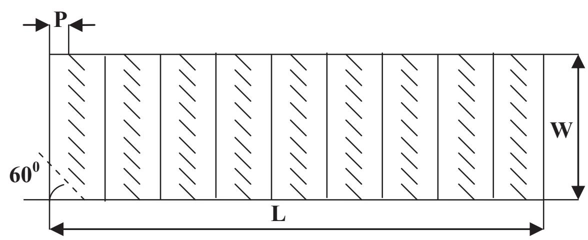


Fig. 24. Combination of transverse and inclined rib roughness [70,76,77].

from 2000 to 12,000, relative roughness height from 0.0189 to 0.038 and relative roughness pitch from 8 to 12. The maximum value of Nusselt number was found corresponds to relative roughness height (e/D) of 0.0379 and relative pitch (P/e) of 10. While minimum value of friction factor was found correspond to relative roughness height (e/D) of 0.0289 and relative pitch (P/e) of 10. Based on experimental data collected during investigation, correlations for Nusselt number and friction factor were developed for the investigated system.

Varun et al. [70] carried out an experimental investigation to study the heat transfer and friction characteristics by using a combination of inclined as well as transverse ribs on the absorber plate of a solar air heater as shown in Fig. 24. The experimental investigation encompassed the Reynolds number (Re) ranges from 2000 to 14,000, relative roughness pitch (P/e) range of 3–8, relative roughness height (e/D) range of 0.030, pitch of ribs (P) range of 5–13 mm, roughness height (e) 1.6 mm and aspect ratio (W/H) of 10. For relative roughness pitch (P/e) value of 8, the best thermal performance was reported. Based on experimental data collected during investigation, correlations for Nusselt number and friction factor was developed for the investigated system.

Layek et al. [71] carried out an experimental investigation on heat and fluid flow characteristics of fully developed turbulent flow in a rectangular duct having repeated integral transverse chamfered rib-groove roughness on one broad wall as shown in Fig. 18. The roughened wall was uniformly heated while the remaining three walls were insulated. These boundary conditions correspond closely to those found in solar air heaters. Six roughened plates were tested placing a 60° V-groove at the center line in between two consecutive chamfered ribs. The rib's top was chamfered having chamfer angles of 5°, 12°, 15°, 18°, 22° and 30° while Relative roughness pitch, P/e, relative groove position, g/P, and relative roughness height, e/D, were kept constant at 10, 0.5 and 0.03 respectively. The flow Reynolds number of the duct varied in the range of approximately 3000–21,000, most suitable for solar air heater. Roughened absorber plates increased the Nusselt number and friction factor by 2.6 and 3.35 times as compared to smooth surface. The maximum enhancement of Nusselt number was found for chamfer angle of 18° but the friction factor increased monotonously with increase in chamfer angle. A substantial improvement in the thermo-hydraulic performance was obtained, as indicated by the performance parameter value lying between 1.4 and 1.76 for the range of experimentation.

Karmare and Tikekar [72] experimentally investigated thermo-hydraulic performance of roughened solar air heaters with metal rib grits as shown in Fig. 19. The range of variation of system and operating parameters was investigated within the limits of, e/D: 0.035–0.044, P/e: 15–17.5 and l/s as 1.72, against variation of Reynolds number, Re: 3600–17,000. The study showed substantial enhancement in thermal efficiency (10–35%), over solar air heater with smooth collector plate. The thermal efficiency enhancement was also accompanied by a considerable increase in the pumping power requirement due to the increase in the friction factor (80–250%).

Aharwal et al. [73] carried out an experimental investigation on heat transfer and friction characteristics of solar air heater ducts with integral repeated discrete square ribs on the absorber plate as shown in Fig. 22. The effect of geometrical parameters, especially, the gap width and gap position was investigated. The experimental investigation encompassed the Reynolds number (Re) ranges from 3000–18,000; relative gap position (d/W) range of 0.16–0.5; relative gap width (g/e) range of 0.5–2.0; relative roughness pitch (P/e) range of 4–10; relative roughness height (e/D) range of 0.018–0.037; angle of attack (α) range of 30–90° while width to height ratio (W/H) was kept constant at 5.83. As compared to the smooth surface, the rib-roughened surface yielded an increase of about 2.83 and 3.60 times in the Nusselt number and friction factor, respectively, for the range of parameters investigated. The maximum heat transfer enhancement was observed at a relative gap position of 0.25 for relative gap width of 1.0, relative roughness pitch of 8.0, angle of attack of 60° and relative roughness height of 0.037. The maximum value of friction factor occurred for discrete transverse ribs with relative roughness pitch of 8.0. Based on the experimental data, correlations for Nusselt number and friction factor were developed as function of roughness parameters of inclined discrete square ribs and flow Reynolds number.

Bopche and Tandale [74] carried out an experimental investigation to study the heat transfer coefficient and friction factor of specially prepared inverted U-shaped turbulators on the absorber surface of an air heater duct as shown in Fig. 25. Fig. 26 shows schematic diagram of experimental set-up for this investigation. The roughened wall was uniformly heated while the remaining three walls were insulated. These boundary conditions correspond closely to those found in solar air heaters. The experiments encompassed the Reynolds number range from 3800 to 18000; ratio of turbulator height to duct hydraulic mean diameter is varied from, e/D=0.0186 to 0.03986 (D=37.63 mm and e=0.7 to 1.5 mm) and turbulator pitch to height ratio was varied from,

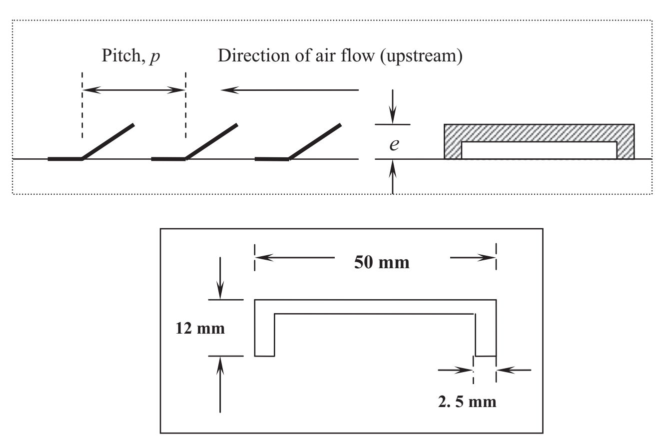


Fig. 25. Inverted U-shaped turbulator roughness [74].

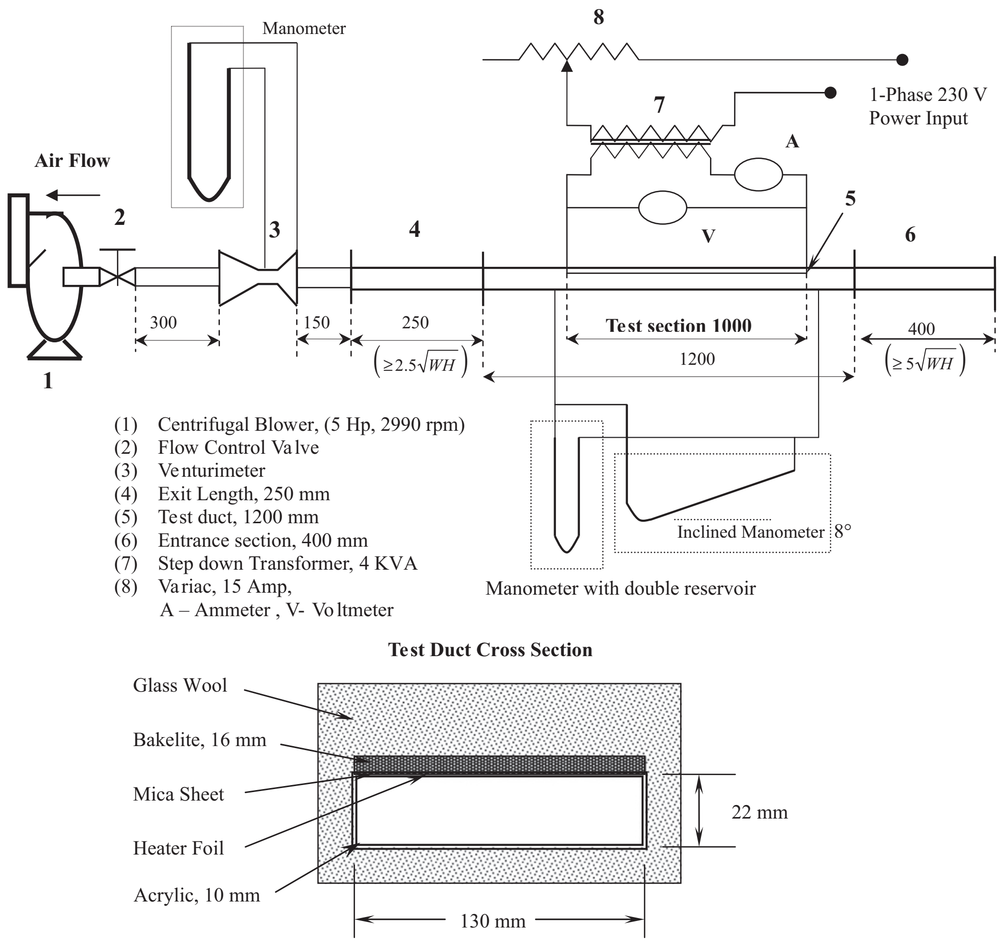


Fig. 26. Schematic diagram of experimental set-up [74].

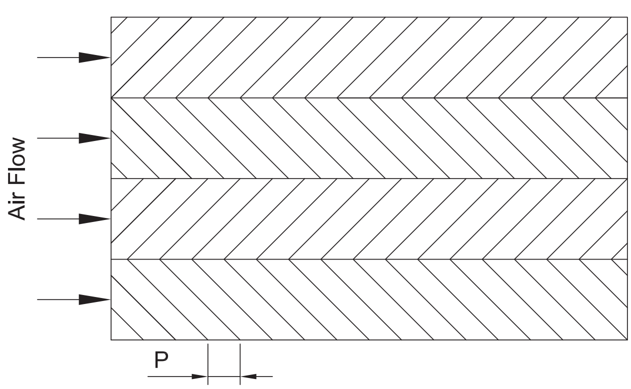


Fig. 27. Discrete W-shaped rib roughness [75].

$P/e = 6.67$ to 57.14 ($P = 10$–40 mm). The angle of attack of flow on turbulators, $\alpha = 90^\circ$ kept constant during the whole experimentation. As compared to the smooth duct, the turbulator roughened duct enhanced the heat transfer and friction factor by 2.82 and 3.72 times, respectively. The correlations were developed for averaged Nusselt number and friction factor for turbulator roughened duct.

Kumar et al. [75] experimentally investigated heat transfer and friction characteristics of discrete W-shaped rib roughened solar air heater as shown in Fig. 27, with an aspect ratio of 8:1. The experiment encompassed Reynolds number (Re) range from 3000 to 15,000, relative roughness height (e/D) in the range of 0.0168–0.0338, relative roughness pitch (P/e) 10 and the angle of attack (α) in the range of 30–75°. Correlations for heat transfer and friction were developed as a function of roughness and flow parameters. Nusselt number increased with an increase of Reynolds number. The maximum enhancement of Nusselt number was found to be 1.44, 1.54, 1.67 and 1.61 times that for smooth duct for angles of attack of 30°, 45°, 60° and 75° for relative roughness height of 0.0168 whereas for relative roughness height of 0.0338, the maximum enhancement in Nusselt number was found to be 1.88, 1.99, 2.16 and 2.08 times for corresponding angles of attack of 30°, 45°, 60° and 75° respectively. Friction factor decreased with an increase of Reynolds number. For relative roughness height of 0.0168, the maximum enhancement in friction factor was found to be 1.53, 1.71, 1.82 and 1.76 times that of smooth duct for angles of attack of 30°, 45°, 60° and 75° respectively whereas for relative roughness height of 0.0338, the maximum enhancement was found to be 2.34, 2.61, 2.75 and 2.69 times for corresponding values of angles of attack of 30°, 45°, 60° and 75° respectively. The maximum enhancement of Nusselt number and friction factor as a result of providing artificial roughness was found to be 2.16 and 2.75 times that of smooth duct for an angle of attack of 60° and relative roughness height of 0.0338.

Varun et al. [76] carried out an experimental study to investigate the effective efficiency of a solar air heater duct provided with transverse and inclined ribs as artificial roughness elements on the absorber plate as shown in Fig. 24. The range of parameters considered for the investigation; Reynolds number (Re) 2000–14,000, relative roughness pitch (P/e) 3–8 and a fixed value of relative roughness height (e/D) of 0.030.The maximum value of effective efficiency was found for roughness parameters corresponding to relative roughness

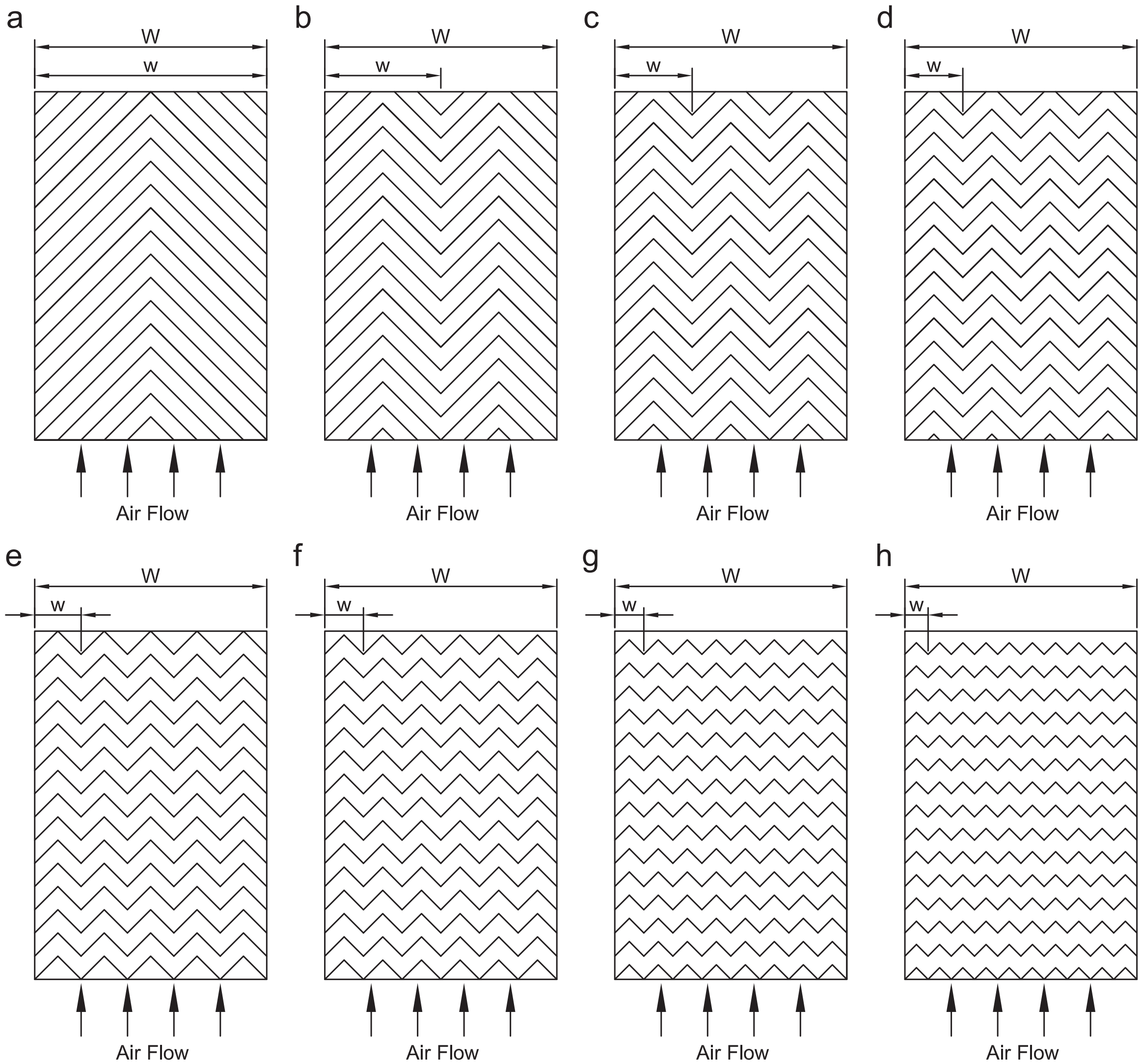


Fig. 28. Multiple V-rib roughness [78]. (a) W/w=1, (b) W/w=2, (c) W/w=3, (d) W/w=4, (e) W/w=5, (f) W/w=6, (g) W/w=8 and (h) W/w=10.

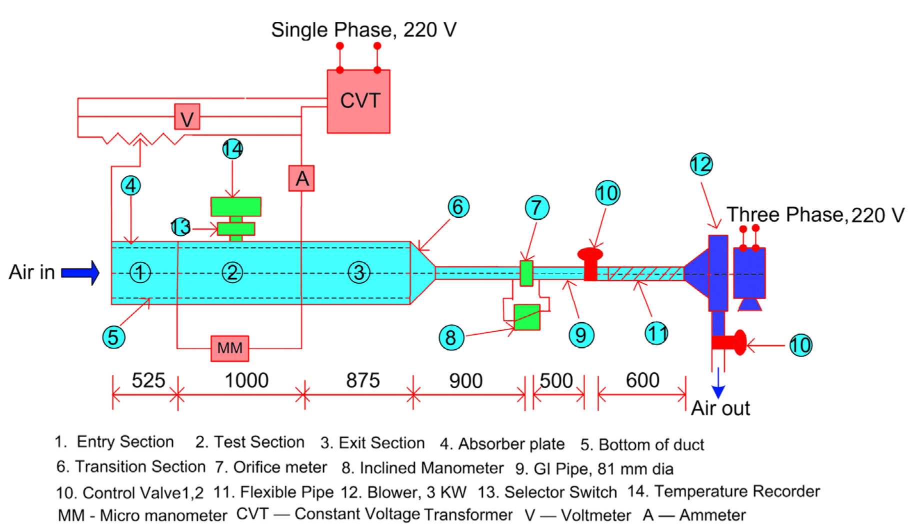


Fig. 29. Schematic diagram of experimental set-up [78].

pitch (P/e) of 8 under the range of parameters investigated. An attempt was also made to optimize the thermal efficiency for the same system under similar conditions by Taguchi method.

Mittal and Varun [77] carried out an experimental investigation of the thermo-hydraulic performance of a solar air heater having transverse and inclined ribs as artificial roughness elements on the

absorber plate as shown in Fig. 24 and the comparison of its performance with that of a conventional smooth one. The experiments covered the Reynolds number ranges in between 1500 and 13,000, relative roughness pitch (P/e) between angled discrete and transverse full ribs of 8, 6 and 3, for a fixed value of relative roughness height (e/D) of 0.03 and aspect ratio (W/H) of 10. It was observed that the thermo-hydraulic performance of rib roughened solar air heater having $p/e=8$ was best among the three different types of rib geometry used.

Hans et al. [78] carried out an experimental investigation to study the effect of multiple v-rib roughness on heat transfer coefficient and friction factor in an artificially roughened solar air heater duct as shown in Fig. 28. The experiment encompassed Reynolds number (Re) from 2000 to 20,000, relative roughness height (e/D) values of 0.019–0.043, relative roughness pitch (P/e) range of 6–12, angle of attack (α) range of 30–75° and relative roughness width (W/w) range of 1–10. Correlations for Nusselt number and friction factor in terms of roughness geometry and flow parameters were developed. Fig. 29 shows schematic diagram of experimental set-up for this investigation. A maximum enhancement of Nusselt number and friction factor due to presence of such an artificial roughness was found to be 6 and 5 times, respectively, in comparison to the smooth duct for the range of parameters considered. The maximum heat transfer enhancement was found to occur for a relative roughness width (W/w) value of 6 while friction factor attains maximum value for relative roughness width (W/w) value of 10. It was also found that Nusselt number and friction factor attain maxima corresponding to angle of attack (α) value of 60°. Maximum enhancement of Nusselt number and friction factor was observed corresponding to relative roughness pitch (P/e) value of 8 while Nusselt number and friction factor increased monotonically with increase in the value of relative roughness height (e/D).

Lanjewar et al. [79] carried out an experimental investigation of heat transfer and friction factor characteristics of a rectangular duct roughened with W-shaped ribs arranged at an inclination with respect to the flow direction on its underside on one broad wall as shown in Fig. 30. W-shaped ribs was tested both pointing in downstream W-down and upstream W-up to the flow. The range of parameters for this study was decided on the basis of practical considerations of the system and operating conditions. The duct had a width to height ratio (W/H) of 8.0, relative roughness pitch (P/e) of 10, relative roughness height (e/D) of 0.03375 and angle of attack of flow (α) of 30–75°. The air flow rate corresponds to Reynolds number between 2300 and 14,000. Maximum enhancement in Nusselt number as a result of providing artificial roughness was 136% for angle of attack of 60° for W-down ribs and 124% for angle of attack of 60° for W-up ribs over smooth plate. Maximum enhancement in Friction factor as a result of providing artificial roughness was 101% for angle of attack of 60° for W-down ribs and 135% for angle of attack of 60° for W-up ribs over the smooth duct. Maximum thermo-hydraulic performance for W-down ribs was 1.98 while it was 1.81 for W-up ribs in the range of parameters investigated. Heat transfer and friction factor correlations were developed.

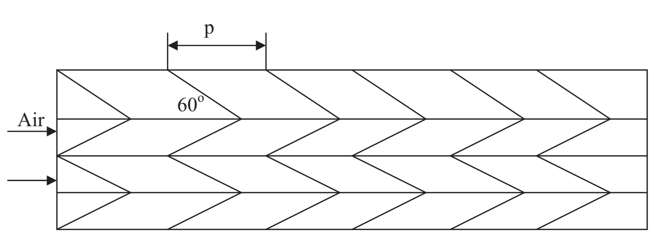


Fig. 30. W-shaped rib roughness [79,81].

Singh et al. [80] experimentally investigated the heat and fluid flow characteristics of rectangular duct having its one broad wall heated and roughened with periodic 'discrete V-down rib' as shown in Fig. 31. The experiment encompassed Reynolds number (Re) from 3000 to 15000 with relative gap width (g/e) range of 0.5–2.0, relative gap position (d/w) range of 0.20–0.80, relative roughness pitch (P/e), angle of attack (α) and relative roughness height (e/D) range of 4–12, 30–75° and 0.015–0.043 respectively. The maximum enhancement of Nu and f for the roughened duct in comparison to that for smooth duct was found to be 3.04 and 3.11 folds respectively, for the investigated range of parameters. The maximum value of Nu and f occurred at P/e of 8.0, and these decreased on the both sides of this pitch. At all Re, the value of Nu is more for discrete V-down rib than that for continuous V-down rib. This is because gap in continuous rib results in enhancement of local Nu at the downstream side of the gap thereby causing increase in average Nu. This local Nu enhancement is caused by increased flow-mixing and turbulence resulting from accelerated flow through the gap (Fig. 32). Statistical correlations for Nu and f were developed as function of Re and rib roughness parameters.

Lanjewar et al. [81] carried out an experimental investigation of heat transfer and friction factor characteristics of rectangular duct roughened with W-shaped ribs on its underside on one broad wall arranged at an inclination with respect to flow direction as shown in Fig. 30. Range of parameters for this study was decided on basis of practical considerations of system and operating conditions. Duct had width to height ratio (W/H) of 8.0, relative roughness pitch (P/e) of 10, relative roughness height (e/D) 0.018–0.03375 and angle of attack of flow (α) 30–75°. Air flow rate corresponds to Reynolds number between 2300 and 14,000. Maximum enhancement of Nusselt

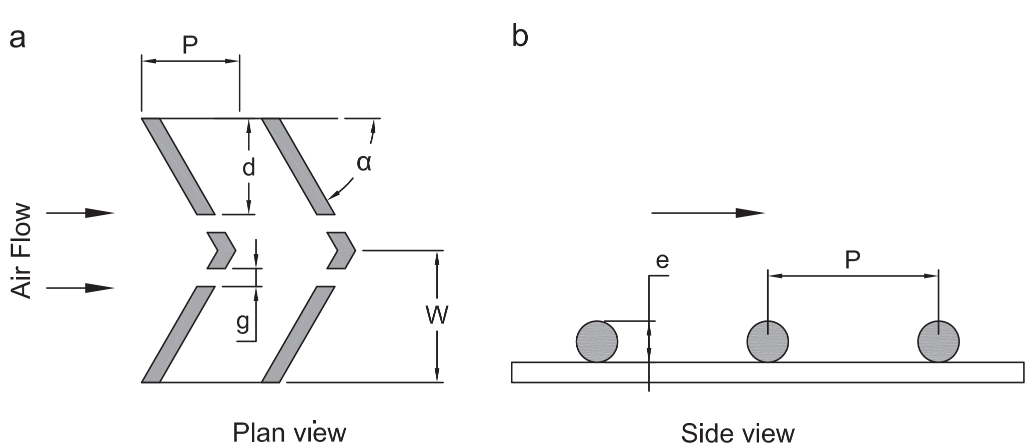


Fig. 31. Discrete V-down rib roughness [80,85].

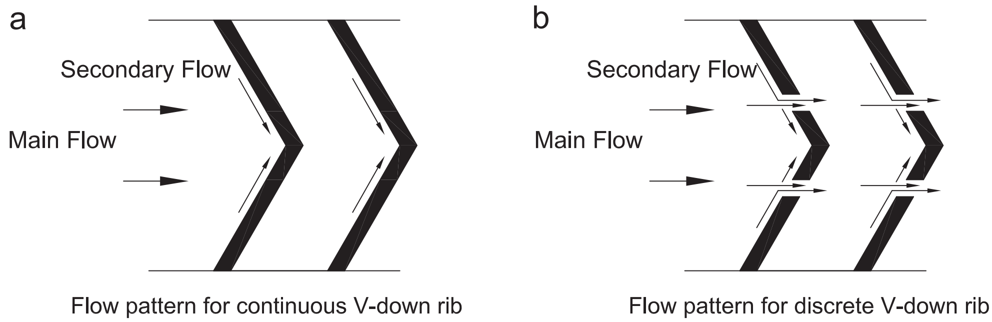


Fig. 32. Flow pattern for continuous V-down rib and discrete V-down rib [80].

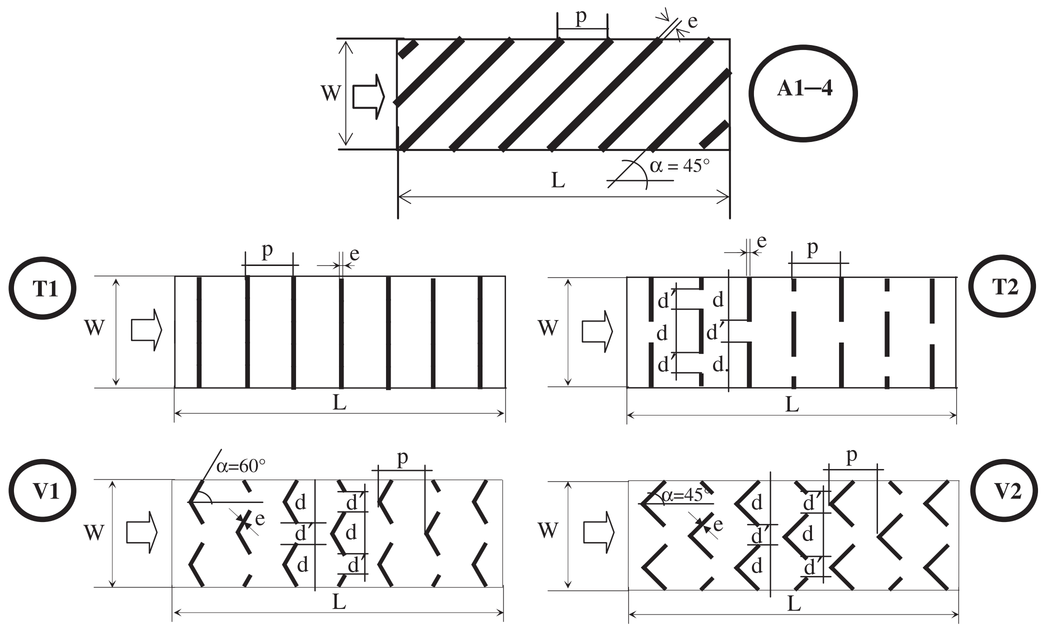


Fig. 33. Geometry of rib configurations studied: A1-4: angled continuous ribs, T1: transverse continuous ribs, T2: transverse broken ribs, V1-2: discrete V-shaped ribs [82].

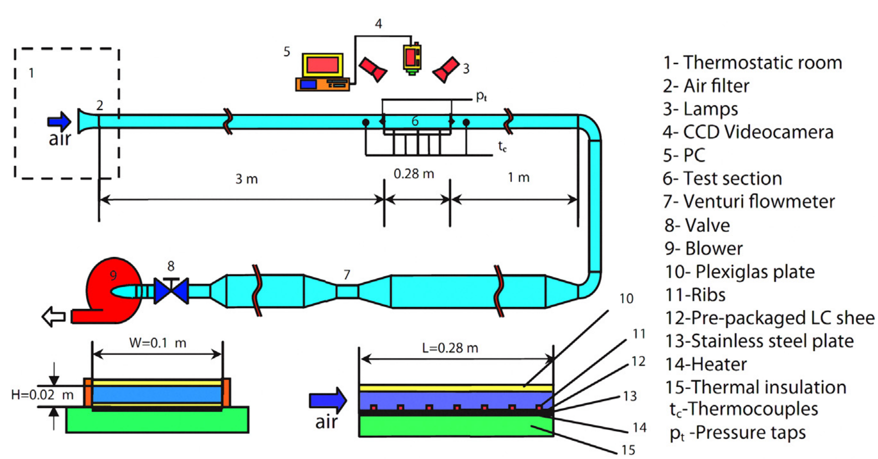


Fig. 34. Schematic layout of experimental setup and test section [82].

number and friction factor as result of providing artificial roughness was found to be respectively 2.36 and 2.01 times that of smooth duct for angle of attack of 60°. Thermo-hydraulic performance improved with angle of attack of flow and relative roughness height and maxima occurred at angle of attack of 60°. Correlations were developed for heat transfer coefficient and friction factor for roughened duct.

Tanda [82] experimentally investigated the heat transfer coefficients and friction factors for a rectangular channel having one wall roughened by repeated ribs and heated at uniform flux, while the remaining three walls were smooth and insulated. Angled continuous ribs, transverse continuous and broken ribs, and discrete V-shaped ribs were considered as rib configurations as shown in Fig. 33. Different types of roughness elements were considered in this study: (i) 45° inclined, continuous ribs, (ii) transverse continuous ribs, (iii) transverse broken ribs, and (iv) discrete V-shaped ribs. For all the rib geometries, the rib height to

hydraulic diameter (e/D, relative roughness height) was fixed and equal to 0.09, while the rib pitch to height ratio (p/e) was set at 13.33, with the exception of the inclined ribs, which were explored also for P/e=6.66, 10 and 20. Moreover, the discrete V-shaped ribs presented an angle (with respect to the longitudinal direction) of 45° or 60°. Fig. 34 shows schematic layout of experimental setup and test section. It was found that all the rib configurations considered performed better than a reference smooth channel in the medium-low range of the Reynolds number, which was that typically encountered in solar air heater applications. In particular, roughening the heat transfer surface by transverse broken ribs appeared to be the most promising enhancement technique of the investigated rib geometries.

Sethi et al. [83] carried out an experimental investigation of heat transfer and friction factor characteristics of a solar air heater duct having dimple shaped elements arranged in angular fashion (arc) as roughness elements on absorber plate as shown in Fig. 35. The experiment encompassed duct aspect ratio (W/H) of 11, relative roughness pitch (P/e) range of 10–20, relative roughness height (e/D) range of 0.021–0.036, arc angle (α) range of 45–75° and Reynolds number (Re) ranges from 3600 to 18,000. The maximum value of Nusselt number was found corresponding to relative roughness height of 0.036, relative roughness pitch of 10 and arc angle of 60°.

Kumar et al. [84] carried out an experimental investigation of the effect of geometrical parameters of Multi v-shaped ribs with gap on heat transfer and fluid flow characteristics of rectangular duct with heated plate having rib roughness on its underside as shown in Fig. 36. The experimental investigation encompassed the Reynolds number (Re) range from 2000 to 20,000, relative width ratio (W/w) of 6, relative gap distance (G_d/L_v) of 0.24–0.80, relative gap width (g/e) of 0.5–1.5, relative roughness height (e/D) of 0.043, relative roughness pitch (P/e) of 10, angle of attack (α) of 60°. The maximum enhancement in Nusselt number and friction factor was observed 6.32 and 6.12 times of that of the smooth duct, respectively. The thermo-hydraulic performance parameter was found the best for the relative gap distance of 0.69 and the relative gap width of 1.0.

Singh et al. [85] experimentally investigated the thermo-hydraulic performance of rectangular ducts roughened with a new configuration of 'V-down rib having gap' on one wide wall as shown in Fig. 31. Small symmetrical gap equal to rib height was created at the center of both legs of V of continuous V-down rib. The duct had aspect ratio (AR) of 12 and the Reynolds number (Re) ranged from 3000 to 15,000. To simulate the indoor testing of solar air heater, the roughened side of rectangular duct was heated with constant heat flux electric heater while the other sides were insulated. The roughness had relative roughness height of 0.043 and relative roughness pitch of 8. Five rib roughened plates having flow-attack-angle (α) from 30° to 75° were tested. The highest friction factor and Nusselt number occurred at flow attack angle of 60°. The highest thermo-hydraulic performance parameter was 2.06 corresponding to flow-attack angle of 60°.

Yadav et al. [86] carried out an experimental investigation to study the effect of heat transfer and friction characteristics of turbulent flow of air passing through rectangular duct which was roughened by circular protrusions arranged in angular arc fashion as shown in Fig. 35. The roughened wall was uniformly heated while other three walls were kept insulated. The thermal and friction characteristics were governed by duct aspect ratio (W/H), hydraulic diameter (D), relative roughness pitch (P/e), relative roughness height (e/D), arc angle (α) and Reynolds number (Re). Experiments encompassed that the Reynolds number ranges from 3600 to 18100, P/e ranges from 12 to 24, e/D ranges from 0.015 to 0.03 and arc angle of protrusions arrangement ranges from 45° to 75°. The maximum enhancement in heat transfer and friction factor was 2.89 and 2.93 times as compared with smooth duct. Correlations for Nusselt number and friction factor were developed. The maximum heat transfer enhancement and friction factor attained maximum value for relative roughness height (e/D) value of 0.03 and relative roughness pitch (P/e) value of 12. It was found that Nusselt number attained maxima corresponding to arc angle

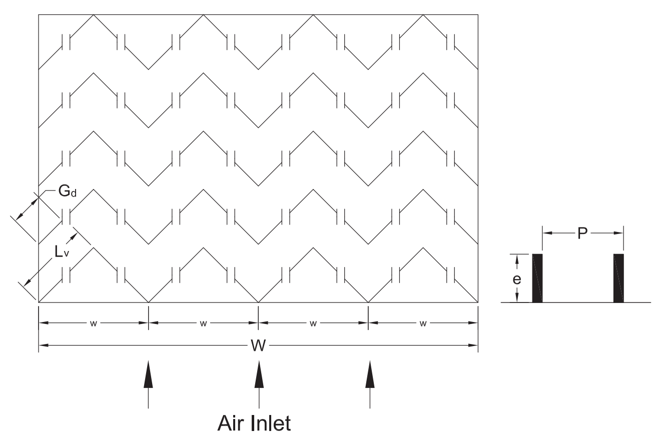
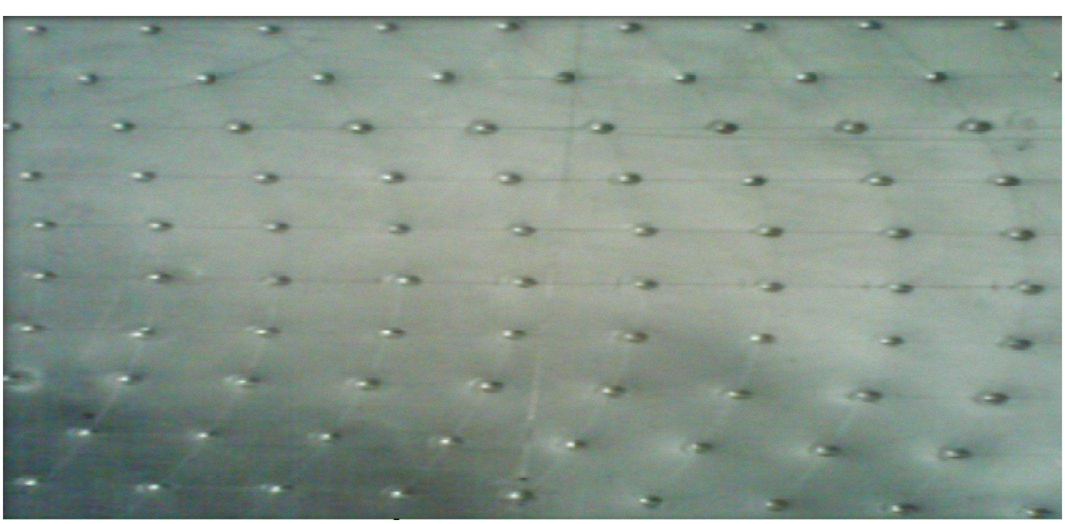


Fig. 36. Multi V-shaped rib roughness with gap [84,88].


Fig. 35. Dimple/circular shaped roughness elements arranged in arc shape [83,86].

(α) value of 60° and friction factor attained maxima corresponding to arc angle (α) value of 60°. Correlations were developed for heat transfer coefficient and friction factor for roughened duct.

Bharadwaj et al. [87] carried out an experimental study to determine the effect on the heat transfer and friction characteristics of an equilateral triangular solar air heater duct using inclined continuous ribs (Fig. 7) as roughness element on the absorber plate. The experimental study covered the range of Reynolds numbers from 5600 to 28,000, relative roughness height (e/D) 0.021–0.043, relative roughness pitch (P/e) 8–16 and angle of attack (α) 30–60°. The duct had an aspect ratio (W/H) of 1.15. The effects of flow parameters and roughness parameters on heat transfer and friction factor were discussed. The maximum value of Nusselt number occurred at the relative roughness pitch (P/e) of 12, whereas maximum friction factor occurred at the relative roughness pitch (P/e) of 8. The maximum value of the thermo-hydraulic performance parameter occurred at a relative roughness pitch (P/e) of 12 and an angle of attack of 60°.

Kumar et al. [88] presented the results of an experimental investigation of heat transfer and friction in the flow of air in rectangular ducts having multi V-shaped rib with gap roughness (Fig. 36) on one broad wall. As compared to the smooth duct the presence of multi V-shaped rib with gap artificial roughness yielded Nusselt number up to 6.74 times while the friction factor increased up to 6.37 times in the range of parameters investigated. The maximum value of friction factor occurred for multi v-shaped with gap rib with relative roughness width of 10. Based on the experimental data, correlations for Nusselt number and friction factor were.

Prasad [89] presented the experimental results on heat transfer and thereby thermal performance of artificially roughened solar air heaters for fully developed turbulent flow data collected under actual outdoor conditions. Thin G.I. wires of varying diameter were provided on the flow side of the absorber plate normal to the fluid flow direction as a roughness element (Fig. 5). Author reported that such solar air heaters were found to give considerably high value of collector heat removal factor, collector efficiency factor and thermal

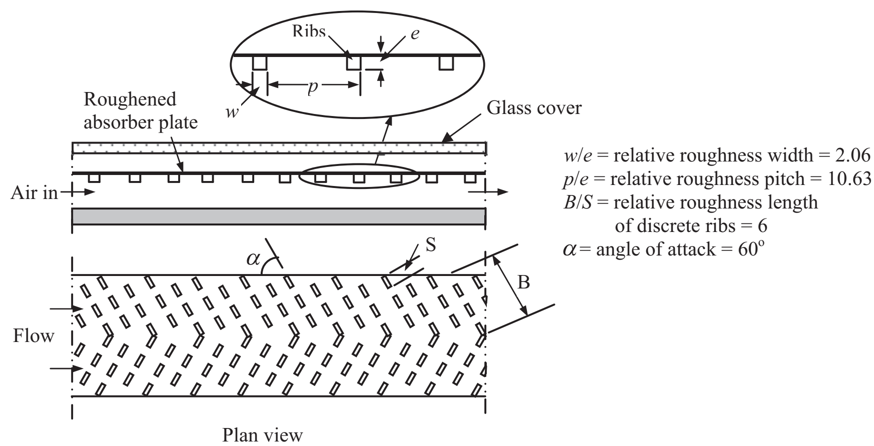


Fig. 37. Roughened absorber plate [90].

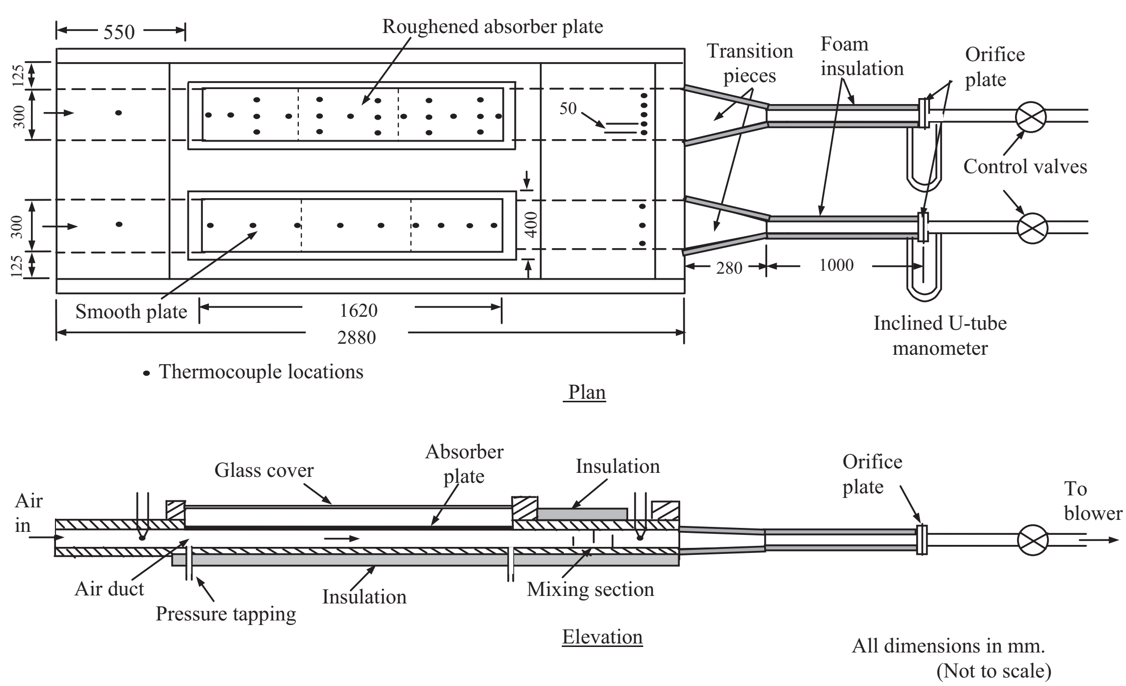


Fig. 38. Schematic diagram of experimental set-up [90].

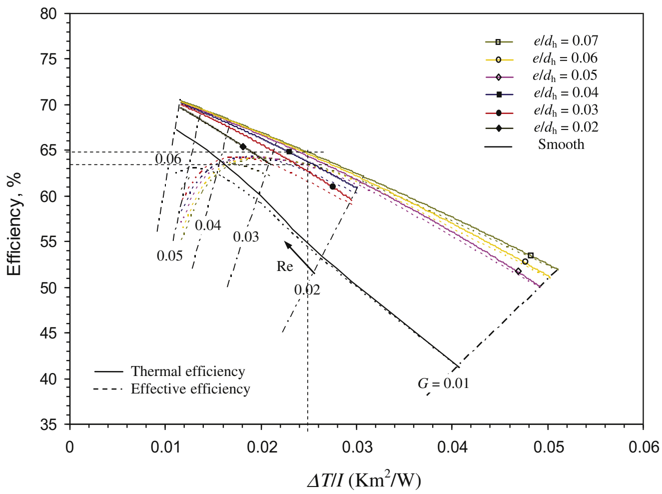


Fig. 39. Performance plots of solar air heaters with 60° V-down discrete rectangular rib roughness [90].

efficiency as compared to the corresponding values of those of smooth collectors. In the range of the operating parameters investigated, the ratio of the respective values of the heat removal factor, collector efficiency factor and thermal efficiency for the roughened collectors to the smooth collectors were found to be 1.786, 1.806 and 1.842 respectively.

Karwa and Chitoshiya [90] presented the results of an experimental study of thermo-hydraulic performance of a solar air heater with 60° V-down discrete rib roughness on the airflow side of the absorber plate along with that for a smooth duct air heater (Fig. 37). Fig. 38 shows schematic layout of experimental setup and test section. The enhancement in the thermal efficiency due to the roughness on the absorber plate was found to be 12.5–20% depending on the airflow rate; higher enhancement was at the lower flow rate. The results of a detailed thermo-hydraulic performance study of solar air heater with v-down discrete rib roughness using the mathematical model were also presented along with the effect of variation of various parameters on the performance. The results were available in the form of plots of thermal and effective efficiencies versus the temperature rise parameter $\Delta T/I$ (Fig. 39). It can be seen from the plots in Fig. 39 that, at the low mass flow rates, the roughened duct air heaters have significantly higher thermal and effective efficiencies as compared to a smooth duct solar air heater. This enhancement is the result of the increased heat transfer coefficient due to the artificial roughness on the absorber plate leading to a higher heat collection rate and lower absorber plate temperature and hence reduced heat loss from the collector. It is to note that, at low flow rates the thermal and effective efficiency values differ marginally only because of the very small pumping power requirement at low flow rates.

Varun et al. [91], Hans et al. [92], Bhushan and Singh [93] and Kumar et al. [94] also reported different investigations on roughness elements of different shapes, sizes and orientations carried out for solar air heater in order to obtain an optimum arrangement of roughness element geometry. For detail information about theoretical/analytical studies on artificially roughened solar air heater, readers are referred to Ref. [95–102].

8. Effect of roughness parameters on heat transfer performance

There are several parameters that characterize the roughness elements, but in case of solar air heater the most preferred roughness geometry is repeated rib type, which is described by the dimensionless parameters viz. relative roughness height e/D, relative roughness pitch P/e, angle of attack α, etc. The friction factor and Stanton/Nusselt number are function of these dimensionless parameters, assuming that the rib thickness is small relative to rib spacing or pitch. The effects of various parameters of artificial roughness geometry on heat transfer and friction characteristics based on the literature are given below:

8.1. Effect of rib

The most important effect produced by the presence of a rib on the flow pattern is the generation of two flow separation regions, one on each side of the rib. The vortices generated are responsible for the turbulence and hence the enhancement in heat transfers as well as in the friction losses takes place.

8.2. Effect of rib cross-section

Rib cross-section affects the size of separated region and level of disturbance in the flow. The friction factor is less for circular cross section ribs in comparison to that of rectangular or square cross section ribs on account of reduction in the size of separated region. This results in decrease in inertial losses and increase in skin friction, thereby, decreasing the friction factor. As the size of separated region diminishes, level of disturbance in flow also decreases which affects the heat transfer adversely. Another possible factor contributing to the Nusselt number decrease is the reduction in heat transfer surface area associated with circular cross-section ribs. It is reported that by changing the rib cross section from rectangular to trapezoidal the friction factor is reduced; while there is minor effect on reduction of Nusselt number and this effect disappears at higher values of Reynolds number.

8.3. Effect of rib height (e)

Fig. 40 clarifies the effect of the roughness height (e) as follows:

If $e \ll \delta$, roughness has no effect.
If $e \gg \delta$, roughness has more effect on fluid pressure as compared to heat transfer, owing to probable interference of turbulency induced in the already turbulent core.
If $e \geq \delta$, the intended purpose of noticeable increase in heat transfer and moderate fluid pressure could be served.

8.4. Effect of relative roughness pitch (P/e)

Fig. 41 shows the flow patterns downstream of a rib with variation in relative roughness pitch. The behavior has been explained on the basis of flow separation. Due to flow separation downstream of a rib, reattachment of the shear layer does not occur for a relative roughness pitch of less than about 8. For small P/e the flow which separates after each rib does not reattach before it reaches the succeeding rib. Maximum heat transfer has been found to occur in the vicinity of a reattachment point. It is reasonable to accept that a similar effect can be produced by decreasing the relative roughness pitch (P/e) for a fixed relative roughness height (e/D). For relative roughness pitch considerably less than about 8, the reattachment will not occur at all resulting in the decrease of heat transfer enhancement. However, an increase in pitch beyond about 10 also results in decreasing the enhancement. For larger relative roughness pitch at a P/e value of about 10 the reattachment point is reached and a boundary layer begins to grow before the succeeding rib is encountered. However,

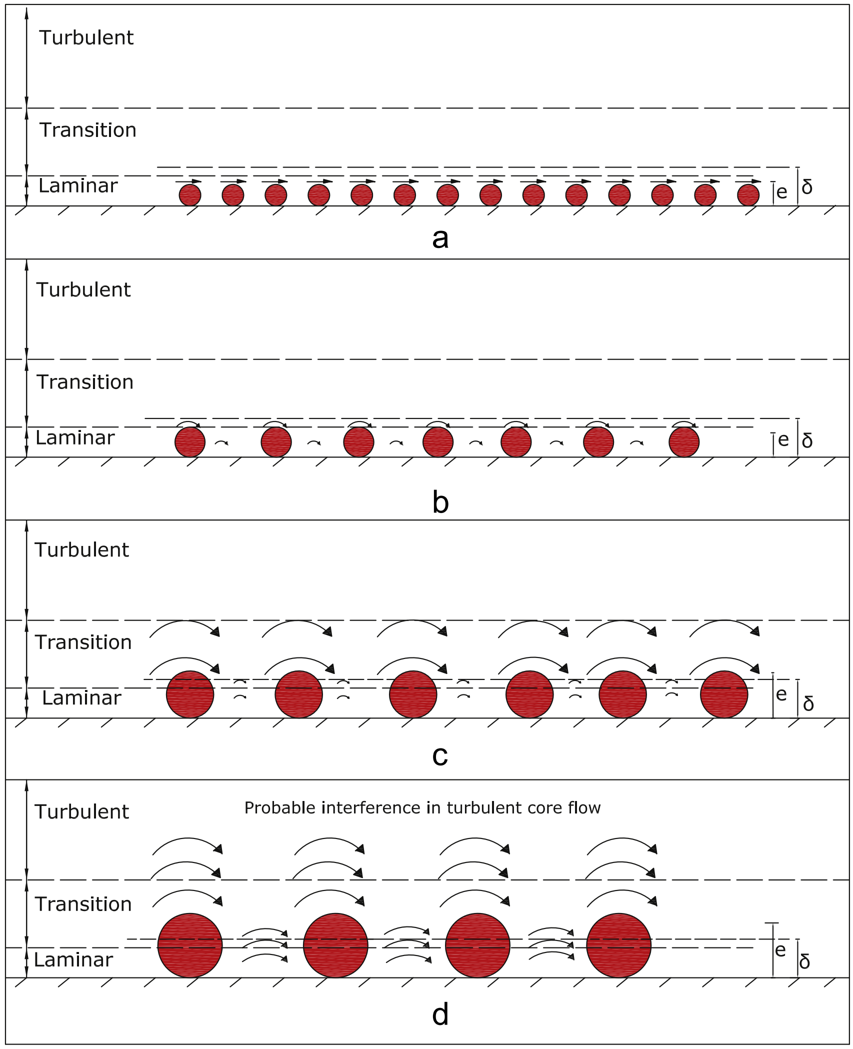


Fig. 40. Effect of roughness height [58]. (a) $e << \delta$, (b) $e = \delta$, (c) $e \geq \delta$ (Optimum condition) and (d) $e > \delta$.

enhancement decreases with an increase in P/e beyond about 10. Table 3 shows the optimum value of relative roughness pitch corresponding to maximum value of a heat transfer coefficient for different types of artificial roughness geometries.

8.5. *Effect of relative roughness height (e/D)*

Fig. 42 shows the flow patterns downstream of a rib with variation in relative roughness height. The enhancement of heat transfer coefficient depends on the flow rate and the relative roughness height. As e/D increases, both the friction factor and Nusselt number increase. The rate of increase of average friction factor increases whereas the rate of increase of average Nusselt number decreases, with the increase of relative roughness height. At very low Reynolds number the effect of e/D is insignificant on enhancement of Nusselt number. If the roughness height is less than thickness of laminar sub-layer then there will not be any enhancement in heat transfer, hence the minimum roughness height should be of same order as thickness of laminar sub-layer at the lowest flow Reynolds number. The maximum rib height should be such that the fin and flow passage blockage effects are negligible. Table 4 shows the optimum value of relative roughness height corresponding to maximum value of a heat transfer coefficient for different types of artificial roughness geometries.

8.6. *Effect of angle of attack (α)*

Various researchers have experimentally investigated, the effect of angle of attack on the flow pattern. Besides a relative roughness pitch and relative roughness height, the parameter that has been found to be most influential to flow pattern is the angle of inclination of the rib i.e. angle of attack of flow with respect to the rib position. As the angle of attack decreases, the friction factor reduces rapidly; however, there is marginal decrease in Nusselt number with change in angle of attack from 90° to 45°.The inclined rib gives a higher heat transfer rate than the transverse rib because of the secondary flow induced by the rib, in addition to breaking the viscous sub-layer and producing local wall turbulence. It is pointed out that the two fluid vortices immediately upstream and downstream of a transverse rib are essentially stagnant relative to main stream flow which raises the local fluid temperature in the vortices and wall temperature near the rib resulting in low heat transfer. The vortices in the case of inclined ribs move along the rib so subsequently to join the main stream causing the fluid to enter near the leading end of rib and coming out near the trailing end. These moving vortices therefore bring in cooler channel fluid in contact with leading end, raising the heat transfer rate while the trailing end heat transfer is relatively lower. This phenomenon therefore results in strong span wise variation of heat transfer. Table 5 shows the optimum value of Angle of

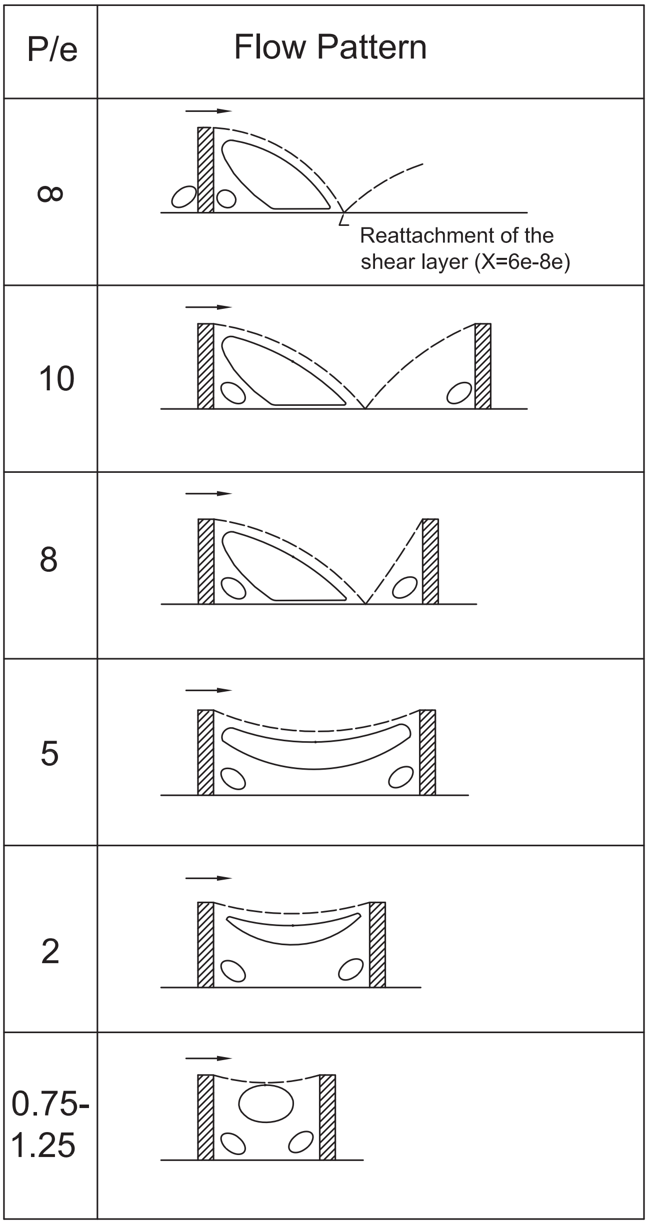


Fig. 41. Flow pattern downstream the roughness as a function of relative roughness pitch [58].

attack (α) corresponding to maximum value of a heat transfer coefficient for different types of artificial roughness geometries. Table 6 shows the optimum value of aspect ratio corresponding to maximum value of a heat transfer coefficient for different types of artificial roughness geometries.

Based on the experimental studies carried out by various investigators, correlation for Nusselt number and friction factor were developed. These correlations along with the range of investigated parameters are given in Table 7.

9. Design considerations/strategy for an artificially roughened solar air heater

Beckman et al. [103] have recommended standard design dimensions for solar air heating systems. The length of the duct has been recommended to range from 1.25 to 2.5 m. The spacing between the absorber plate and the glass cover should range from 1 to 4 cm. The second glass cover is usually mounted 1–2 cm above the first one as recommended by Lof [104]. The depth of the bed is so decided that the optical depth (product of extinction coefficient and actual bed depth) does not exceed 6 as recommended by Chiou et al. [105]. The test apparatus has been recommended to have an upstream flow straightener and a downstream mixing duct across the test section; the respective minimum lengths for these sections based on flow cross-section area A_f should be $6\sqrt{A_f}$ and $6.5\sqrt{A_f}$ [53]. The length of straight M.S. pipe is based on the pipe diameter, d_1 and its minimum length should be taken as $5d_1$ on the upstream side and $10d_1$ on the downstream side of the orifice plate, as recommended by Ehlinger [106]. A pyranometer should be fixed at an inclination equal to that of the duct to measure the correct intensity of solar radiation falling on the inclined test duct. Roughness elements should be considered only on one wall, which is the only heated wall comprising the absorber plate. Recommendations of Verma and Prasad [58] should also be considered for the selection of appropriate value of roughness height. The range of Reynolds number, 3800–18,000 should be chosen based on the suggestions given by Gupta et al. [96]. Gupta et al. [96] suggested that the solar air heater systems operating in a specified range of Reynolds number (3800–18,000) would show better thermo-hydraulic performance.

The experimental test rig used for the investigations should be designed keeping in view the above design considerations. Performance of any system represents the degree of utilization of input to the system. It is required to analyze thermal and hydraulic performance of an artificially roughened solar air heater for making an efficient design of such type of a system. To design of an optimal artificially roughened solar air heater following thermal and hydraulic parameters need to be measured:

9.1. Thermal performance

Thermal performance concerns with heat transfer process within the collector. Thermal performance of solar air heater can be computed with the help of Hottel–Whillier–Bliss equation reported by Duffie and Beckman [10];

$$Q_u = A_C\ F_R\left[I(\tau\alpha)_e - U_L(T_i - T_a)\right] \tag{7}$$

or

$$q_u = \frac{Q_u}{A_c} = F_R\left[I(\tau\alpha)_e - U_L(T_i - T_a)\right] \tag{8}$$

The rate of valuable energy gain by flowing air in the duct of a solar air heater can be calculated from the following equation;

$$Q_u = m\,c_p\,(T_o - T_i) = hA_c\,(T_{pm} - T_{am}) \tag{9}$$

The value of heat transfer coefficient (h) can be increased by various active and passive augmentation techniques. It can be represented in non-dimensional form of Nusselt number (Nu);

$$Nu = hl/k \tag{10}$$

Nusselt number for smooth duct of a solar air heater can also be obtained by Dittus–Boelter equation [12];

$$Nu_s = 0.023Re^{0.8}Pr^{0.4} \tag{11}$$

Further, thermal efficiency of a solar air heater can be expressed by the following equation;

$$\eta_{th} = \frac{q_u}{I} = F_R\,[(\tau\alpha)_e - U_L(T_i - T_a)/I] \tag{12}$$

Table 3
Optimum value of relative roughness pitch (P/e) corresponding to maximum value of heat transfer.

S. No.	Investigators	Rib geometry	Optimum value of relative roughness pitch (P/e)
1	Prasad and Mullick [37]	Transverse wire rib roughness	$P/e=12.7$
2	Gupta et al. [54]	Inclined continuous rib roughness	$P/e=10$
3	Verma and Prasad [58]	Transverse wire rib roughness	$P/e=10$
4	Karwa et al. [59]	Chamfered rib roughness	$P/e=4.58$
5	Momin et al. [60]	V-shaped rib roughness	$P/e=10$
6	Bhagoria et al. [61]	Transverse wedge shaped rib roughness	$P/e=7.57$
7	Karwa [62]	Transverse, inclined, V-up continuous, V-down continuous, V-up discrete and V-down discrete rib roughness	$P/e=10$
8	Jaurker et al. [64]	Rib-grooved roughness	$P/e=6$
9	Layek et al. [65]	Chamfered rib-grooved roughness	$P/e=6$
10	Karmare and Tikekar [66]	Metal grit rib roughness	$P/e=17.5$
11	Saini and Saini [67]	Arc shaped rib roughness	$P/e=10$
12	Aharwal et al. [68]	Inclined continuous rib roughness with gap	$P/e=10$
13	Saini and Verma [69]	Dimple-shaped rib roughness	$P/e=10$
14	Varun et al. [70]	Combination of transverse and inclined rib roughness	$P/e=8$
15	Layek et al. [71]	Chamfered rib-grooved roughness	$P/e=10$
16	Aharwal et al. [73]	Inclined continuous rib roughness with gap	$P/e=8$
17	Bopche and Tandale [74]	Inverted U-shaped turbulators	$P/e=6.67$
18	Kumar et al. [75]	Discrete W-shaped rib roughness	$P/e=10$
19	Varun et al. [76]	Combination of transverse and inclined rib roughness	$P/e=8$
20	Mittal and Varun [77]	Combination of transverse and inclined rib roughness	$P/e=8$
21	Hans et al. [78]	Multi V-shaped rib roughness	$P/e=8$
22	Lanjewar et al. [79]	W-shaped rib roughness	$P/e=10$
23	Singh et al. [80]	Discrete V-down rib roughness	$P/e=8$
24	Lanjewar et al. [81]	W-shaped rib roughness	$P/e=10$
25	Sethi et al. [83]	Dimple shaped elements arranged in angular fashion (arc)	$P/e=10$
26	Kumar et al. [84]	Multi v-shaped rib roughness with gap	$P/e=10$
27	Singh et al. [85]	Discrete V-down rib roughness	$P/e=8$
28	Yadav et al. [86]	Circular protrusions arranged in angular arc shape	$P/e=12$
29	Bharadwaj et al. [87]	Inclined continuous rib roughness	$P/e=12$
30	Kumar et al. [88]	Multi V-shaped rib roughness with gap	$P/e=10$
31	Prasad [89]	Transverse wire rib roughness	$P/e=12$
32	Karwa and Chitoshiya [90]	60° V-down discrete rib roughness	$P/e=10.63$

9.2. Hydraulic performance

Hydraulic performance of a solar air heater concerns with pressure drop (ΔP) in the duct. Pressure drop accounts for energy consumption by blower to propel air through the duct. The pressure drop for fully developed turbulent flow through duct with $Re<50{,}000$ is given as

$$f=\frac{(\Delta P/l)\,D}{2\rho v^2} \tag{13}$$

Friction factor for smooth duct of a solar air heater can also be obtained by Blasius equation [13];

$$f_s=0.079\,R_e^{-0.25} \tag{14}$$

9.3. Thermo-hydraulic performance

It is necessary that while evaluating the performance of a solar air heater with respect to the enhancement of thermal gain, the energy spent in propelling air should also be taken into account. It is desirable that design of solar air heater should be made in such a way that it should transfer maximum heat energy to the flowing fluid with minimum consumption of blower energy. Therefore in order to analyze overall performance of a solar air heater, thermo-hydraulic performance should be evaluated by considering thermal and hydraulic characteristics of the collector simultaneously. An important thermo-hydraulic performance evaluation parameter which is used to compare the heat transfer of artificially roughened duct to that of a smooth duct under constant pumping power constraints as defined by Webb and Eckert [107];

$$\text{Thermohydraulic Performance Parameter}=\frac{(Nu/Nu_s)}{(f/f_s)^{1/3}} \tag{15}$$

A value of this parameter greater than unity ensures the effectiveness of using an enhancement device and can be used to compare the performance of number of arrangements to decide the best among these. The Thermohydraulic Performance Parameter (THPP) based on constant pumping power represents heat transfer enhancement for constant pumping power and widely used in literature for evaluating the relative performance of different arrangement of ribs geometry.

10. A numerical study to determine the most suitable roughness geometry

A number of experimental studies have been reported on solar air heater, roughened with different kinds of roughness geometry used for creating artificial roughness for performance enhancement. However, no comprehensive comparative study has been carried out or found in the literature so far, in order to investigate the relative performance of different types of artificially roughened solar air heater. The objective of this section is to perform such a study. This review of literature reveals that the artificial roughness that results in the desirable increase in the heat transfer also results in an undesirable increase in the pressure drop due to the increased friction; thus the design of the solar air heater duct and absorber surface of duct should, therefore, be executed with the objectives of high heat transfer rates and low friction losses. Therefore, it is necessary that while evaluating the performance of a solar air heater with respect to the enhancement of thermal gain, the energy spent in propelling air should also be taken into account. An important thermo-hydraulic performance evaluation parameter that facilitates simultaneous consideration of thermal and hydraulic performance is given by Webb and Eckert [107] as $(Nu_r/Nu_s)/(f_r/f_s)^1/^3$. This parameter is used to compare the heat

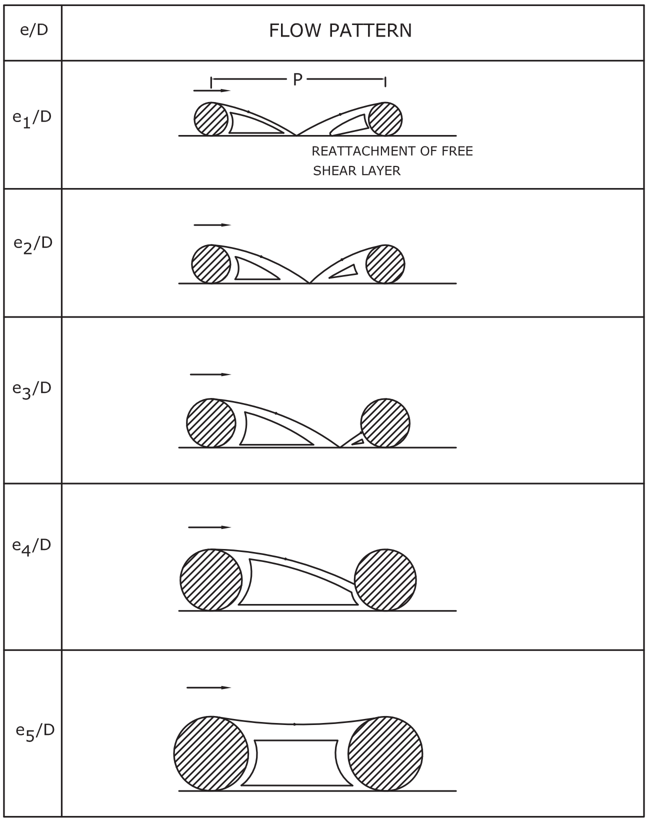


Fig. 42. Flow patterns downstream the roughness as a function of relative roughness height [58].

transfer of artificially roughened duct to that of a smooth duct under constant pumping power constraints. A value of this parameter greater than unity ensures the effectiveness of using an enhancement device and can be used to compare the performance of number of arrangements to decide the best among these.

Performance of any system represents the degree of utilization of input to the system. In this section a total number of twenty known different shapes and orientations of roughness elements are considered for comparative analysis. In order to evaluate the Nusselt number, friction factor and thermohydraulic performance parameter for different types of artificially roughened solar air heater, for different values of Reynolds number, numerical calculations have been carried out within the same investigated range of operating and system parameters. In order to obtain the results numerically, codes are developed in MATLAB-7.6.0.324 using fixed values of operating and system parameters. The fixed values of operating and system parameters used for the present numerical investigations have been chosen, keeping in view the above design considerations. The fixed values of operating and system parameters considered under the present investigation are as given in Table 8. The values of Nusselt number and friction factor for different rib shapes are computed by using the correlations (Table 7) for heat transfer and friction factor developed by various investigators.

After selected the high-performance roughness surface geometries, we carried out an investigation on those elements in order to compare their performance when they operate in the same conditions. Fig. 43 shows the variation of Nusselt number with Reynolds number for different roughness geometries used in solar air heater duct. In all cases, the presence of artificial roughness produces higher Nusselt number than that of smooth solar air heater, as expected. The artificial roughness can lead to superior

Table 4
Optimum value of relative roughness height (e/D) corresponding to maximum value of heat transfer.

S. no.	Investigators	Rib geometry	Optimum value of relative roughness height (e/D)
1	Prasad and Mullick [37]	Transverse wire rib roughness	$e/D=0.019$
2	Gupta et al. [54]	Inclined continuous rib roughness	$e/D=0.023$
3	Saini and Saini [55]	Expanded metal mesh roughness	$e/D=0.0387$
4	Verma and Prasad [58]	Transverse wire rib roughness	$e/D=0.022$
5	Karwa et al. [59]	Chamfered rib roughness	$e/D=0.0441$
6	Momin et al. [60]	V-shaped rib roughness	$e/D=0.032$
7	Bhagoria et al. [61]	Transverse wedge shaped rib roughness	$e/D=0.033$
8	Sahu and Bhagoria [63]	90° broken transverse rib roughness	$e/D=0.0338$
9	Jaurker et al. [64]	Rib-grooved roughness	$e/D=0.0363$
10	Layek et al. [65]	Chamfered rib-grooved roughness	$e/D=0.04$
11	Karmare and Tikekar [66]	Metal grit rib roughness	$e/D=0.044$
12	Saini and Saini [67]	Arc shaped rib roughness	$e/D=0.0422$
13	Aharwal et al. [68]	Inclined continuous rib roughness with gap	$e/D=0.0377$
14	Saini and Verma [69]	Dimple-shaped rib roughness	$e/D=0.0379$
15	Varun et al. [70]	Combination of transverse and inclined rib roughness	$e/D=0.030$
16	Layek et al. [71]	Chamfered rib-grooved roughness	$e/D=0.03$
17	Aharwal et al. [73]	Inclined continuous rib roughness with gap	$e/D=0.037$
18	Bopche and Tandale [74]	Inverted U-shaped turbulators	$e/D=0.03985$
19	Kumar et al. [75]	Discrete W-shaped rib roughness	$e/D=0.0388$
20	Varun et al. [76]	Combination of transverse and inclined rib roughness	$e/D=0.030$
21	Mittal and Varun [77]	Combination of transverse and inclined rib roughness	$e/D=0.030$
22	Hans et al. [78]	Multi V-shaped rib roughness	$e/D=0.043$
23	Lanjewar et al. [79]	W-shaped rib roughness	$e/D=0.03375$
24	Singh et al. [80]	Discrete V-down rib roughness	$e/D=0.043$
25	Lanjewar et al. [81]	W-shaped rib roughness	$e/D=0.03375$
26	Sethi et al. [83]	Dimple shaped elements arranged in angular fashion (arc)	$e/D=0.036$
27	Kumar et al. [84]	Multi v-shaped rib roughness with gap	$e/D=0.043$
28	Singh et al. [85]	Discrete V-down rib roughness	$e/D=0.043$
29	Yadav et al. [86]	Circular protrusions arranged in angular arc shape	$e/D=0.03$
30	Bharadwaj et al. [87]	Inclined continuous rib roughness	$e/D=0.043$
31	Kumar et al. [88]	Multi V-shaped rib roughness with gap	$e/D=0.043$
32	Prasad [89]	Transverse wire rib roughness	$e/D=0.0279$
33	Karwa and Chitoshiya [90]	60° V-down discrete rib roughness	$e/D=0.047$

Table 5
Optimum value of angle of attack (α) corresponding to maximum value of heat transfer.

S. no.	Investigators	Rib geometry	Optimum value of angle of attack (α)
1	Gupta et al. [54]	Inclined continuous rib roughness	$\alpha=60°$
2	Saini and Saini [55]	Expanded metal mesh roughness	$\alpha=61.9°$
3	Muluwork [56]	Staggered discrete V-shaped rib roughness	$\alpha=60°$
4	Momin et al. [60]	V-shaped rib roughness	$\alpha=60°$
5	Aharwal et al. [68]	Inclined continuous rib roughness with gap	$\alpha=60°$
6	Aharwal et al. [73]	Inclined continuous rib roughness with gap	$\alpha=60°$
7	Bopche and Tandale [74]	Inverted U-shaped turbulators	$\alpha=90°$
8	Kumar et al. [75]	Discrete W-shaped rib roughness	$\alpha=60°$
9	Varun et al. [76]	Combination of transverse and inclined rib roughness	$\alpha=60°$
10	Mittal and Varun [77]	Combination of transverse and inclined rib roughness	$\alpha=60°$
11	Hans et al. [78]	Multi V-shaped rib roughness	$\alpha=60°$
12	Lanjewar et al. [79]	W-shaped rib roughness	$\alpha=60°$
13	Singh et al. [80]	Discrete V-down rib roughness	$\alpha=60°$
14	Lanjewar et al. [81]	W-shaped rib roughness	$\alpha=60°$
15	Kumar et al. [84]	Multi V-shaped rib roughness with gap	$\alpha=60°$
16	Singh et al. [85]	Discrete V-down rib roughness	$\alpha=60°$
17	Yadav et al. [86]	Circular protrusions arranged in angular arc shape	$\alpha=60°$
18	Bharadwaj et al. [87]	Inclined continuous rib roughness	$\alpha=60°$
19	Kumar et al. [88]	Multi V-shaped rib roughness with gap	$\alpha=60°$
20	Karwa and Chitoshiya [90]	60° V-down discrete rib roughness	$\alpha=60°$

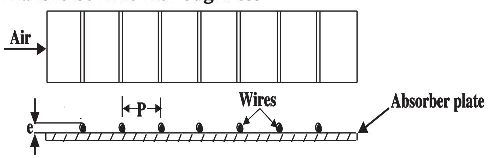
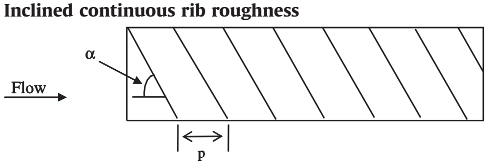
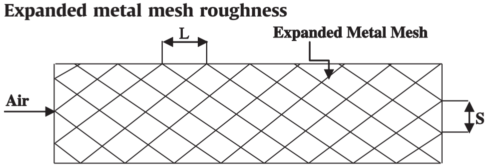
Table 6
Optimum value of duct aspect ratio (W/H) corresponding to maximum value of heat transfer.

S. no.	Investigators	Rib geometry	Optimum value of duct aspect ratio (W/H)
1	Karwa et al. [57]	Chamfered rib roughness	$W/H=9.66$
2	Bhagoria et al. [61]	90° broken Transverse rib roughness	$W/H=5$
3	Sahu and Bhagoria [63]	Transverse wedge shaped rib roughness	$W/H=8$
4	Karmare and Tikekar [66]	Metal grit rib roughness	$W/H=10$
5	Saini and Saini [67]	Arc shaped rib roughness	$W/H=12$
6	Aharwal et al. [68]	Inclined continuous rib roughness with gap	$W/H=5.87$
7	Varun et al. [70]	Combination of transverse and inclined rib roughness	$W/H=10$
8	Karmare and Tikekar [72]	Metal grit rib roughness	$W/H=10$
9	Aharwal et al. [73]	Inclined continuous rib roughness with gap	$W/H=5.83$
10	Bopche and Tandale [74]	Inverted U-shaped turbulators	$W/H=6$
11	Kumar et al. [75]	Discrete W-shaped rib roughness	$W/H=8$
12	Varun et al. [76]	Combination of transverse and inclined rib roughness	$W/H=10$
13	Mittal and Varun [77]	Combination of transverse and inclined rib roughness	$W/H=10$
14	Lanjewar et al. [79]	W-shaped rib roughness	$W/H=8$
15	Singh et al. [85]	Discrete V-down rib roughness	$W/H=12$
16	Yadav et al. [86]	Circular protrusions arranged in angular arc shape	$W/H=11$
17	Bharadwaj et al. [87]	Inclined continuous rib roughness	$W/H=1.15$
18	Kumar et al. [88]	Multi V-shaped rib roughness with gap	$W/H=12$
19	Prasad [89]	Transverse wire rib roughness	$W/H=8$
20	Karwa and Chitoshiya [90]	60° V-down discrete rib roughness	$W/H=7.8$

heat transfer performance because of the secondary flow induced by the rib. This secondary flow has the form of two counter-rotating vortices, which carry cold fluid from the central core region toward the ribbed walls. These cells, interacting with the main flow, affect the flow reattachment and recirculation between ribs and interrupt boundary layer growth downstream of the reattachment regions. From this figure, it is observed that the Nusselt number of the roughened duct with respect to the smooth duct, increase with increasing values of Reynolds number in all cases as expected. The velocity increases with increasing value of Reynolds number, which results in enhanced heat transfer rate. As the Reynolds number increases the roughness elements begin to project beyond the laminar sub-layer. Laminar Sub-layer thickness decreases with an increase in the Reynolds number. In addition to this there is local contribution to the heat removal by the vortices originating from the roughness elements. This increases the heat transfer rate as compared to the smooth surface. This is also because the roughness elements disturb the development of the boundary layer of the fluid flow and increase the turbulent intensity caused by increase in turbulent dissipation rate and turbulent kinetic energy.

It is found that among the entire roughness elements investigated, the multi V-shaped rib roughness with gap has the highest Nusselt number as compared to other roughness geometries for the investigated range of parameters. It can be seen that at low Reynolds number ($Re=3800$), the Nusselt number increases in the following sequence: smooth surface, inclined continuous rib, metal grit rib dimple-shaped rib, discrete V-down rib, transverse wire rib, W-shaped rib, V-shaped rib, transverse wedge shaped rib, discrete W-shaped rib, rib-grooved roughness, combination of transverse and inclined rib, staggered discrete V-shaped rib, U-shaped turbulators, inclined continuous rib roughness with gap, chamfered rib-grooved roughness, circular protrusions arranged in angular arc shape, arc shaped rib roughness, multi

Table 7
Summary of experimental investigations of artificially roughened solar air heaters.

Roughness Geometry	Investigators	Range of Parameters	Correlations Heat Transfer and Friction Factor	Principal Findings
Transverse wire rib roughness 	Prasad and Mullick [37]	e/D: 0.019 P/e: 12.7 Re: 10,000-40,000	Not reported.	14% improvement in thermal performance was reported at a Reynolds number of 40,000 over smooth duct.
	Verma and Prasad [58]	Re: 5000-20,000 P/e: 10-40 e^+: 8-42 e/D: 0.01-0.03 m: 0.01-0.06	$Nu_r = 0.08596\left(\frac{P}{e}\right)^{-0.054}(e/D)^{0.072}Re^{0.732}$, $for\ e^+ \le 24$ $Nu_r = 0.02954\left(\frac{P}{e}\right)^{-0.016}(e/D)^{0.021}Re^{0.802}$, $for\ e^+ > 24$ $f_r = 0.0245\left(\frac{P}{e}\right)^{-0.206}(e/D)^{0.243}Re^{-1.25}$	71% improvement in optimal thermo-hydraulic performance was reported corresponding to e^+_{opt}= 24 over smooth duct.
	Prasad [89]	e/D: 0.0092–0.0279 m: 0.0063-0.0259 kg/s P/e: 10–40 Re: 2959–12,631	Not reported.	The ratio of the respective values of the parameters F_R, F' and η_{th} for the roughened solar air heaters to the smooth collectors were found to be 1.786, 1.806 and 1.842 respectively.
Inclined continuous rib roughness 	Gupta et al. [54]	e/D: 0.018-0.032 e^+: 5-70 P/e: 10 Re: 5000-50,000 W/H: 6.8-11.5 α: 30°-90°	$Nu_r(for\ e^+ < 35) = 0.0024\left(\frac{e}{D}\right)^{0.001}\left(\frac{W}{H}\right)^{-0.06}Re^{1.084}\times\exp\left[-0.04\left(1-\frac{\alpha}{60}\right)^2\right]$ $Nu_r(for\ e^+ \ge 35) = 0.0071\left(\frac{e}{D}\right)^{-0.24}\left(\frac{W}{H}\right)^{-0.028}Re^{0.88}\times\exp\left[-0.475\left(1-\frac{\alpha}{60}\right)^2\right]$ $f_r = 0.1911\left(\frac{e}{D}\right)^{0.196}\left(\frac{W}{H}\right)^{-0.093}Re^{-0.165}\ exp\left[-0.993\left(1-\frac{\alpha}{70}\right)^2\right]$	1.8 and 2.7 times enhancement in Nu_r and f_r were reported over duct with transverse ribs.
	Bharadwaj et al. [87]	e/D: 0.021–0.043 P/e: 8–16 Re: 5600–28,000 W/H: 1.15 α: 30°–60°	Not reported.	Maximum value of thermohydraulic performance was found to be 2.35 for P/e= 12 and α=60°
Expanded metal mesh roughness 	Saini and Saini [55]	e/D: 0.012-0.0390 L/e: 25-71.87 Re: 1900-13,000 S/e: 15.62-46.87	$Nu_r = 4\times10^{-4}\left(\frac{e}{D}\right)^{0.625}Re^{1.22}\times\left(\frac{S}{10e}\right)^{2.22}\times\exp[\{-1.25\left(\ln(S/10e)^2\right)\}]\times(L/10e)^{2.66}\exp\left[\{-0.824\left(\ln(L/10e)^2\right)\}\right]$ $f_r = 0.815\,Re^{-0.361}\left(\frac{L}{e}\right)^{0.266}\left(\frac{S}{10e}\right)^{-0.190}\left(\frac{10e}{D}\right)^{0.591}$	4 and 5 times enhancement in Nu_r and f_r were reported over smooth duct.

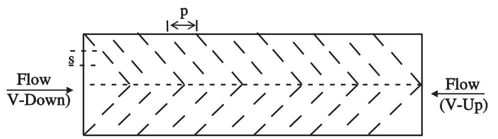
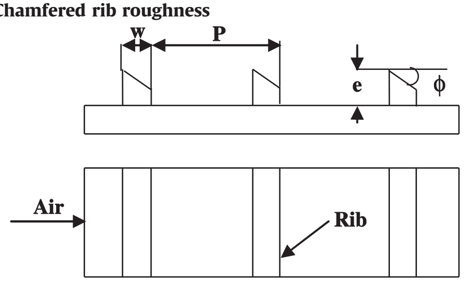
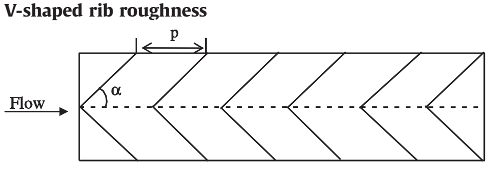
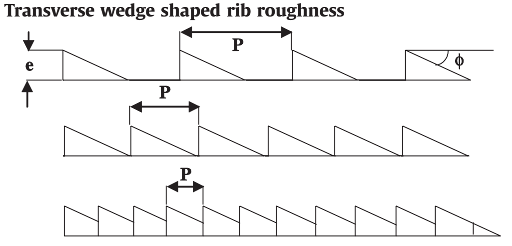
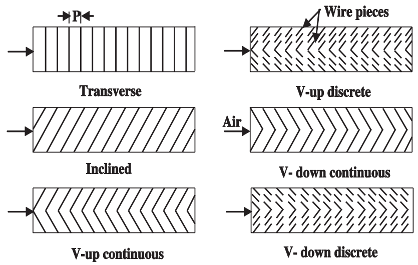
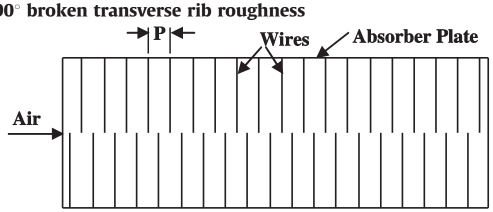
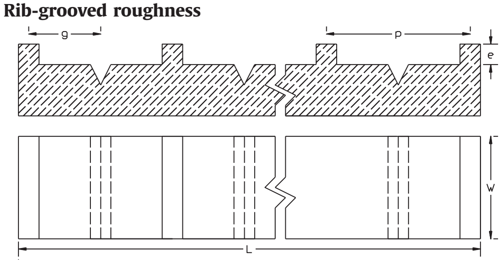
Staggered discrete V-shaped rib roughness 	Muluwork [56]	*B/S*: 3-9 *e/D*: 0.01-0.05 *P'/P*: 0.2-0.8 *Re*: 3032-17652 *S'/S*: 1.1-2.3 α: 30°-90°	$Nu_r = 0.05344\,Re^{1.299}\left(\frac{B}{S}\right)^{1.346}\left(\frac{S'}{S}\right)^{1.112}\left(\frac{e}{D}\right)^{0.270}\left(\frac{P'}{P}\right)^{0.762}$ $\times \exp -2.25\, ln\left(\frac{P'}{P}\right)^{2} exp\left[-0.376\left(ln\left(1-\frac{\alpha}{60}\right)^{2}\right)\right]$ $f_r = 0.7117\,Re^{-0.299}\left(\frac{B}{S}\right)^{0.636}\left(\frac{S'}{S}\right)^{-0.712}(P'/P)^{-0.0936}$ $\times \exp[-1.26(\ln(1-\alpha/70))^{2}]$	Nusselt number for V-down discrete ribs was found to be higher than the corresponding V-up and transverse discrete roughened surfaces.
Chamfered rib roughness 	Karwa et al. [57]	*e/D*: 0.014-0.032 *L/D*: 32-66 *P/e*: 4.5-8.5 ϕ: -15°-18° *Re*: 3000-20,000 *W/H*: 4.8-12	$for\ 7 \le e^{+} < 20$ $g = 103.77e^{-0.006\varphi}\left(\frac{W}{H}\right)^{0.5}\left(\frac{P}{e}\right)^{-2.56} \times \exp[0.7343\left\{\ln\left(\frac{P}{e}\right)\right\}^{2}](e^{+})^{-0.31}$ $for\ 20 \le e^{+} \le 60$ $g = 32.26e^{-0.006\varphi}\left(\frac{W}{H}\right)^{0.5}\left(\frac{P}{e}\right)^{-2.56} \times \exp[0.7343\left\{\ln\left(\frac{P}{e}\right)\right\}^{2}](e^{+})^{0.08}$ $for\ 5 \le e^{+} < 20$ $R = 1.66e^{-0.00786\varphi}\left(\frac{W}{H}\right)^{-0.4}\left(\frac{P}{e}\right)^{2.659} \times \exp[-0.762\left\{\ln\left(\frac{P}{e}\right)\right\}^{2}](e^{+})^{-0.075}$ $for\ 20 \le e^{+} \le 60$ $R = 1.325e^{-0.00786\varphi}\left(\frac{W}{H}\right)^{-0.4}\left(\frac{P}{e}\right)^{2.659} \times \exp[-0.762\left\{\ln\left(\frac{P}{e}\right)\right\}^{2}]$	2 and 3 times enhancement in St_r and f_r were reported over smooth duct.
	Karwa et al. [59]	*e/D*: 0.0197-0.0441 *P/e*: 4.58, 7.09 ϕ: -15° *Re*: 3750-16,350 *W/H*: 6.88-9.38	Not reported.	50-120% and 80-290% enhancement in Nu_r and f_r were reported over smooth duct.
V-shaped rib roughness 	Momin et al. [60]	*e/D*: 0.02-0.034 *P/e*: 10 *Re*: 2500-18,000 *W/H*: 10.15 α: -30°-90°	$Nu_r = 0.067\,Re^{0.888}\left(\frac{e}{D}\right)^{0.424}\left(\frac{\alpha}{60}\right)^{-0.077}\exp\left[-0.782\left(ln\frac{\alpha}{60}\right)^{2}\right]$ $f_r = 6.266\,Re^{-0.425}\left(\frac{e}{D}\right)^{0.565}\left(\frac{\alpha}{60}\right)^{-0.093}\exp\left[-0.719\left(ln\frac{\alpha}{60}\right)^{2}\right]$	2.30 and 2.83 times enhancement in Nu_r and f_r were reported respectively over smooth duct for $\alpha = 60°$.
Transverse wedge shaped rib roughness 	Bhagoria et al. [61]	*e/D*: 0.015-0.033 *P/e*: 60.17x ϕ: -8°- 15° $\phi^{-1.0264}<P/e<12.12$ *Re*: 3000-18,000 *W/H*: 5	$Nu_r = 1.89 \times 10^{-4}\,Re^{1.21}\left(\frac{e}{D}\right)^{0.426}\left(\frac{P}{e}\right)^{2.94}$ $\times \exp\left[-0.71\left(ln\frac{P}{e}\right)^{2}\right](\varnothing/10)^{-0.018}$ $\exp\left[-1.5\left(ln\frac{\varnothing}{10}\right)^{2}\right]$ $f_r = 12.44\,Re^{-0.18}\left(\frac{e}{D}\right)^{0.99}\left(\frac{P}{e}\right)^{-0.52}\left(\frac{\varnothing}{10}\right)^{0.49}$	2.4 and 5.3 times enhancement in Nu_r and f_r were reported over smooth duct for $P/e = 7.57$ and $\phi = 10°$.

Table 7 (*continued*)

Roughness Geometry	Investigators	Range of Parameters	Correlations Heat Transfer and Friction Factor	Principal Findings
Transverse, inclined, V-up continuous, V-down continuous, V-up discrete and V-down discrete rib roughness  	Karwa [62]	B/S: 3.0 e/D: 0.0467-0.05 P/e: 10 Re: 2800-15,000 W/H: 7.19—7.75 α: 60°-90°	***Heat transfer function:*** for inclined rib $g = 12.765 - 0.05095e^{+} + 0.000506(e^{+})^2$ for V-up continuous rib $g = 12.387 - 0.04547e^{+} + 0.000408(e^{+})^2$ for V-down continuous rib $g = 12.502 - 0.11609e^{+} + 0.001239(e^{+})^2$ for V-up discrete rib $g = 11.249 - 0.013120e^{+} + 0.001479(e^{+})^2$ for V-down discrete rib $g = 11.070 - 0.14900e^{+} + 0.001757(e^{+})^2$ ***Roughness function:*** for inclined rib $R = 3.7135\ (e^{+})^{0.12770}$ for V-up continuous rib $R = 3.5080\ (e^{+})^{0.12195}$ for V-down continuous rib $R = 3.4595\ (e^{+})^{0.13048}$ for V-up discrete rib $R = 4.0917\ (e^{+})^{0.16083}$ for V-down discrete rib $R = 3.5341\ (e^{+})^{0.19102}$	65-90%, 87-112%, 102-137%, 110-147%, 93-134%, 102-142% enhancement in St_r was reported over smooth duct for transverse, inclined, V-up continuous, V-down continuous, V-up discrete and V-down discrete rib arrangement respectively. 2.68-2.94, 3.02–3.42, 3.40–3.92, 3.32–3.65, 2.35–2.47 and 2.46–2.58 times enhancement in friction factor ratio was reported over smooth duct for transverse, inclined, V-up continuous, V-down continuous, V-up discrete and V-down discrete rib arrangement respectively.
90° broken transverse rib roughness  	Sahu and Bhagoria [63]	e/D: 0.0338 e: 1.5 P: 10- 30 Re: 3000-12,000 W/H: 8	Not reported.	1.25–1.4 times enhancement in heat transfer coefficient was reported over smooth duct for roughness pitch (P)=20.
Rib-grooved roughness  	Jaurker et al. [64]	e/D: 0.0181-0.0363 g/P: 0.3-0.7 P/e: 4.5-10 Re: 3000-21,000	$Nu_r = 0.00206\,Re^{0.936}\left(\frac{e}{D}\right)^{0.349}\left(\frac{P}{e}\right)^{3.318}\left(\frac{g}{P}\right)^{1.108} \times \exp\left[-0.868\left\{\ln\left(\frac{P}{e}\right)\right\}^2\right] \times \exp\left[2.486\left\{\ln\left(\frac{g}{P}\right)\right\}^2 + 1.406\left\{\ln\left(\frac{g}{P}\right)\right\}^3\right]$ $f_r = 0.001227\,Re^{-0.199}\left(\frac{e}{D}\right)^{0.585}\left(\frac{P}{e}\right)^{7.19}\left(\frac{g}{P}\right)^{0.645} \times \exp\left[-1.854\left\{\ln\left(\frac{P}{e}\right)\right\}^2\right] \times \exp[1.513\left\{\ln\left(\frac{g}{P}\right)\right\}^2 + 0.8662\{\ln(g/P)\}^3]$	2.7 and 3.6 times enhancement in Nu_r and f_r were reported over smooth duct for P/e=6.

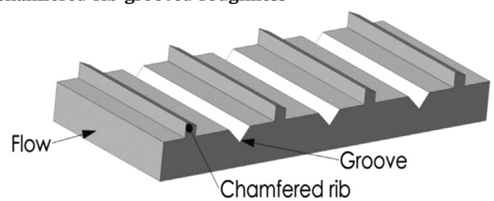
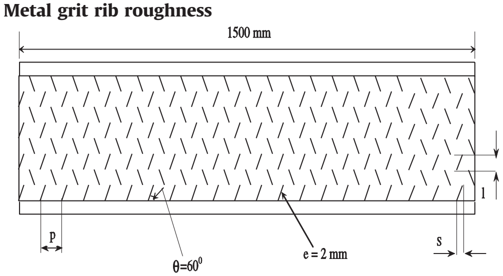
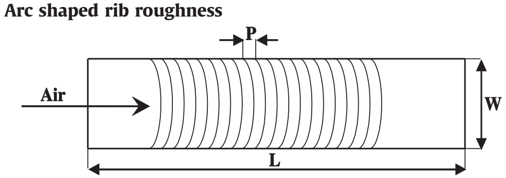
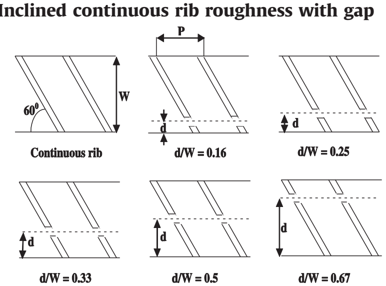
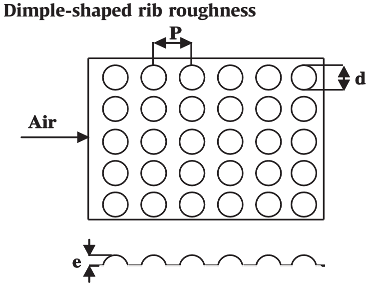
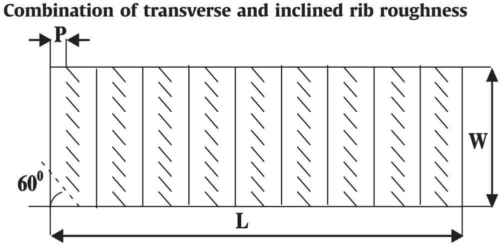
Chamfered rib-grooved roughness 	Layek et al. [65]	*e/D*: 0.022-0.04 *g/P*: 0.3-0.6 *P/e*: 4.5-10 ϕ: -5°-30° *Re*: 3000-21,000	$Nu_r = 0.00225\,Re^{0.92}\left(\frac{e}{D}\right)^{0.52}\left(\frac{P}{e}\right)^{1.72}\left(\frac{g}{P}\right)^{-1.21}\varnothing^{1.24} \times \exp\left[\{-0.22(\ln\varnothing)^2\}\right]$ $\exp\left[-0.46\left\{\ln\left(\frac{P}{e}\right)\right\}^2\right] \times \exp\left[-0.74\left\{\ln\left(\frac{g}{P}\right)\right\}^2\right]$ $f_r = 0.00245\,Re^{-0.124}\left(\frac{e}{D}\right)^{0.365}\left(\frac{P}{e}\right)^{4.32}\left(\frac{g}{P}\right)^{-1.124} \times \exp[0.005\varnothing]$ $\exp\left[-1.09\left\{\ln\left(\frac{P}{e}\right)\right\}^2\right] \times \exp\left[-0.68\left\{\ln\left(\frac{g}{P}\right)\right\}^2\right]$	3.24 and 3.78 times enhancement in Nu_r and f_r were reported over smooth duct for $P/e = 6$.
	Layek et al. [71]	*e/D*: 0.030 *g/p*: 0.5 *P/e*: 10 ϕ: -5°- 30° *Re*: 3000–21,000	Not reported.	2.6 and 3.35 times enhancement in Nu_r and f_r were reported over smooth duct.
Metal grit rib roughness 	Karmare and Tikekar [66]	*e/D*: 0.035-0.044 *Re*: 4000–17,000 *P/e*: 12.5–36 *l/s*: 1.72–1	$Nu_r = 2.4\times10^{-3}\;Re^{1.3}\left(\frac{e}{D}\right)^{0.42}\left(\frac{l}{s}\right)^{-0.146}\left(\frac{P}{e}\right)^{-0.27}$ $f_r = 15.55\,Re^{-0.26}\left(\frac{e}{D}\right)^{0.91}\left(\frac{l}{s}\right)^{-0.27}\left(\frac{P}{e}\right)^{-0.51}$	Upto 2 and 3 times enhancement in Nu_r and f_r were reported over smooth duct.
	Karmare and Tikekar [72]	*e/D*: 0.035-0.044 *l/s*: 1.72 *P/e*: 15-17.5 *Re*: 3600-17,000	Not reported.	10–35% enhancement in thermal efficiency was reported over smooth duct.
Arc shaped rib roughness 	Saini and Saini [67]	*e/d*: 0.0213–0.0422 *P/e*: 10 *Re*: 2000–17,000 *W/H*: 12 $\alpha/90$: 0.3333–0.6666	$Nu_r = 0.001047\,Re^{1.3186}\left(\frac{e}{D}\right)^{0.3772}\left(\frac{\alpha}{60}\right)^{-0.1198}$ $f_r = 0.14408\;Re^{-0.17103}\left(\frac{e}{D}\right)^{0.1765}\left(\frac{\alpha}{60}\right)^{0.1185}$	3.8 and 1.75 times enhancement in Nu_r and f_r were reported over smooth duct.

Table 7 (*continued*)

Roughness Geometry	**Investigators**	**Range of Parameters**	**Correlations** **Heat Transfer and Friction Factor**	**Principal Findings**
Inclined continuous rib roughness with gap  	Aharwal et al. [68]	*d/W*: 0.167–0.5 *e* & *b*: 2mm *e/D*: 0.0377 *g/e*: 0.5–2 *P/e*: 10 *Re*: 3000–18,000 *W/H*: 5.87 α: 60°	Not reported.	2.59 and 2.9 times enhancement in Nu_r and f_r were reported over smooth duct.
	Aharwal et al. [73]	*b*: 2 mm *e/D*: 0.018—0.037 α: 30°-90° *Re*: 3000–18,000 *W/H*: 5.87 *d/W*: 0.167–0.5 e:1-2 mm *g/e*: 0.5–2 *P/e*: 4-10	$Nu_r = 0.012\left(\frac{e}{D}\right)^{0.51} Re^{1.148}\left[\left\{1-\left(0.25-\frac{d}{W}\right)^2\left\{0.01(1-\frac{g}{e})^2\right\}\right\}\right]$ $f_r = 0.5\left(\frac{e}{D}\right)^{0.72} Re^{-0.0836}$	2.83 and 3.60 times enhancement in Nu_r and f_r were reported over smooth duct.
Dimple-shaped rib roughness  	Saini and Verma [69]	*e/D*: 0.0189-0.038 *P/e*: 8-12 *Re*: 2000–12,000	$Nu_r = 5.2\times10^{-4} Re^{1.27}\left(\frac{e}{D}\right)^{0.033}\left(\frac{p}{e}\right)^{3.15} \times\exp\left[-2.12\left(ln\frac{P}{e}\right)^2\right]\times\exp\left[-1.3\left(\ln\frac{e}{D}\right)^2\right]$ $f_r = 0.642\, Re^{-0.465}\left(\frac{e}{D}\right)^{-0.0214}\left(\frac{p}{e}\right)^{-0.465} \times\exp\left[0.054\left(ln\frac{P}{e}\right)^2\right]\times\exp\left[0.840\left(\ln\frac{e}{D}\right)^2\right]$	The maximum value of Nu_r was found corresponds to *e/D*=0.0379 and *P/e*=10
Combination of transverse and inclined rib roughness  	Varun et al. [70]	*e/D*: 0.030 *e*: 1.6mm *P/e*: 3-8 *P*: 5-13 *Re*: 2000–14,000 *W/H*: 10	$Nu_r = 0.0006\, Re^{1.213}\left(\frac{P}{e}\right)^{0.0104}$ $f_r = 1.08585\, Re^{-0.3685}\left(\frac{P}{e}\right)^{0.0114}$	Best thermal performance was reported over smooth duct for *P/e*=8.
	Varun et al. [76]	*e/D*: 0.030 *e*: 1.6mm *P/e*: 3-8 *P*: 5-13 *Re*: 2000–14,000 *W/H*: 10	Not reported.	The maximum value of effective efficiency was reported over smooth duct for *P/e*=8.
	Mittal and Varun. [77]	*e/D*: 0.030 *e*: 1.6mm	Not reported.	The maximum value of thermohydraulic performance was

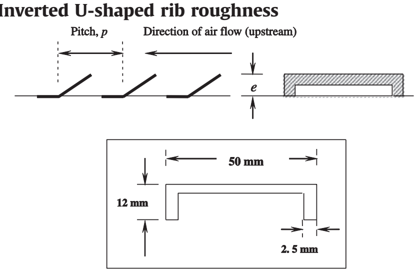
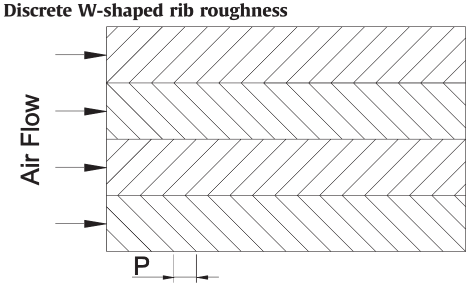
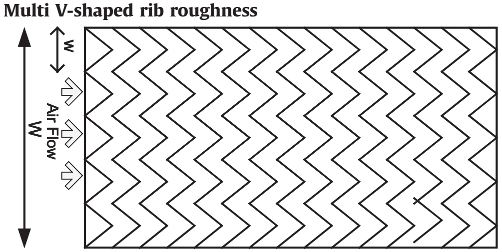
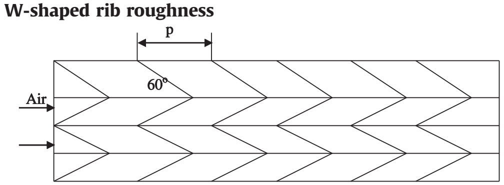
		P/e: 3-8 *P*: 5-13 *Re*: 1500–13,000 *W/H*: 10		reported over smooth duct for *P/e*=8.
Inverted U-shaped rib roughness  	Bopche and Tandale [74]	*e/D*: 0.018–0.0396 *e*: 0.7-1.5 mm *P/e*: 6.669-57.14 *P*: 10- 40 mm *Re*: 3800–18,000 *W/H*: 6 *α*: 90°	$Nu_r = 0.5429\, Re^{0.7054} \left(\frac{e}{D}\right)^{0.3619} \left(\frac{P}{e}\right)^{-0.1592}$ $f_r = 1.2134\, Re^{-0.2376} \left(\frac{e}{D}\right)^{0.3285} \left(\frac{P}{e}\right)^{-0.4259}$	2.82 and 3.72 times enhancement in Nu_r and f_r were reported over smooth duct.
Discrete W-shaped rib roughness  	Kumar et al. [75]	*e/D*: 0.0168–0.0338 *e*: 0.75–1.5mm *P/e*: 10 *Re*: 3000–15,000 *W/H*: 8:1 *α*: 30°–75°	$Nu_r = 0.105\, Re^{0.873} \left(\frac{e}{D}\right)^{0.453} \times \left(\frac{\alpha}{60}\right)^{-0.081} \exp\left[-0.59 \left(ln\frac{\alpha}{60}\right)^2\right]$ $f_r = 5.68\, Re^{-0.4} \left(\frac{e}{D}\right)^{0.59} \times \left(\frac{\alpha}{60}\right)^{-0.081} \exp\left[-0.59 \left(ln\frac{\alpha}{60}\right)^2\right]$	2.16 and 2.75 times enhancement in Nu_r and f_r were reported over smooth duct corresponds to *e/D*=0.0338 and *α*=60°.
Multi V-shaped rib roughness  	Hans et al. [78]	*e/D*: 0.019–0.043 *α* : 30°–75° *Re*: 2000–20,000 *W/w*: 1–10 *P/e*: 6–12	$Nu_r = 3.35 \times 10^{-5}\ Re^{0.92} \left(\frac{e}{D}\right)^{0.77} \left(\frac{P}{e}\right)^{8.54} \left(\frac{W}{w}\right)^{0.43} \left(\frac{\alpha}{90}\right)^{-0.49}$ $\times \exp\left[\left\{-0.1177(\ln\frac{W}{w})^2\right\}\right]\ \exp\left[-2.0407\left\{\ln\left(\frac{P}{e}\right)\right\}^2\right]$	6 and 5 times enhancement in Nu_r and f_r were reported over smooth duct corresponds to *P/e*=8 and *α*=60°.

Table 7 (*continued*)

Roughness Geometry	Investigators	Range of Parameters	Correlations Heat Transfer and Friction Factor	Principal Findings
			$\times \exp\left[-0.61\left\{\ln\left(\frac{\alpha}{90}\right)\right\}^2\right]$ $f_r = 4.47\times 10^{-4}\,\mathrm{Re}^{-0.3188}\left(\frac{e}{D}\right)^{0.73}\left(\frac{P}{e}\right)^{8.9}\left(\frac{W}{w}\right)^{0.22}\left(\frac{\alpha}{90}\right)^{-0.39}$ $\times \exp\left[\left\{-0.52(\ln\frac{\alpha}{90})^2\right\}\right]\ \exp\left[-2.133\left\{\ln\left(\frac{P}{e}\right)\right\}^2\right]$	
W-shaped rib roughness  	Lanjewar et al. [79]	P/e: 10 e: 1.5 mm e/D: 0.03375 W/H: 8 Re: 2300–14,000 α: 30°-75° e^+: 8–44	***Heat transfer function:*** for W-down 75° $g = 12.6813 - 0.03606e^+ + 0.0069(e^+)^2$ for W-down 60° $g = 11.86 - 0.03321e^+ + 0.0062(e^+)^2$ for W-down 45° $g = 11.4519 - 0.3116e^+ + 0.0062(e^+)^2$ for W-down 30° $g = 13.8061 - 0.04434e^+ + 0.0089(e^+)^2$ for W-up 75° $g = 21.3772 - 0.8365e^+ + 0.0140(e^+)^2$ for W-up 60° $g = 18.3937 - 0.6578e^+ + 0.0106(e^+)^2$ for W-up 45° $g = 19.9017 - 0.7837e^+ + 0.0135(e^+)^2$ for W-up 30° $g = 20.4328 - 0.9177e^+ + 0.0174(e^+)^2$ ***Roughness function:*** for W-down 75° $R = 4.5496(e^+)^{0.1716}$ for W-down 60° $R = 4.3375(e^+)^{0.1824}$ for W-down 45° $R = 4.4037(e^+)^{0.1945}$ for W-down 30° $R = 4.8641(e^+)^{0.1889}$ for W-up 75° $R = 3.4705(e^+)^{0.2281}$ for W-up 60° $R = 3.1321(e^+)^{0.2566}$ for W-up 45° $R = 3.4126(e^+)^{0.2437}$ for W-up 30° $R = 4.2970(e^+)^{0.2262}$	Maximum value of thermo-hydraulic performance was found to be 1.98 for W-down ribs and 1.81 for W-up ribs.

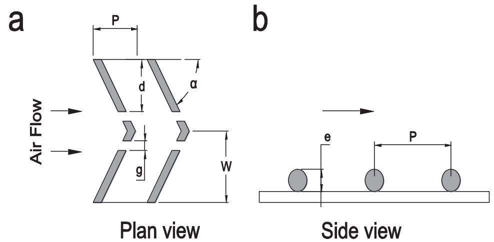
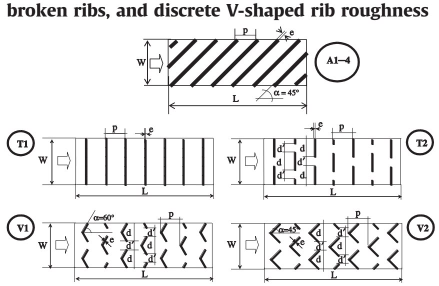
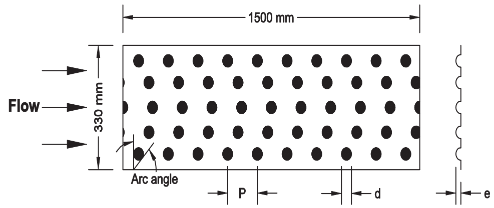
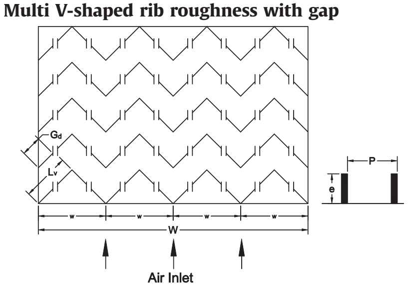
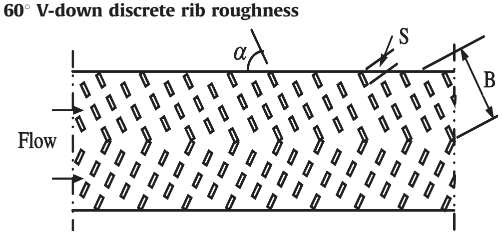
	Lanjewar et al. [81]	e/D: 0.018-0.03375 e: 0.8-1.5 mm P/e: 10 Re: 2300–14,000 W/H: 8 α: 30°-75°	$Nu_r = 0.0613\ Re^{0.9079}\left(\frac{e}{D}\right)^{0.4487}\left(\frac{\alpha}{60}\right)^{-0.1331}\ \exp\left[-0.5307\left(ln\frac{\alpha}{60}\right)^2\right]$ $f_r = 0.6182\ Re^{-0.2254}\left(\frac{e}{D}\right)^{0.4622}\left(\frac{\alpha}{60}\right)^{-0.0817}\ \exp\left[-0.28\left(ln\frac{\alpha}{60}\right)^2\right]$	2.36 and 2.01 times enhancement in Nu_r and f_r were reported over smooth duct corresponds to $P/e=10$, $\alpha=60$ and $e/D=0.03375$.
Discrete V-down rib roughness 	Singh et al. [80]	d/w: 0.2-0.8 e/D: 0.015-0.043 g/e: 0.5-2.0P/e: 4-12 Re: 3000–15,000 α: 30°-75°	$Nu_r = 2.36\times10^{-3}\ Re^{0.90}\left(\frac{e}{D}\right)^{0.47}\left(\frac{P}{e}\right)^{3.52}\left(\frac{g}{e}\right)^{-0.014}\left(\frac{d}{w}\right)^{-0.043}\left(\frac{\alpha}{60}\right)^{-0.023}$ $\times\exp\left[\left\{-0.72(\ln\frac{\alpha}{60})^2\right\}\right]\ \exp\left[-0.84\left\{\ln\left(\frac{P}{e}\right)\right\}^2\right]\times\exp\left[-0.15\left\{\ln\left(\frac{g}{e}\right)\right\}^2\right]$ $\times\exp\left[-0.05\left\{\ln\left(\frac{d}{w}\right)\right\}^2\right]$ $f_r = 4.13\times10^{-2}\ Re^{-0.126}\left(\frac{e}{D}\right)^{0.70}\left(\frac{P}{e}\right)^{2.74}\left(\frac{g}{e}\right)^{0.031}\left(\frac{d}{w}\right)^{-0.058}\left(\frac{\alpha}{60}\right)^{-0.034}\times$ $\exp\left[\left\{-0.93(\ln\frac{\alpha}{60})^2\right\}\right]$ $\exp\left[-0.685\left\{\ln\left(\frac{P}{e}\right)\right\}^2\right]\times\exp\left[-0.21\left\{\ln\left(\frac{g}{e}\right)\right\}^2\right]\times\exp\left[-0.058\left\{\ln\left(\frac{d}{w}\right)\right\}^2\right]$	3.04 and 3.11 times enhancement in Nu_r and f_r were reported over smooth duct corresponds to $P/e=8$, $\alpha=60$ and $e/D=0.043$.
	Singh et al. [85]	e/D: 0.043 P/e: 8 Re: 3000–15,000 W/H: 12 α: 30°- 75°	Not reported.	2.06 times enhancement in thermal performance was reported over smooth duct for flow-attack angle of 60°.
Angled continuous ribs, transverse continuous & broken ribs, and discrete V-shaped rib roughness 	Tanda [82]	e/D: 0.09 e: 3 mm P/e: 6.66-20 Re: 5000–40,000 W/H: 5 α: 45° and 60°	Not reported.	Roughening the heat transfer surface by transverse broken ribs appeared to be the most promising enhancement technique of the investigated rib geometries.
	Sethi et al. [83]	e/D: 0.021–0.036 e/d: 0.5		

Table 7 (*continued*)

Roughness Geometry	Investigators	Range of Parameters	Correlations Heat Transfer and Friction Factor	Principal Findings
Dimple/ circular shaped elements arranged in angular fashion (arc)  		*P/e*: 10–20 *Re*: 3600–18,000 *W/H*: 11 α: 45°–75°	$Nu_r = 7.1\times10^{-3}\ Re^{1.1386}\left(\frac{e}{D}\right)^{0.3629}\left(\frac{P}{e}\right)^{-0.047}\left(\frac{\alpha}{60}\right)^{-0.0048}$ $\times\exp\left[-0.7792\left(\ln\left(\frac{\alpha}{60}\right)\right)^2\right]$ $f_r = 4.869\times10^{-1}\ Re^{-0.223}\left(\frac{e}{D}\right)^{0.2663}\left(\frac{P}{e}\right)^{-0.059}\times\left(\frac{\alpha}{60}\right)^{-0.0042}$ $\times\exp[-0.4801\ (\ln(\frac{\alpha}{60}))^2]$	The maximum value of Nu_r was reported over smooth duct for $P/e = 10$ and $e/D = 0.036$.
	Yadav et al. [86]	*e/D*: 0.015–0.03 *e/d*: 0.3 *P/e*: 12–24 *Re*: 3600–18,100 *W/H*: 11 α: 45°–75°	$Nu_r = 0.154\ Re^{1.017}\left(\frac{e}{D}\right)^{0.521}\left(\frac{P}{e}\right)^{-0.038}\left(\frac{\alpha}{60}\right)^{-0.213}\times\exp\left[-2.023\left(\ln\left(\frac{\alpha}{60}\right)\right)^2\right]$ $f_r = 7.027\ Re^{-0.56}\left(\frac{e}{D}\right)^{0.176}\left(\frac{P}{e}\right)^{-0.18}\left(\frac{\alpha}{60}\right)^{0.038}\times\exp[-1.412\ (\ln(\frac{\alpha}{60}))^2]$	2.89 and 2.93 times enhancement in Nu_r and f_r were reported over smooth duct.
Multi V-shaped rib roughness with gap  	Kumar et al. [84]	*e/D*: 0.043 *g/e*: 0.5–1.5 G_d/L_v: 0.24–0.80 *P/e*: 10 *Re*: 2000–20,000 *W/H*: 12 *W/w*: 6 α: 60°	Not reported.	6.32 and 6.12 times enhancement in Nu_r and f_r were reported over smooth duct.
	Kumar et al. [88]	*e/d*: 0.022–0.043 *g/e*: 0.5–1.5 G_d/L_v: 0.24-0.80 *P/e*: 6-12 *Re*: 2000–17,000 *W/w*: 1-10 α: 30°–75°	$Nu_r = 8.532\times10^{-3}\ Re^{0.932}\left(\frac{e}{D}\right)^{0.175}$ $\left(\frac{P}{e}\right)^{1.196}\left(\frac{g}{e}\right)^{-0.0708}\left(\frac{G_d}{L_v}\right)^{-0.0348}\left(\frac{\alpha}{60}\right)^{-0.0239}\left(\frac{W}{w}\right)^{0.506}$ $\times\exp\left[\left\{0.1153(\ln\frac{\alpha}{60})^2\right\}\right]\exp\left[-0.2805\left\{\ln\left(\frac{P}{e}\right)\right\}^2\right]\times\exp\left[-0.223\left\{\ln\left(\frac{g}{e}\right)\right\}^2\right]$ $\times\exp\left[-0.0753\left\{\ln\left(\frac{W}{w}\right)\right\}^2\right]\times\exp\left[-0.0653\left\{\ln\left(\frac{G_d}{L_v}\right)\right\}^2\right]$ $f_r = 3.1934\times Re^{0.3151}\left(\frac{e}{D}\right)^{0.268}\left(\frac{P}{e}\right)^{-0.7941}\left(\frac{g}{e}\right)^{-0.1769}\left(\frac{G_d}{L_v}\right)^{0.0610}\left(\frac{\alpha}{60}\right)^{0.1553}\left(\frac{W}{w}\right)^{0.113}$ $\times\exp\left[\left\{-0.1527(\ln\frac{\alpha}{60})^2\right\}\right]\exp\left[0.1468\left\{\ln\left(\frac{P}{e}\right)\right\}^2\right]$ $\times\exp\left[-0.6349\left\{\ln\left(\frac{g}{e}\right)\right\}^2\right]\times\exp\left[0.0974\left\{\ln\left(\frac{W}{w}\right)\right\}^2\right]\times\exp\left[-0.1065\left\{\ln\left(\frac{G_d}{L_v}\right)\right\}^2\right]$	6.74 and 6.37 times enhancement in Nu_r and f_r were reported over smooth duct.
60° V-down discrete rib roughness  	Karwa and Chitoshiya [90]	*B/S*: 6 *e/D*: 0.047 *I*: 550-670 W/m^2 *P/e*: 10.63 *Re*: 2750–11,150 *W/H*: 7.8 α: 60°	Not reported.	Enhancement in the thermal efficiency due to the roughness on the absorber plate was found to be 12.5-20% depending on the airflow rate.

V-shaped rib roughness, expanded metal mesh roughness and multi V-shaped rib roughness with gap. It can also be observed that at high Reynolds number ($Re = 18{,}000$), the Nusselt number increases in the following sequence: metal grit rib, inclined continuous rib, transverse wedge shaped rib, discrete W-shaped rib, dimple-shaped rib, V-shaped rib, W-shaped rib, transverse wire rib, combination of transverse and inclined rib, rib-grooved roughness, circular protrusions arranged in angular arc shape, inclined continuous rib roughness with gap, discrete V-down rib, inverted U-shaped turbulators, chamfered rib-grooved roughness, staggered discrete V-shaped rib, arc shaped rib, expanded metal mesh, multi V-shaped rib and multi V-shaped rib roughness with gap.

Fig. 44 shows the variation of friction factor with Reynolds number for different roughness geometries used in solar air heater duct. In all cases, the presence of artificial roughness produces higher friction factor than that of smooth solar air heater, as expected. Presence of artificial roughness (rib), which is inserted into a duct of a solar air heater, results in an obstruction of the flow. The flow blockage due to the presence of the rib is a vital factor to cause a high pressure drop. All types of investigated artificial roughness cause a regular boundary layer separation and re-attachment. This is reflected in an increased pressure drop and therefore an increased friction factor in the roughened duct compared to a smooth duct. With higher blockage of the duct of a solar air heater, pressure drop increases with no significant increase in heat transfer. From this figure, it is seen that the average friction factor of the roughened duct with respect to the smooth duct, tends to decrease as the Reynolds number increases in all cases as expected because of the suppression of laminar sub-layer.

It is found that among the entire roughness elements investigated, the multi V-shaped rib roughness with gap has the highest friction factor as compared to other roughness geometries for the investigated range of parameters. It can be seen that at low Reynolds number ($Re = 3800$) the friction factor increases in the following sequence: arc shaped rib, W-shaped rib, staggered discrete V-shaped rib, combination of transverse and inclined rib, dimple-shaped rib, discrete W-shaped rib, inclined continuous rib, V-shaped rib, circular protrusions arranged in angular arc shape, metal grit rib, discrete V-down rib, transverse wire rib, rib-grooved roughness, inclined continuous rib roughness with gap, chamfered rib-grooved, inverted U-shaped rib, expanded metal mesh, transverse wedge shaped rib, multi V-shaped rib and multi V-shaped rib roughness with gap. It can also be observed that at high Reynolds number ($Re = 18{,}000$), the friction factor increases in the following sequence: arc shaped rib, staggered discrete V-shaped rib, W-shaped rib, combination of transverse and inclined rib, inclined continuous rib, dimple-shaped rib, discrete W-shaped rib, transverse wire rib, V-shaped rib, discrete V-down rib, metal grit rib, circular protrusions arranged in angular arc shape, rib-grooved roughness, chamfered rib-grooved, inclined continuous rib roughness with gap, inverted U-shaped rib, transverse wedge shaped rib, multi V-shaped rib, multi V-shaped rib roughness with gap and expanded metal mesh.

Use of artificial roughness on the absorber plate generates local wall turbulence or interrupts the laminar sub-layer due to flow separation and reattachment between the consecutive ribs, which

Table 8
Fixed value of geometrical and operating parameters.

Geometrical and operating parameters	Fixed value
Length of duct, '*L*' (mm)	1000
Height of duct, '*H*' (mm)	25
Width of duct, '*W*' (mm)	250
Duct aspect ratio, '*W*/*H*'	10
Angle of attack of flow, 'α'	60°
Intensity of solar radiation, '*I*' (W/m^2)	1000
Chamfer angle, 'φ'	10°
Relative roughness pitch, '*P*/*e*'	10
Relative roughness height, '*e*/*D*'	0.03
Density of air, 'ρ' (kg/m^3)	1.105
Specific heat of air, 'C_p' (J/kg k)	1008
Thermal conductivity of air, '*k*' (J/kg m k)	0.026
Viscosity of air, 'μ' (kg/s m)	1.865×10^{-5}
Reynolds number, '*Re*'	3800, 5000, 8000, 12000, 5000, 18000 (6 values)

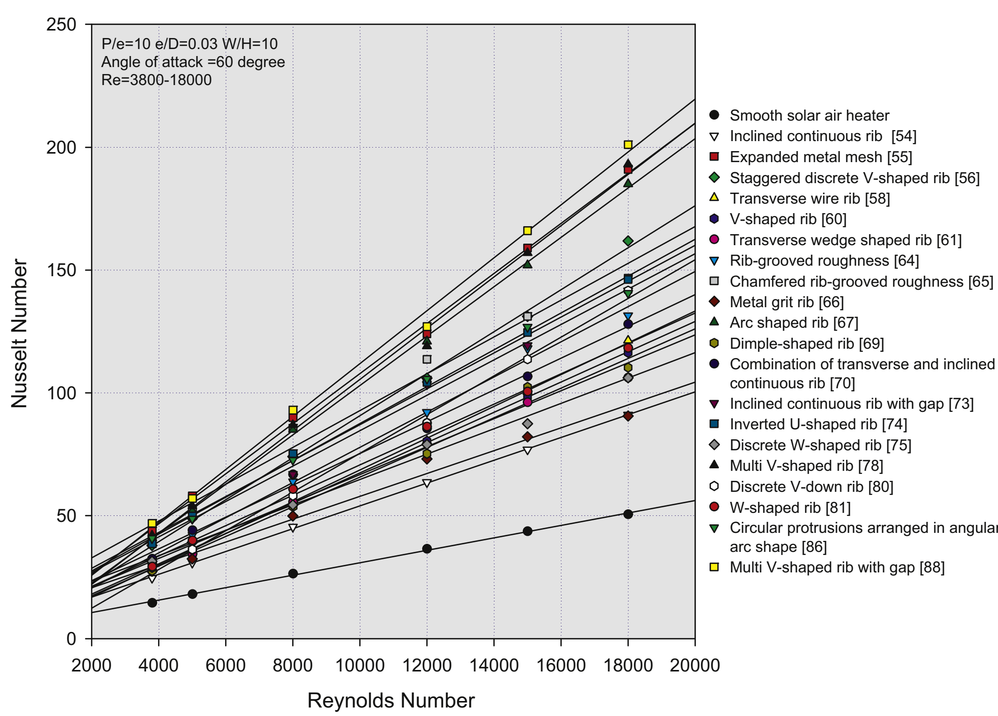


Fig. 43. Nusselt number vs. Reynolds number for artificially roughened solar air heater having different types of roughness geometry and for smooth solar air heater.

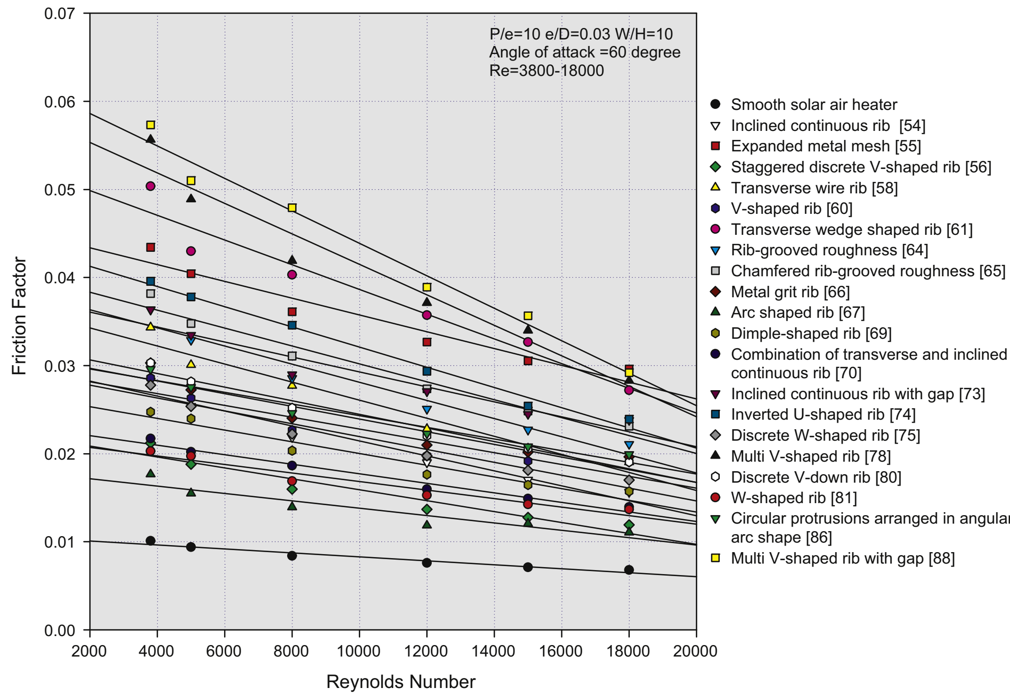


Fig. 44. Friction factor vs. Reynolds number for artificially roughened solar air heater having different types of roughness geometry and for smooth solar air heater.

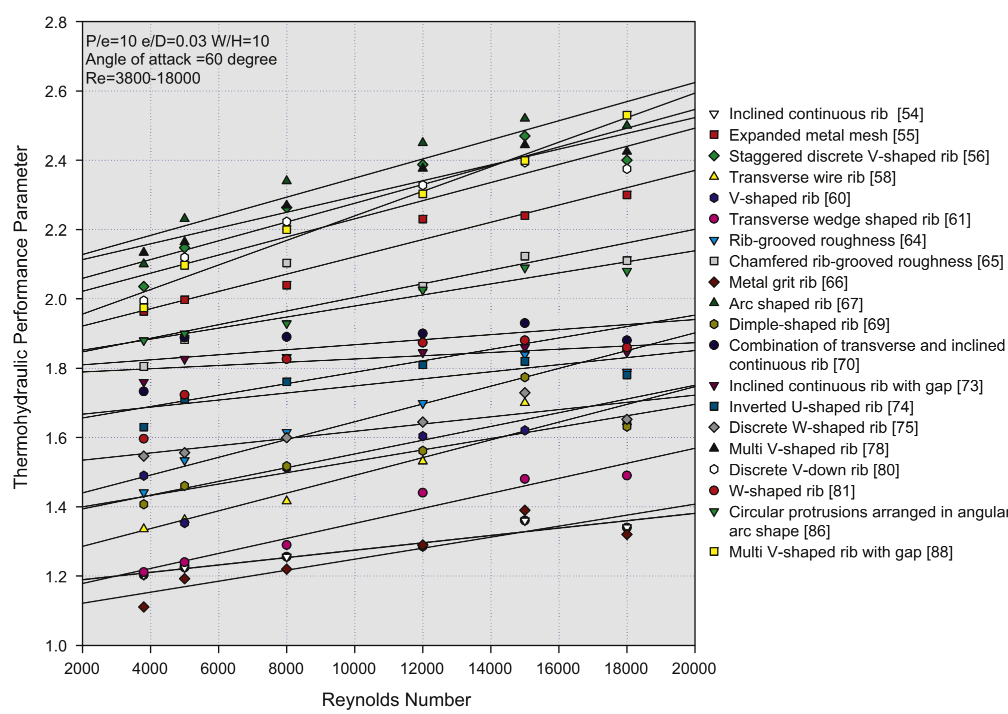


Fig. 45. Thermohydraulic performance parameter vs. Reynolds number for artificially roughened solar air heater having different types of roughness geometry.

reduces thermal resistance and significantly boost the rate of heat transfer. However, the uses of artificial roughness on the heat transfer surface results in higher pressure drop and hence greater pumping power requirements. So, it is necessary that turbulence must be generated only in the region very close to the absorber plate, i.e. in the laminar sub-layer only. Hence, in order to make the use of artificial roughness more effective, the height of roughness should be kept small, primarily in the laminar sub-layer region, so that the increases in the friction will not be disproportionate to the increase in heat transfer. It has been observed that the rate of increment of average heat transfer is comparatively less than the rate of increment of average friction factor for increasing rib height. It is, therefore, necessary to determine the optimal roughness geometry such that the heat transfer coefficient is maximized while keeping the friction losses at the minimum possible value. A parameter that facilitates simultaneous consideration of

thermal and hydraulic performance as defined by Webb and Eckert [107] is given by Eq. (15). The result of this parameter higher than one declares the usefulness of applying an enhancement scheme and used to compare the performance of number of arrangements to decide the best among these.

Fig. 45 shows the variation of thermohydraulic performance parameter with Reynolds number for different types of roughness geometries used in solar air heater duct. The thermo-hydraulic performance parameter initially tends to increase with the rise of Reynolds number and then decreases with the further rise of Reynolds number. This appears due to the fact that at relatively higher values of relative roughness height, the reattachment of free shear layer might not occur and the rate of heat transfer enhancement will not be proportional to that of friction factor as stated by Prasad and Saini [95].

It is found that among the entire roughness elements investigated, arc shaped rib geometry has the highest thermohydraulic performance parameter at a value of $Re=15{,}000$ as compared to other roughness geometries for the investigated range of parameters. It can be seen that at low Reynolds number ($Re=3800$) the thermohydraulic performance parameter increases in the following sequence: metal grit rib, inclined continuous rib, transverse wedge shaped rib, transverse wire rib, dimple-shaped rib, rib-grooved roughness, V-shaped rib, discrete W-shaped rib, W-shaped rib, inverted U-shaped rib, combination of transverse and inclined rib, inclined continuous rib roughness with gap, chamfered rib-grooved, circular protrusions arranged in angular arc shape, expanded metal mesh, multi V-shaped rib roughness with gap, discrete V-down rib, staggered discrete V-shaped rib, arc shaped rib and multi V-shaped rib. It can also be seen that at high Reynolds number ($Re=18{,}000$), the thermohydraulic performance parameter increases in the following sequence: metal grit rib, inclined continuous rib, transverse wedge shaped rib, dimple-shaped rib, V-shaped rib, transverse wire rib, discrete W-shaped rib, inverted U-shaped rib, rib-grooved roughness, inclined continuous rib roughness with gap, W-shaped rib, combination of transverse and inclined rib, circular protrusions arranged in angular arc shape, chamfered rib-grooved, expanded metal mesh, discrete V-down rib, staggered discrete V-shaped rib, multi V-shaped rib, arc shaped rib and multi V-shaped rib roughness with gap.

Yadav and bhagoria [44] suggested the following three criteria for the selection of best rib geometry for heat transfer enhancement of a solar air heater:

(1) Selection of best rib geometry on the basis of maximum heat transfer enhancement only.
(2) Selection of best rib geometry on the basis of minimum pumping penalty only (i.e. economically benefited).
(3) Selection of best rib geometry on the basis of constant pumping power penalty (i.e. thermo-hydraulic performance parameter).

As we know that the application of artificial roughness on the heat transfer surface has been recommended to enhance the heat transfer coefficient by several investigators. Inclusion of artificial roughness, on the other hand, results in higher friction factor causing more pumping power required. If designer's primary aim is only heat transfer enhancement and not the pumping power, then artificially roughened solar air heater having multi V-shaped rib roughness with gap on the absorber plate can be employed for heat transfer augmentation. A maximum 6.74 times enhancement in heat transfer can be obtained by using multi V-shaped rib roughness with gap. If designer's primary aim is only heat transfer enhancement with minimum pumping power penalty, then artificially roughened solar air heater having arc shaped rib roughness on the absorber plate can be employed for heat transfer augmentation. If designer's primary aim is heat transfer enhancement with constant pumping power penalty (i.e. thermo-hydraulic performance parameter), then artificially roughened solar air heater having arc shaped rib roughness on the absorber plate can be employed for heat transfer augmentation.

11. Conclusions

This article presents a detailed review of the experimental investigations carried out by various researchers in order to enhance the heat transfer by the use of artificial roughness of different shapes, sizes and orientations. The effects of various rib parameters on heat transfer and fluid flow processes are discussed in detail. Heat transfer and friction factor correlations reported in literature are also presented in tabular form. These correlations may be used to predict the thermal as well as hydraulic performance of solar air heater having roughened duct. In this article a comparative study is also carried out to select best roughness element geometry for maximum convective heat transfer with minimum constant pumping losses. Total number of twenty known different shapes and orientations of roughness elements are considered for comparative analysis. In order to obtain the results numerically, codes are developed in MATLAB-7.6.0.324 using fixed values of operating and system parameters. On the basis of the review of the literature and comparative study of artificially roughened solar air heaters, the conclusions can be summarized as follows:

(1) The use of artificial roughness on a surface is an effective technique to enhance heat transfer to fluid flowing in the duct. Artificially roughened solar air heaters have enhanced rate of heat transfer as compared to the smooth solar air heaters under the same geometric/operating conditions.
(2) It has been found that roughness geometries being used in solar air heaters are of many types depending upon shapes, size, arrangement and orientations of roughness elements on the absorber plate.
(3) There are several parameters that characterize the roughness elements, but for solar air heater the most preferred roughness geometry is repeated rib type which is described by the dimensionless parameters viz. relative roughness height (e/D), relative roughness pitch, (P/e), angle of attack (α), channel aspect ratio (W/H) etc.
(4) Transverse rib roughness enhances the heat transfer coefficient by flow separation and generation of vortices on the upstream and downstream of rib and reattachment of flow in the inter-rib spaces.
(5) It can be concluded that the use of artificial roughness results in higher friction and hence higher pumping power requirements. It is desirable that design of solar air heater should be made in such a way that it should transfer maximum heat energy to the flowing fluid with minimum consumption of blower energy.
(6) It is found that among the entire roughness elements investigated, the multi V-shaped rib roughness with gap has the highest Nusselt number as compared to other roughness geometries for the investigated range of parameters.
(7) It is found that among the entire roughness elements investigated, the multi V-shaped rib roughness with gap has the highest friction factor as compared to other roughness geometries for the investigated range of parameters.
(8) It is found that among the entire roughness elements investigated, arc shaped rib geometry has the highest thermohydraulic performance parameter as compared to other roughness geometries for the investigated range of parameters.

Experimental approaches used for the design and development of an artificially roughened solar air heater are mostly tedious, expensive

and time consuming. Computational Fluid Dynamics (CFD) approach has emerged as a cost effective alternative and it provides speedy solution to design and optimization of an artificially roughened solar air heater. In recent years CFD approach has been used as it is a powerful tool for dealing with the wide range of parameters and complicated analysis which cannot be done through experimental investigations. Nowadays CFD has also been applied in the design of artificially roughened solar air heater. The solutions obtained from CFD simulations are largely within the acceptable range proving that CFD is an effective tool for predicting the behavior and performance of an artificially roughened solar air heater.

There is tremendous scope for future study of artificially roughened solar air heater with different combination of roughness element with gap at different positions/angle of attack. Based on present critical review it has been found that the research on the following geometries of the artificial roughness is relatively limited and may attract more interest in the future research:

(a) Combination of transverse I-shaped and V-up wire rib roughness
(b) Combination of transverse I-shaped and V-down wire rib roughness
(c) Chamfered rib-semi-circular grooved roughness
(d) Circular rib-semi-circular grooved roughness
(e) Discreet arc shaped rib roughness.

In summary, the purpose of this article is to illustrate the use of artificial roughness in design of solar air heater. There is tremendous scope for future study of artificially roughened solar air heater. The information presented here will be beneficial for beginners in this area of research. This article is very helpful for researchers in carrying out the experimental investigations to find out and optimize the new roughness element geometries for the maximum enhancement of heat transfer. Authors hope that this article has opened the horizons of use of artificial roughness in the design of enhanced solar air heater to researchers.

References

[1] Maczulak A. Renewable energy: sources and methods. 1st ed. New York: Infobase Publishing; 2011.
[2] Quaschning V. Understanding renewable energy systems. 3rd ed. London: Earthscan; 2005.
[3] Kaltschmitt M, Streicher W, Wiese A. Renewable energy: technology, economics and environment. 1st ed. New York: Springer; 2007.
[4] Twidell J, Weir T. Renewable energy: sources. 2nd ed. New York: Taylor & Francis; 2006.
[5] Li X. Green energy: basic concepts and fundamentals. 1st ed. New York: Springer; 2011.
[6] Kalogirou S. Solar energy engineering: processes and systems. London: Academic Press; 2009.
[7] Sukhatme SP, Nayak JP. Solar energy. 3rd ed. New Delhi: Tata McGraw Hill; 2011.
[8] Tyagi VV, Panwar NL, Rahim NA, Kothari R. Review on solar air heating system with and without thermal energy storage system. Renew Sustain Energy Rev 2012;16:2289–303.
[9] Garg HP, Prakash J. Solar energy fundamentals and applications. 1st ed. New Delhi: Tata McGraw-Hill; 2000.
[10] Duffie JA, Beckman WA. Solar engineering of thermal processes. 2nd ed.. New York: Wiley; 1980.
[11] Khan BH. Non-conventioal energy resources. 2nd ed.. New Delhi: Tata McGraw Hill; 2012.
[12] McAdams WH. Heat transmission. New York: McGraw-Hill; 1942.
[13] Fox W, Pritchard P, McDonald A. Introduction to fluid mechanics. New York: John Wiley & Sons; 2010.
[14] Constantinos AB. A review of augmentation techniques for heat transfers surfaces in single phase heat exchangers. Energy 1990;15:899–906.
[15] Joule JP. On the surface condensation of steam. Philos Trans R Soc Lond 1861;151:133–60.
[16] Nikuradse J. Laws of flow in rough pipes, VDI Forsch 1933; 361, English translation. National Advisory Committee for Aeronautics Technical Memorandum, p. 1292; Nov 1950.
[17] Nunner W. Heat transfer and pressure drop in rough pipes. VDI-Forsch 1956;22:445-B, English trans, AERE Lib./Trans p. 786; 1958.
[18] Dippery DF, Sabersky RH. Heat and momentum transfer in smooth and rough tubes at various Prandtl number. Int J Heat Mass Transfer 1963;6:329–53.
[19] Webb RL, Eckert ERG, Goldstein RJ. Heat transfer and friction in tubes with repeated-rib roughness. Int J Heat Mass Transf 1971;14:601–17.
[20] Sheriff N, Gumley P. Heat transfer and friction properties of surfaces with discrete roughness. Int J Heat Mass Transf 1966;9:1297–320.
[21] Kays WB. Convective heat and mass transfer. New York: McGraw Hill Book Co;; 1966.
[22] Lewis MJ. Optimizing the thermo-hydraulic performance of rough surfaces. Int J Heat Mass Transf 1975;18:1243–8.
[23] Han JC, Glicksman LR, Rohsenow WM. An investigation of heat transfer and friction for rib-roughened surfaces. Int J Heat Mass Transf 1978;21 (8):1143–56.
[24] Han JC. Heat transfer and friction in channels with two opposite rib-roughened walls. J Heat Transf 1984;106(4):774–81.
[25] Han JC, Park JS, Lei CK. Heat transfer enhancement in channels with turbulence promoters. J Eng Gas Turbines Power 1985;107(3):628–35.
[26] Han JC. Heat transfer and friction characteristics in rectangular channels with rib turbulators. J Heat Transf 1988;110(2):321–9.
[27] Han JC, Park JS. Developing heat transfer in rectangular channels with rib turbulators. Int J Heat Mass Transf 1988;31(1):183–95.
[28] Han JC, Ou S, Park JS, Lei CK. Augmented heat transfer in rectangular channels of narrow aspect ratios with rib turbulators. Int J Heat Mass Transf 1989;32(9):1619–30.
[29] Han JC, Zhang YM, Lee CP. Augmented heat transfer in square channels with parallel, crossed, and V-shaped angled ribs. J Heat Transf 1991;113: 590–6.
[30] Han JC, Zhang YM. High performance heat transfer ducts with parallel broken and V-shaped broken ribs. Int J Heat Mass Transf 1992;35(2):513–23.
[31] Han JC, Zhang YM, Lee CP. Influence of surface heat flux ratio on heat transfer augmentation in square channel with parallel, crossed and V-shaped angled ribs. J Turbomach 1992;114(4):872–80.
[32] Park JS, Han JC, Huang Y, Ou S. Heat transfer performance comparisons of five different rectangular channels with parallel angled ribs. Int J Heat Mass Transf 1992;35(11):2891–903.
[33] Chandra PR, Alexande CR, Han JC. Heat transfer and friction behaviors in rectangular channels with varying number of ribbed wall. Int J Heat Mass Transf 2003;46(3):481–95.
[34] Lau SC, Rd Mcmillin, Han JC. Turbulent heat transfer and friction in a square channel with discrete rib turbulators. J Turbomach 1991;113(3):360–7.
[35] Lau SC, Rd Mcmillin, Han JC. Heat transfer characteristics of turbulent flow in a square channel with angled discrete ribs. J Turbomach 1991;113(3):367–74.
[36] Zhang YM, Gu WZ, Han JC. Heat transfer and friction in rectangular channels with ribbed or ribbed-grooved walls. J Heat Transfer 1994;116(1):58–65.
[37] Prasad K, Mullick SC. Heat transfer characteristics of a solar air heater used for drying purposes. Appl Energy 1983;13(2):83–93.
[38] Chaube A, Sahoo PK, Solanki SK. Analysis of heat transfer augmentation and flow characteristics due to rib roughness over absorber plate of a solar air heater. Renew Energy 2006;31(3):317–31.
[39] Chaube A, Sahoo PK, Solanki SK. Effect of roughness shape on heat transfer and flow friction characteristics of solar air heater with roughened absorber plate. WIT Trans Eng Sci 2006;53:43–51.
[40] Karmare SV, Tikekar AN. Analysis of fluid flow and heat transfer in a rib grit roughened surface solar air heater using CFD. Sol Energy 2010;84(3): 409–17.
[41] Gandhi BK, Singh KM. Experimental and numerical investigations on flow through wedge shape rib roughened duct. Inst Eng (India) J MC 2010;90 (January):13–8.
[42] Sharma AK, Thakur NS. CFD based fluid flow and heat transfer analysis of a V-shaped roughened surface solar air heater. Int J Eng Sci Technol 2012; 4(5):2115–21.
[43] Kumar S, Saini RP. CFD based performance analysis of a solar air heater duct provided with artificial roughness. Renew Energy 2009;34(5):1285–91.
[44] Yadav AS, Bhagoria JL. A CFD based performance analysis of an artificially roughened solar air heater having equilateral triangular sectioned rib roughness on the absorber plate. Int J Heat Mass Transf 2014;70:1016–39.
[45] Yadav AS, Bhagoria JL. Heat transfer and fluid flow analysis of solar air heater: a review of CFD approach. Renew Sustain Energy Rev 2013;23:60–79.
[46] Yadav AS, Bhagoria JL. A CFD based heat transfer and fluid flow analysis of a solar air heater provided with circular transverse wire rib roughness on the absorber plate. Energy 2013;55:1127–42.
[47] Yadav AS, Bhagoria JL. Modeling and simulation of turbulent flows through a solar air heater having square sectioned transverse rib roughness on the absorber plate. Sci World J 2013;2013:12.
[48] Yadav AS, Bhagoria JL. A numerical investigation of turbulent flows through an artificially roughened solar air heater. Numer Heat Transf A 2014;65: 679–98.
[49] Yadav AS, Bhagoria JL. Numerical investigation of flow through an artificially roughened solar air heater. Int J Ambient Energy 2014 (in press) http://dx.doi.org/10.1080/01430750.2013.823107.
[50] Yadav AS, Bhagoria JL. Heat transfer and fluid flow analysis of an artificially roughened solar air heater: a CFD based investigation. Front Energy 2014 (in press) http://dx.doi.org/10.1007/s11708-014-0297-7.

[51] Yadav AS, Bhagoria JL. A CFD analysis of a solar air heater having triangular rib roughness on the absorber plate. Int J ChemTech Res 2013;5(2):964–71.
[52] Yadav AS, Bhagoria JL. A CFD based heat transfer and fluid flow analysis of a conventional solar air heater. J Eng Sci Manag Educ 2013;6(2):137–46.
[53] ASHRAE Standard 93. Method of testing to determine the thermal performance of solar collectors. Atlanta: American Society of Heating, Refrigeration and Air Conditioning Engineers; 2003.
[54] Gupta D, Solanki SC, Saini JS. Heat and fluid flow in rectangular solar air heater ducts having transverse rib roughness on absorber plates. Sol Energy 1993;51(1):31–7.
[55] Saini RP, Saini JS. Heat transfer and friction factor correlations for artificially roughened ducts with expanded metal mesh as roughened element. Int J Heat Mass Transf 1997;40:973–86.
[56] Muluwork KB. Investigations on fluid flow and heat transfer in roughened absorber solar heaters. India: IIT, Roorkee-247667; 2000 (Ph.D. Dissertation).
[57] Karwa R, Solanki SC, Saini JS. Heat transfer coefficient and friction factor correlations for the transitional flow regime in rib-roughened rectangular ducts. Int J Heat Mass Transf 1999;42:1597–615.
[58] Verma SK, Prasad BN. Investigation for the optimal thermohydraulic performance of artificially roughened solar air heaters. Renew Energy 2000;20:19–36.
[59] Karwa R, Solanki SC, Saini JS. Thermo-hydraulic performance of solar air heaters having integral chamfered rib roughness on absorber plates. Energy 2001;26:161–76.
[60] Momin AME, Saini JS, Solanki SC. Heat transfer and friction in solar air heater duct with v-shaped rib roughness on absorber plate. Int J Heat Mass Transf 2002;45:3383–96.
[61] Bhagoria JL, Saini JS, Solanki SC. Heat transfer coefficient and friction factor correlations for rectangular solar air heater duct having transverse wedge shaped rib roughness on the absorber plate. Renew Energy 2002;25:341–69.
[62] Karwa RK. Experimental studies of augmented heat transfer and friction in asymmetrically heated rectangular ducts with ribs on heated wall in transverse, inclined, v-continuous and v-discrete pattern. Int Commun Heat Mass Transf 2003;30:241–50.
[63] Sahu MM, Bhagoria JL. Augmentation of heat transfer coefficient by using 90° broken transverse ribs on absorber plate of solar air heater. Renew Energy 2005;30:2057–63.
[64] Jaurker AR, Saini JS, Gandhi BK. Heat transfer and friction characteristics of rectangular solar air heater duct using rib-grooved artificial roughness. Sol Energy 2006;80:895–907.
[65] Layek A, Saini JS, Solanki SC. Heat transfer and friction characteristics for artificially roughened ducts with compound turbulators. Int J Heat Mass Transf 2007;50:4845–54.
[66] Karmare SV, Tikekar AN. Heat transfer and friction factor correlation for artificially roughened duct with metal grit ribs. Int J Heat Mass Transf 2007;50:4342–51.
[67] Saini SK, Saini RP. Development of correlations for Nusselt number and friction factor for solar air heater with roughened duct having arc-shaped wire as artificial roughness. Sol Energy 2008;82:1118–30.
[68] Aharwal KR, Gandhi BK, Saini JS. Experimental investigation on heat-transfer enhancement to a gap in an inclined continuous rib arrangement in a rectangular duct of solar air heater. Renew Energy 2008;33:585–96.
[69] Saini RP, Verma J. Heat transfer and friction factor correlations for a duct having dimple-shaped artificial roughness for solar air heaters. Energy 2008;33:1277–87.
[70] Varun RP, Saini, Singal SK. Investigation of thermal performance of solar air heater having roughness elements as a combination of inclined and transverse ribs on absorber plate. Renew Energy 2008;33:1398–405.
[71] Layek A, Saini JS, Solanki SC. Effect of chamfering on heat transfer and friction characteristics of solar air heater having absorber plate roughened with compound turbulators. Renew Energy 2009;34:1292–8.
[72] Karmare SV, Tikekar AN. Experimental investigation of optimum thermohydraulic performance of solar air heaters with metal rib grits roughness. Sol Energy 2009;82:6–13.
[73] Aharwal KR, Gandhi BK, Saini JS. Heat transfer and friction characteristics of solar air heater ducts having integral inclined discrete ribs on absorber plate. Int J Heat Mass Transf 2009;52:5970–7.
[74] Bopche SB, Tandale MS. Experimental investigations on heat transfer and frictional characteristics of a turbulator roughened solar air heater duct. Int J Heat Mass Transf 2009;52:2834–48.
[75] Kumar A, Bhagoria JL, Sarviya RM. Heat transfer and friction correlations for artificially roughened solar air heater duct with discrete W-shaped ribs. Energy Convers Manag 2009;50:2106–17.
[76] Varun A, Patnaik, Saini RP, Singal SK, Siddhartha. Performance prediction of solar air heater having roughened duct provided with transverse and inclined ribs as artificial roughness. Renew Energy 2009;34:2914–22.
[77] Mittal MK, Varun. Thermohydraulic performance of solar air heater provided with artificial roughness on the absorber plate. Inst Eng J IE(I)–MC 2009;90(July):43–8.
[78] Hans VS, Saini RP, Saini JS. Heat transfer and friction factor correlations for a solar air heater duct roughened artificially with multiple V-ribs. Sol Energy 2010;84:898–911.
[79] Lanjewar A, Bhagoria JL, Sarviya RM. Experimental study of augmented heat transfer and friction in solar air heater with different orientations of W-Rib roughness. Exp Thermal Fluid Sci 2011;35:986–95.
[80] Singh S, Chander S, Saini JS. Heat transfer and friction factor correlations of solar air heater ducts artificially roughened with discrete V-down ribs. Energy 2011;36:5053–64.
[81] Lanjewar A, Bhagoria JL, Sarviya RM. Heat transfer and friction in solar air heater duct with W-shaped rib roughness on absorber plate. Energy 2011;36:4531–41.
[82] Tanda G. Performance of solar air heater ducts with different types of ribs on the absorber plate. Energy 2011;36:6651–60.
[83] Sethi M, Varun, Thakur NS. Correlations for solar air heater duct with dimpled shape roughness elements on absorber plate. Sol Energy 2012;86:2852–61.
[84] Kumar A, Saini RP, Saini JS. Experimental investigation on heat transfer and fluid flow characteristics of air flow in a rectangular duct with Multi v-shaped rib with gap roughness on the heated plate. Sol Energy 2012;86:1733–49.
[85] Singh S, Chander S, Saini JS. Investigations on thermo-hydraulic performance due to flow-attack-angle in V-down rib with gap in a rectangular duct of solar air heater. Appl Energy 2012;97:907–12.
[86] Yadav S, Kaushal M. Varun, Siddhartha. Nusselt number and friction factor correlations for solar air heater duct having protrusions as roughness elements on absorber plate. Exp Therm Fluid Sci 2013;44:34–41.
[87] Bharadwaj G, Kaushal M, Goel V. Heat transfer and friction characteristics of an equilateral triangular solar air heater duct using inclined continuous ribs as roughness element on the absorber plate. Int J Sustain Energy 2013;32(6):515–30.
[88] Kumar A, Saini RP, Saini JS. Development of correlations for Nusselt number and friction factor for solar air heater with roughened duct having multi v-shaped with gap rib as artificial roughness. Renew Energy 2013;58:151–63.
[89] Prasad BN. Thermal performance of artificially roughened solar air heaters. Sol Energy 2013;91:59–67.
[90] Karwa R, Chitoshiya G. Performance study of solar air heater having v-down discrete ribs on absorber plate. Energy 2013;55:939–55.
[91] Saini RP, Varun, Singal SK. A review on roughness geometry used in solar air heaters. Sol Energy 2007;81:1340–50.
[92] Hans VS, Saini RP, Saini JS. Performance of artificially roughened solar air heaters—a review. Renew Sustain Energy Rev 2009;13:1854–69.
[93] Bhushan B, Singh R. A review on methodology of artificial roughness used in duct of solar air heaters. Energy 2010;35:202–12.
[94] Kumar A, Saini RP, Saini JS. Heat and fluid flow characteristics of roughened solar air heater ducts—a review. Renew Energy 2012;47:77–94.
[95] Prasad BN, Saini JS. Effect of artificial roughness on heat transfer and friction factor in a solar air heater. Sol Energy 1988;41(6):555–60.
[96] Gupta D, Solanki SC, Saini JS. Thermo-hydraulic performance of solar airheaters with roughened absorber plates. Sol Energy 1997;61(1):33–42.
[97] Mittal MK, Varun, Saini RP, Solanki SK. Effective efficiency of solar air heaters having different types of roughness elements on the absorber plate. Energy 2007;32:739–45.
[98] Layek A, Saini JS, Solanki SC. Second law optimization of a solar air heater having chamfered rib-grooveroughness on absorber plate. Renew Energy 2007;32:1967–80.
[99] Gupta MK, Kaushik SC. Performance evaluation of solar air heater for various artificial roughness geometries based on energy, effective and exergy efficiencies. Renew Energy 2009;34(3):465–76.
[100] Gupta MK, Kaushik SC. Performance evaluation of solar air heater havingexpanded metal mesh as artificial roughness on absorber plate. Int J Therm Sci 2009;48:1007–16.
[101] Singh S, Chander S, Saini JS. Exergy based analysis of solar air heater having discrete V-down rib roughness on absorber plate. Energy 2012;37(1):749–58.
[102] Karwa R, Shrivastava V. Thermal performance of solar air heater having absorber plate with V-down discrete rib roughness for space heating applications. J Renew Energy 2013;2013:13.
[103] Beckman WA, Klein SA, Duffie JA. Solar heating design by the f-chart method. New York: Wiley; 1977.
[104] Lof GOG. Flat plate and concentrating collectors. In: Dickinson WC, Cheremisinoff PN, editors. Solar Energy Technology Hand Book, Part A. New York: Marcel Dekker; 1980.
[105] Chiou JP, El-Wakil MM, Duffie JA. A slit and expanded aluminium-foil matrix solar collector. Sol Energy 1965;9:73–80.
[106] Ehling AH. Flow of air and gases. In: Salisburv JK, editor. Kent's Mechanical Engineers Handbook, Power Vol. New York: Wiley; 1950.
[107] Webb RL, Eckert ERG. Application of rough surface to heat exchanger design. Int J Heat Mass Transf 1972;15(9):1647–58.